PREDICTIVE AND DIAGNOSTIC METHODS FOR VAPOR COMPRESSION CHILLER

SATHTHASIVAM, JAYAPRAKASH

NATIONAL UNIVERSITY OF SINGAPORE
2010

PREDICTIVE AND DIAGNOSTIC METHODS FOR VAPOR COMPRESSION CHILLER

SATHTHASIVAM, JAYAPRAKASH

B.ENG. (Mechanical-Aeronautics, UTM)

A THESIS SUBMITTED

FOR THE DEGREE OF DOCTOR OF PHILOSOPHY

DEPARTMENT OF MECHANICAL ENGINEERING

NATIONAL UNIVERSITY OF SINGAPORE

2010

OM NAMAH SHIVAYA

To Beloved God, Family and Friends;

For All Their Love and Understanding

Acknowledgements

Firstly, I would like to convey my warmest gratitude to Professor Ng Kim Choon for his priceless guidance and support throughout this project. I am thankful for all the resources and references that he has provided. Secondly, my deepest appreciation goes to Professor James E. Braun from Purdue University for providing comprehensive laboratory chiller data that were utilized to validate the proposed FDD technique. Special thanks go to Mr. Sacadevan Raghavan of Air Conditioning Laboratory for his kind assistance in setting up the chiller test rig. I also would like to acknowledge advice and helpful feedback from Professor T. Agami Reddy of Drexel University. I would also like to take this opportunity to thank my research colleagues who were willing to share and provide information on this project. Finally, I would like to thank individuals for their direct or indirect contributions towards the accomplishment of this report.

SATHTHASIVAM, JAYAPRAKASH

AUGUST 2010

Table of Contents

Table of Contents

Table of Contents

Table of Contents

Table of Contents

Summary

The aim of thesis work is to develop a reliable and accurate Fault Detection and Diagnosis (FDD) tool for vapor compression chillers. Faults that normally occur in chillers can be categorized as:- (i) Abrupt and (ii) Degrading faults. Abrupt faults occur spontaneously and are easily detectable where obvious impacts on the chiller system operation can be observed. On the other hand, degrading faults are difficult to detect at the initial stages and develop gradually over time. Common degrading faults in chillers are refrigerant leakage and condenser fouling. In this study, we will only focus on the occurrence of degrading faults as they are more difficult to detect and affect the system efficiency over a period of time. Three degrading faults namely (i) Refrigerant leakage (ii) Condenser fouling and (iii) Refrigerant overcharge were simulated on a scroll chiller in this thesis work.

The test runs were firstly conducted under fault-free conditions and was then followed by other faulty test runs. Fouling was simulated by blocking the condenser water tubes. Refrigerant leakage was simulated by undercharging the system while overcharge was performed by adding more refrigerant. Fault-free models were then developed for the selected fault detection parameters namely, (i) suction superheat temperature (ii) condenser approach temperature (iii) condenser sub-cooling (iv) overall condenser heat transfer coefficient and (v) condenser entropy generation. These models were developed using simple linear regression technique.

Two statistical methods were employed in this study to detect and diagnose the three faults. The faults were detected using the Cumulative Summation (CUSUM) technique while the diagnosis was accomplished using the Bayes Theorem. Although five fault detection parameters were investigated, it was found that condenser approach and condenser sub-

cooling temperatures were more than sufficient to evaluate the three degrading faults investigated in this study. These parameters are readily available in industrial chillers. A fault is considered detected if the non-reset drift (negative or positive) of any of the two fault detection parameters surpasses the second decision limit. A simple lag analysis is also proposed to enhance the diagnostic results. Once a fault is detected, the diagnosis routine is then activated to compute the fault probability.

The proposed FDD scheme was able to diagnose the leakage fault at the lowest severity level of 10% with an acceptable probability of 86.8%. The occurrence of 10% fouling was also successfully diagnosed with a probability of 91.6%. Refrigerant overcharge of 10% and above was correctly diagnosed with a probability of 79.8%. The proposed CUSUM-Bayes approach was also validated using faulty data sets obtained from an external 90 Rton chiller.

The capability of the developed scheme to diagnose faults on the existing scroll test rig and external centrifugal chiller was clearly demonstrated in the thesis work. The scheme was developed using only a handful number of measurements that is usually available in chillers. Apart from that, the proposed scheme can be easily programmed as a commercial software due to its simple and straight forward equations.

List of Tables

List of Tables

List of Figures

List of Figures

List of Figures

List of Figures

List of Symbols

A_{int}	Internal area, m^2
A_{ext}	External area, m^2
A_0	Regression Coefficient
A_1	Regression Coefficient
COP	Coefficient of Performance
Cp	Specific heat capacity, kJ/kgK
H	Enthalpy
h_{int}	Internal heat transfer coefficient, kW/m^2K
h_{ext}	External heat transfer coefficient, kW/m^2K
L	Tube length, m
LMTD	Log mean temperature difference, ^oC or K
$\dot{m}$	Mass flow rate, kg/s
N	subgroup size
NS	number of subgroups
P_{in}	Compressor power input, kW
$\dot{Q}$	Heat load, kW
$\dot{Q}_{Evap}$	Evaporator cooling Load, kW
$Q_{leak,eqv}$	Heat Leak, kW

List of Symbols

R	Total Thermal Resistance, K/kW
$R_{f,int}$	Internal fouling factor, m^2K /kW
$R_{f,ext}$	External fouling factor, m^2K /kW
R (j)	jth subgroup range
RB	Range mean
SB	Sigma mean
$\dot{S}_{gen}$	Entropy generation, kW/K
S(j)	jth subgroup sigma
SIGXB	Standard deviation, sigma of the Xbar
T	Temperature, ^oC or K
$T_{C,outlet}$	Chilled water inlet temperature, ^oC or K
$T_{Cond,appr}$	Condenser approach temperature, ^oC or K
$T_{Evap,appr}$	Evaporator approach temperature, ^oC or K
$T_{Evap,out}$	Evaporator refrigerant outlet temperature, ^oC or K
T_{evap}^{in}	Chilled water inlet temperature, ^oC or K
T_{cond}^{in}	Cooling water inlet temperature, ^oC or K
$T_{H,inlet}$	Cooling water inlet temperature, ^oC or K
T_{sat}	Saturation temperature, ^oC or K
$\dot{W}$	Work, kW
XB (j)	jth subgroup mean

List of Symbols

XBB	Xbar mean
X (i,j)	ith value of the variable in subgroup j
X_j	Data input
XMAX (j)	jth subgroup maximum value
XMIN (j)	jth subgroup sigma

Greek Symbols

ε	Effectiveness
ε_{Cond}	Condenser Effectiveness
ε_{Evap}	Evaporator Effectiveness
μ	Mean
σ	Standard deviation, sigma of the Xbar
Ω	decision intervals
Z	Slack value
ψ_H	positive drift
ψ_L	negative drift
ψ_R	Reset drift
ψ_{NR}	Non-reset drift
ϕ_1	Superheat, ^{o}C or K

List of Symbols

ϕ_2	Condenser Approach Temperature, ^{o}C or K
ϕ_3	Condenser sub-cooling Temperature, ^{o}C or K
ϕ_4	Condenser overall heat transfer coefficient, UA_{Cond}, kW/K
ϕ_5	Condenser entropy generation, kW/K

Chapter 1: Introduction

1.1 Background

In large commercial buildings, chillers play a prominent role in providing sufficient cooling capacity while ensuring a comfortable building envelope. Analysis of the utility bills of commercial buildings in Singapore reveal that chillers and other heating, ventilation and air-conditioning (HVAC) equipment consume approximately 30 to 50% of the total electricity. As low tension electricity tariff in Singapore has increased by approximately 18.5% between April 2001 (S$ 0.1987 per kWh) and April 2010 (S$ 0.2356 per kWh) with the highest tariff recorded on October 2008 (S$ 0.3045 per kWh), the significant electricity utilization by chillers and other HVAC operations has proved to be of great concern for building managers and owners. As a result, HVAC manufacturers and researchers have been relentlessly developing various latest designs (variable speed compressors, digital scroll technology, and many more profound technologies) in order to increase the overall system efficiency, thus leading to lower electricity consumption.

Apart from important contributions from system manufacturers and researchers to develop high efficiency chillers, building managers also play a huge role in minimizing power consumption by having strategic HVAC equipment operations and maintenance plans. Well scheduled maintenance plans are essential for achieving interruption-free, reliable and cost effective building operations as well as minimizing down times. Inefficient chillers and other HVAC equipment lead to economic losses to building owners in term of repairs and breakdown cost, compensation to tenants due to business interruptions and higher energy cost due to lower efficiency. This scenario emphasizes the importance of performance monitoring which can be a great tool for building operators to assess the performance of their operating

equipment. By analysing the monitored data, the management has the luxury of scheduling their maintenance plan in advance rather than experiencing unnecessary operation interruptions.

In this regard, performance of chillers and other equipment need to be closely monitored to ensure continuous and optimal operations. Traditionally, performance monitoring is confined to manual data recording where technicians collect data at specified intervals or shifts using log sheets. Unfortunately, manual data logging provides insufficient clues on system performance, as it is incapable of elucidating the genuine trend of the operating system due to the large time interval between the logged data. It is also difficult to appraise the operating state (transient or steady) of the chiller at the time point of the logging. However, with the advent of data acquisitions technologies, automated system monitoring is gaining its popularity in analysing system performances. Besides offering excellent graphical and data base features as well as continuous monitoring, automated system monitoring also minimizes work force utilization. With the aid of apposite sensors and reliable data analyses, it is capable of supporting building operators in assessing the real time efficiency and performance status of the operating HVAC equipment, specifically chillers.

One of the essential elements in HVAC automated performance monitoring is the application of Fault detection and Diagnostic (FDD) in vapor compression chillers. Chiller FDD plays a pivotal role in optimizing energy consumption of a chiller. Faults developing in chillers affect the overall system efficiency. This leads to increase in the energy cost of a building in two ways – usage of energy and maximum contracted capacity. Building owners have to commit to a maximum contracted capacity for the building where diminution in chiller efficiency will augment maximum contracted capacity. Thus, building owners will have to pay additional monthly cost to increase the contracted capacity in addition to the energy cost. Early detection of faults allows building managers to schedule chillers for

preventive maintenance work. It minimizes chiller downtime, avoiding costly and unscheduled repairs. In short, by maintaining chillers at fault-free conditions, they can be operated at optimum efficiencies. Besides minimizing energy cost, FDD applications also promotes condition-based maintenance instead of the current practices where maintenance are scheduled based on operating hours. Based on a 12-hourly daily operation, each chiller will undergo scheduled maintenance annually regardless of the chiller conditions. With a good fault detection and diagnostic system, chiller maintenance can be carried out based on the chiller conditions rather than operating hours. Conditioned based maintenance could lead to saving in the maintenance cost and avoid unexpected breakdowns.

Having realized the benefits and potentials of FDD applications in ensuring economic and efficient chiller operations, it is important to understand the common faults associated to chillers in order to develop a reliable FDD tool. As shown in Figure 1.1, faults that normally occur in chillers can be categorized as:- (i) Abrupt and (ii) Degrading faults. Abrupt faults, also known as sudden or hard faults, occur spontaneously and usually lead to unscheduled maintenance. These faults are easily detectable where obvious impacts on the chiller system operation can be observed. Some of the common sudden faults in chillers are sensor failures, compressor rotor damage, motor burn out and fan belt breakage. On the other hand, degrading faults which are also defined as soft faults are difficult to be detected at the initial stages. These faults developed gradually over the time and reduce the chiller efficiency. Common soft faults in chillers are refrigerant leakage and condenser fouling. In this study, we will be only focusing on the occurrence of soft faults at it is more difficult to be detected and affects the system efficiency over a period of time.

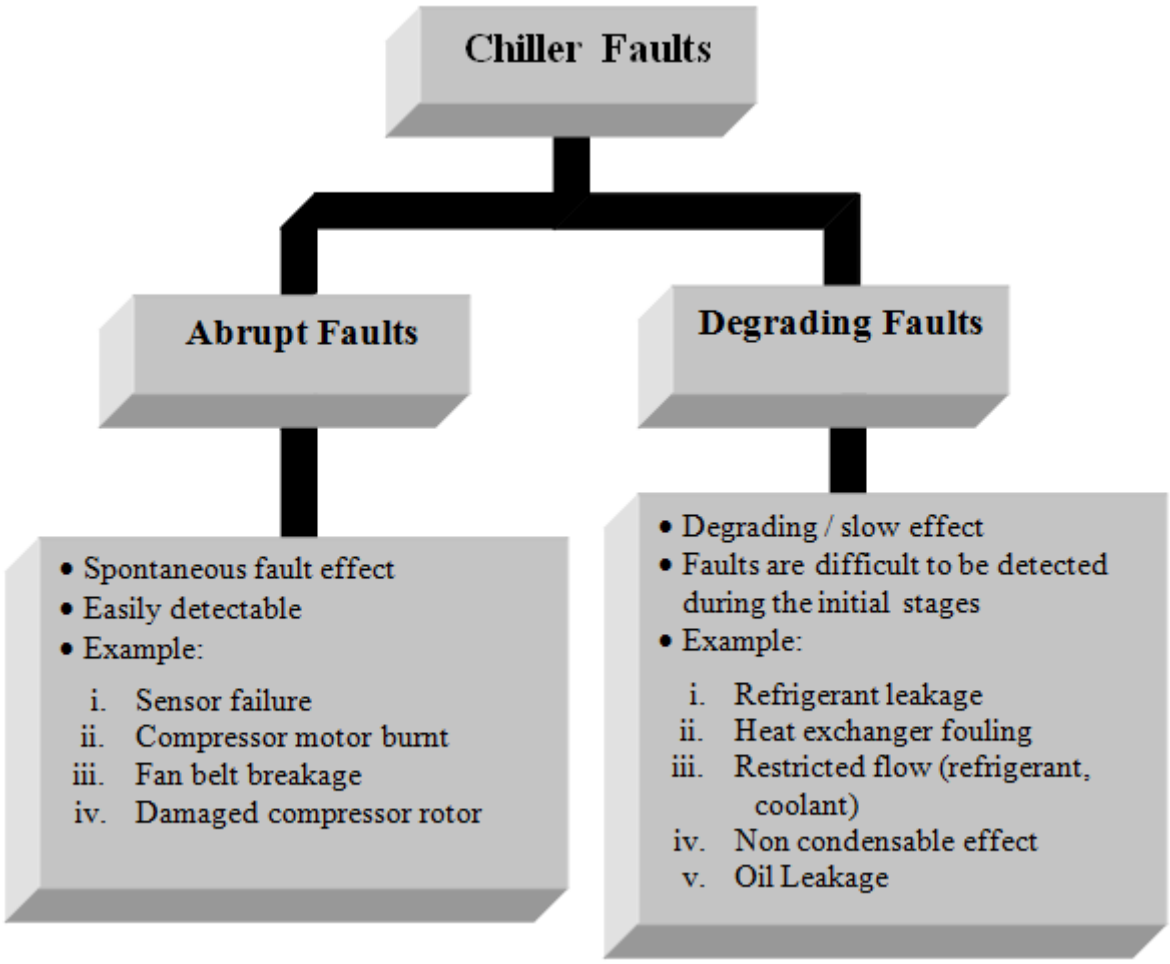

Figure 1.1: Common types of faults in chiller

It is also very important to comprehend the founding principles of fault detection and diagnostic before embarking on a FDD study pertaining to soft faults in vapor compression chillers. In general, FDD encompasses two major procedures:-

a. Fault detection – Physical model or Black box model (which represents a fault-free chiller) is used to compare the measured data from the online chiller. Details of these fault free models are explained in Table 1.1. For instance, COP computed using a physical or black box model is compared with the COP measured from the online chiller. If the percentage of deviation or residual between the two values is well above a predetermined threshold,

then the application will execute the diagnosis mode. This is shown in Figure 1.2.

b. Diagnosis – In this mode, the application will perform a diagnosis to determine root cause of the fault.

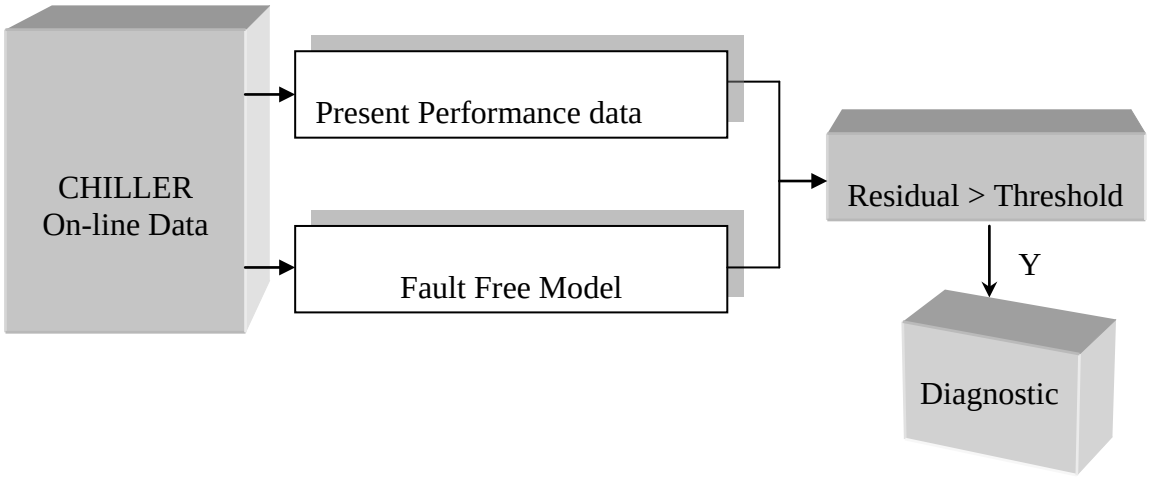

Figure 1.2 : Schematic diagram of FDD application

Table 1.1: Comparison between physical and black box models

Physical Models	**Black Box Models**
Incorporates laws of physics and represents a meaningful approach	Does not require the physical knowledge of the system
Less training data are required	Model largely relies on the training data
Requires plenty of effort in model development	Requires less modelling effort
Can be easily adapted to an another chiller	Custom-made approach.
Example: ASHRAE Toolkit Model Gordon-NG Universal Model	Example: Neural Networks, Polynomial Curve Fitting

1.2 Research Objective

Fault detection and diagnostic application play a vital role in ensuring optimum chiller operations. With a reliable monitoring system, developing soft fault can be detected and diagnosed at earlier stages. This study primarily focuses on developing a trustworthy FDD technique for vapor compression chiller. The specific objectives of this study are summarized as follows:-

i) Construction of Scroll Chiller Test Facility

The construction of the scroll test facility is one of the main tasks of this study. The test facility is developed with the aim of simulating artificial building loads by having two separate mixing chambers namely Cold Chamber and Hot Chamber. These chambers served the evaporator and condensers respectively. The required mixing rate and supply temperatures for the heat exchangers are achieved by modulating the bypass valves which are precisely controlled by self developed PID controllers. Comprehensive details of the experimental set up were covered in chapter 3 of this thesis.

ii) Development of Thermodynamic Fault-Free Model

Five thermodynamic parameters namely, (i) suction superheat temperature (ii) condenser approach temperature (iii) condenser sub-cooling (iv) overall condenser heat transfer coefficient and (v) condenser entropy generation are identified to build the fault-free models associated to the soft faults investigated in this thesis. These parameters are then regressed using simple linear regression technique to obtain the

fault free models. The development of these fault-free models are clearly described in the chapter 4.

iii) Development of Fault Detection Model

As soft faults develop gradually over a period of time, it is imperative to develop a fault detection technique that is capable of detecting minute yet persistent drift at the earliest possible time. We have used the CUSUM technique as the fault detection tool. The modelling of the CUSUM technique is presented in Chapter 3 while the efficacy of this method was demonstrated in the chapter 5.

iv) Development of Fault diagnosis Model

Once a fault has been successfully detected, a diagnostic routine is activated to determine the root cause of the fault. In this study, we have developed the diagnostic routine using the Bayes probability theorem. The diagnostic is accomplished by computing the prior probabilities and likelihood. Further details on this simple yet powerful diagnostic technique can be obtained in the chapter 5.

v) Evaluation of the proposed CUSUM-Bayes on external chiller

Besides the evaluation of the scroll chiller, the developed CUSUM-Bayes methodology is also verified against faulty data sets obtained from an external 90 R-ton centrifugal chiller. The diagnostic results using the proposed methodology are reported in the chapter 5.

1.3 Research Scope

The main scope of this research is described as follows:

a) Only vapor compression chillers are considered.

b) The developed FDD technique is only valid for steady state data.

c) Faults related to control, sensors and instrumentations are not considered.

1.4 Research Contribution

The main contribution of this thesis work is to develop a simple yet reliable FDD model that is capable of diagnosing soft faults in chillers. The fault detection analysis using the CUSUM technique is very suitable for slow drift detection. We have proposed tuning techniques and identified fault detection parameters that are suitable for CUSUM modelling. The proposal of multiple thresholds in detecting faults is also important in avoiding false alarms. Apart from that, we have also proposed lag analyses that include the lag effect between the fault detection parameters. These analyses are vital in determining the inputs required for diagnostic analysis. The diagnostic analysis using Bayes probability is also specifically tuned for soft faults using the prior probabilities and likelihoods. In short, the advantages of the proposed technique over the existing FDD models are as follows:-

a. Earliest possible fault detection using the CUSUM method

b. Multiple thresholds to improve fault detection

c. Lag analyses to improve the Bayes Diagnosis

d. Selection of prior probabilities and likelihood parameters that are suitable for soft faults

e. Capable of performing FDD analysis at real time

Chapter 2: Literature Review on Fault Detection and Diagnostics Applications in Chillers

Introduction

This chapter presents a comprehensive literature review on the applications of chiller Fault Detection and Diagnostics (FDD). There are two main sections in this chapter namely: (i) Chiller Modelling and (ii) FDD methodology and implementation. In the first part, selected publications on the steady state modelling of chillers were reviewed. These reviews comprised both the physical and black box modelling. These modelling techniques are particularly important to generate that fault-free models that can be used to determine the residual or deviations of a particular fault detection parameter. The second part of this chapter specifically focused on the several FDD methodologies studied by various researchers. This section provides a good overview on the implementation of assorted FDD techniques on vapor compression chillers.

2.1 Steady state Chiller Modelling

There are several ways that can be adopted to model vapor compression chillers. Among the common techniques are (i) physical and (ii) black box modelling. Physical modelling or also commonly known as white box modelling utilized laws of physics to characterize the chiller. Among the common white box modelling are ASHRAE HVAC Toolkit developed by ASHRAE TC 4.7 and the Gordon and Ng Universal chiller model. A detailed review will be provided on the Gordon and Ng Universal Chiller model. The ability

of this particular model to physically characterise the steady state condition of the chiller system based on evaporator and condenser thermal resistances and especially entropy generation leads to utilization of such thermodynamic parameters for the purpose of fault detection and diagnostics.

The first version of the Gordon and Ng Universal Chiller model was developed in 1993 exclusively for modelling reciprocating chillers. The proposed steady state model was derived from the first and second laws of thermodynamics to capture some of the governing irreversibilities of chillers such as finite rate heat transfer from the heat exchangers, heat leaks, fluid friction losses, throttling losses, de-superheating and others. The model was then evaluated by regressing experimental data acquired from a laboratory reciprocating chiller to obtain three key coefficients, A_0, A_1 andA_2. The coefficients were then used to predict the system performance and it was reported that the model was capable of replicating the actual performance data to within the experimental uncertainty (Gordon and Ng (1995)).

However, the regressed coefficients (A_0, A_1 andA_2) are not usually appreciated from the thermodynamic point of view as they carry no physical information of the system and are merely recognized as arbitrary numerical values. This ignited the search for an advanced model that can yield “thermodynamically meaningful” regressed coefficients which lead to more accurate and meaningful predictions. The second generation of the Gordon and Ng Universal Chiller (hereinafter named STM), which is much superior to its predecessor due to its physically meaningful regression characteristics, was established two years later. The authors ingenuously substituted the regressed coefficients (A_0, A_1 and A_2) with thermodynamic parameters namely, Total Thermal Resistance (R), Equivalent Heat Leak ($Q_{Leak,\ Eqv}$) and Internal Entropy Generation ($\dot{S}_{gen,Total}$). The revised model is expressed as follows:-

$$\frac{T_{evap}^{in}}{T_{cond}^{in}}\left(1+\frac{1}{COP}\right)-1=\frac{T_{evap}^{in}}{Q_{evap}}\Delta\dot{S}_{\text{gen,Total}}+Q_{leak,eqv}\frac{(T_{cond}^{in}-T_{evap}^{in})}{T_{cond}^{in}\times Q_{evap}}+\frac{R\times Q_{evap}}{T_{cond}^{in}}\left(1+\frac{1}{COP}\right)$$

In general, the thermodynamic model of a chiller system can be evaluated using data obtained from either intrusive measurements such as refrigerant temperatures and pressures or from non-intrusive measurements that require only water temperatures. Gordon and Ng (2000) emphasized that non-intrusive measurements are preferred due to their simplicity and accessibility. Using judiciously selected non-intrusive data, the STM model can be used to predict the system COP by regressing the three critical irreversibility parameters, R, $\Delta\dot{S}_{gen,Total}$, and $Q_{\text{Leak, Eqv}}$, using multiple regression analysis. As explained by Jiang and Reddy (2003), the regression process can be accomplished by using multiple linear regression technique. It has to be emphasized that regression analysis has to be performed correctly in order to retain the physical significance of the model. The following are some of useful guidelines that might prevent erroneous analysis:

a) The coefficients R and $\dot{S}_{gen,Total}$ are positive numerical parameters. These constraints are incorporated in the regression analysis in order to yield a meaningful prediction. Although non positive values might yield a better curve fitting, the prediction is said to be mathematically accurate but physically meaningless. For instance, regressing a negative value coefficient for internal entropy generation is unacceptable from a thermodynamics perspective.

b) The value of $Q_{\text{Leak, Eqv}}$ can be either positive or negative and is less significant compared to the R and ΔS_T parameters.

c) The STM has to be regressed without the inclusion of intercept. The inclusion of intercept yields accurate results but reduces the physical significance of STM (Gordon and Ng, 2000; Andersen and Reddy, 2001; Jiang and Reddy, 2003).

Several researchers have successfully evaluated the STM model for various cases of chiller modelling. Stylianou and Nikanpour (1996) employed the model in their FDD methodology while Wei and Reddy (2003) studied the internal and external predictive ability of STM model using data sets from 46 different types of chillers. Corcoran and Reddy (2003) concluded that STM model is capable of accurately predicting the complete chiller performance map with only four well chosen operating points. Sreedharan and Haves (2001) also reported on a fault detection comparison study using three different models namely (i) STM (ii) ASHRAE Toolkit model and (iii) DOE-2 toolkit. It was concluded that STM has the advantage of being linear in parameters that allow robust parameter estimation method.

Although the regressive approach of STM is capable of predicting reasonably accurate COP, its capabilities for fault detection is limited due to following reasons:

a) The regressed coefficient R is simply an arithmetic addition of evaporator and condenser thermal resistances. Consequently, the sources of faults due to deviation in R are unable to be localized to either the evaporator or the condenser. In short, only partial diagnosis is possible.

b) The regressed coefficients are obtained from different set points. These coefficients represent the whole group of data rather than individual points. Thus, FDD evaluation for a single data point is not possible for regressive approach. Apart from that, the processing time for fault detection by STM regressive approach is apparently longer as several data points are required for regression. In short, real time FDD is not possible.

c) Reddy (2006) asserted that STM is strictly applicable to steady-state chiller operation. The COP prediction of STM at transient conditions is not feasible since STM has been derived from the steady state conditions. The author also claimed that implementation of STM for continuous on-line performance monitoring needs to be further explored although STM works well with off line performance data.

The above mentioned limitations together with the prowess of physically meaningful characteristics of STM inspired me to develop a simple yet reliable FDD scheme.

Other reputed work on the chiller steady state modelling was reported by Browne and Bansal (1997). The proposed steady state model is valid for both hermetic and open drive centrifugal compressor. This unique model considered the real phenomenon like superheating and sub-cooling as well as capacity control using inlet guide vanes. NTU-effectiveness method is used for the modelling of both evaporator and condenser while isenthalphic expansion process is assumed across the throttling valves. Pressure drop in the refrigerant for the condenser and evaporator was assumed as 10% and 5%, of the respective saturation pressures. The proposed steady state model only required readily available data such as dimension of heat exchangers, compressor size and the coolant (cooling and chilled water) properties such as inlet, outlet temperatures and flow rates. The simulation strategy was clearly presented in a flow chart. The modelling result was found to be within 10% of the measured value when tested for three different chillers. Browne and Bansal (2001) also analyzed different modelling strategies for in-situ liquid chiller in 2001. Five different models that predict performance indicators such as cooling capacity, compressor power and condensing temperatures were investigated. The five models were (i) regression model (ii) physical steady state model (iii) physical dynamic model (iv) steady state neural network model and (v) dynamic neural networks. It was concluded that the proposed steady state

model that employed NTU-effectiveness approach was found to be within 5% of the measured data during the quasi steady and slow change chiller operations. However, the model was less effective during the compressor unloading and system shut-down where deviation as large as 20% could be observed.

Another researcher, Swider (2003) investigated various black box models that could be used to predict the Coefficient of Performance (COP) of vapor compression chillers. The models were built using various regression techniques such as simple linear regression, multivariate polynomial regression and bi-quadratic regression. Also investigated in his study were the STM model and 2 types of neural network models. The neural network models were generated using Multilayer Perceptron Layer (MLP) and Radial Basis Function (RBF) techniques respectively. Similar to most of the other steady state models, all the proposed models employed easily available independent variables such as cooling capacity and the inlet temperatures of the chilled and cooling water. The reported result indicated that the neural network models have higher prediction accuracy and generalization abilities compared to the other models. Swider claimed that black box models specifically RBF neural network model could be used to accurately predict the chiller performance if there are large training data available.

Grimmelius et al. (1999) reported on three state-of-the-art methods suitable for condition monitoring. The methods were (i) first principle physical model (ii) feature extraction and (iii) neural networks. These methods were validated against two engineering case studies related diesel engine crack shaft vibration monitoring and condition monitoring of a compression refrigeration plant. The research study revealed that all the methods were suitable for condition monitoring. The authors concluded that the combination of the above methods was more likely to yield the model for condition monitoring purposes.

2.2 FDD methodology and implementation

In this section various FDD techniques employed in chillers will be discussed. Important details on fault simulations and the implementation of the diagnostic scheme will be presented.

The publication of Grimmelius et al. (1995) on on-line failure diagnosis for compression refrigerant plant was among the highest cited FDD papers with respect to vapor compression chillers. This specific publication primarily focused on the (i) lay out of the studied chiller (ii) derivation of failure modes of chillers and (iii) the applied diagnostic methods. A total of 58 failure modes were identified where a cause-effect study was undertaken for each fault. Using the cause-effect analyses, the failure modes symptoms were captured using 20 variables that were easily measured or derived using only temperature, pressure and other simple electrical transducers. Some of the variables are as follows:- (i) suction pressure and temperature (ii) discharge pressure and temperature (iii) oil pressure, temperature and level (iv) crankcase pressure (v) electrical power consumption (vi) Sub-cooling (v) approach temperature (vi) sub-cooling and etc.

On the other hand, the fault-free model was predicted using regression technique which is one of the common black box methods. The independent variables for the regression models were the cooling and chilled water inlet temperatures as well as number of cylinders in operation. The chiller plant investigated in the study comprised three reciprocating compressors complete with water cooled evaporator and condenser as well as other standard accessories. The 270 kW reciprocating chiller used refrigerant R22 and designed for chilled water temperature between 6.5 to 12^{o}C. Rigorous testing were conducted with constant chilled and cooling water flow rates by varying the chilled water temperature from 4 to 14 ^{o}C while the cooling water temperature was varied between 24 and 32 ^{o}C. The data pre-

processing was achieved using geometric moving average technique with a forgetting factor 0.2. A deviation could be confirmed if the measured and regressed value differs more than the limiting threshold which was chosen with a confidence level of 99.7%. Upon detection, the diagnosis routine that employed fuzzy logic algorithm would be activated. The authors concluded that the proposed FDD system was capable of monitoring all normal operating conditions without any false alarms. The regressed models were also capable of yielding fairly good results where faults could be detected and diagnosed at early stage. However, the proposed methodology was not capable of transient analysis and the regressed model has no generalization capability if exposed to data that were not encountered during the regression.

Another widely read publication in Chiller FDD was by Stylianou and Nikanpour (1996); discussed on performance monitoring, fault detection and diagnosis of reciprocating chillers. This paper employed physical modelling, artificial intelligence and pattern recognition methodologies to complete their FDD scheme. The test unit consisted of a 5 R-ton two cylinder semi hermetic compressor complete with shell and tube condenser and evaporator. A total of 11 RTD's, four pressure transducers and two water flow meters were used for data logging purposes. The cooling water temperature was varied from 22 ^{o}C to 34 ^{o}C while the inlet chilled water temperature was varied from 10 ^{o}C to 15 ^{o}C. Five types of faults were investigated in this study, namely (i) Refrigerant leak (ii) Refrigerant flood back at start-up (iii) refrigerant line flow restriction (iv) reduction in the cooling water flow rate and (v) reduction in chilled water flow rate. The FDD routines were divided into three primary modules:- (i) Off cycle module (ii) start-up module and lastly (iii) steady module. The off-cycle module performed the diagnostics from the duration of shut down till start-up. It basically diagnosed the irregularities in the sensors prior to start-up using a first order model that approximates temperature decay. On the other hand, the start-up module was used to detect faults related to refrigerant flow control within 15 minutes from the start-up.

Transient features determined during the commissioning period were used as the based reference for fault detection during unsteady start-up period. Finally, the steady state module developed using Gordon and Universal chiller model was employed to detect and diagnose the faults. Linear regression models were used to generate fault free models. A fault pattern was proposed in their study. A fault would be detected and diagnosed if the residual between the predicted and the measured parameters were beyond the uncertainty band. The authors concluded that the proposed methodology required further modifications especially in the determination of the threshold that triggered the FDD scheme.

Castro (2002) published another study related to reciprocating chiller fault detection and diagnosis. The study was carried out a 12 R-ton air cooled chiller that used a constant speed two stage reciprocating compressor. The condenser was a single row finned tube heat exchanger with two parallel condensing sections that were cooled using two fans while the evaporator was a liquid-to-liquid shell and tube heat exchanger. Thermostatic expansion valve was used to achieve the throttling effect. Castro proposed a methodology named MATCH (model based assessment tool for chillers) to obtain values for the performance indicator required for fault detection and diagnosis. Five types of faults were studied in this study namely (i) Air side condenser fouling (ii) water-side evaporator fouling (iii) liquid line restriction (iv) refrigerant overcharge and (v) refrigerant undercharge. K-nearest neighbour classifier and K-nearest prototype classifier as well as rule-based fault diagnostic algorithms were used to complete the FDD scheme. A detailed explanation on the implementation of the K-nearest neighbour and prototype classifiers as fault detection tool was presented in the study. The author recommended the prototype classifier over the neighbour classifier as the former was less computation intensive. The rule based algorithm was developed from sets of "IF….. And Then…." rules. The proposed MATCH algorithm was able to detect and diagnose condenser fouling, refrigerant undercharge, overcharge at a fault level of 20% and

beyond. However, evaporator fouling and liquid restriction were only captured at 30% fault level and above.

Riemer et al. (2002) proposed the evaluation of FDD using time series analysis. It was explained that the time series is capable of revealing unexpected time varying trends in the data. These trends are the indication of the occurring fault. The authors clearly explained the underlying principle of time series where brief and concise explanations on the cross-correlation, auto-correlation, ARMA and ARIMA models were provided. The time series analysis was demonstrated using data obtained from centrifugal chillers. Parameters like coolant flow rates, coolant inlet and outlet temperatures, evaporator saturation temperature, condenser saturation temperature, compressor discharge temperature and electrical power consumption were monitored using the proposed methodology. It was concluded that ARIMA (3,0,0) was suitable for the chilled water flow rates. Although the technique presented in the paper provided a good overview and useful insight on the implementation of the time series in chiller FDD, the proposed methodologies still needed optimization to reliably detect and diagnose the faults.

Chen and Braun (2001) proposed a simple rule-based method for fault detection and diagnostics of package air conditioners. The proposed method has simpler rules and proved to be an inexpensive FDD method. The FDD scheme was performed on a 5 R-ton rooftop unit that operated using scroll compressor and thermostatic expansion valve. The steady state data required for FDD was obtained at various dry bulb temperatures and relative humidity of the inlet air and the ambient dry-bulb temperatures. Seven different types of faults related to air conditioners were studied where the fault simulation methods and severity level were clearly described. From experimental observation, eight types of performance indicators were specified to detect and diagnose the faults. One of the proposed FDD techniques was the

sensitivity ratio method. For a particular fault, the sensitivity ratio was defined as the ratio of residual of insensitive measurement over residual of the sensitive measurement. The residual was defined as the arithmetic difference between the measured and the predicted value of a performance indicator. The fault free model of a performance indicator was developed using a first order polynomial model using the return air dry bulb temperature and relative humidity as well as ambient dry bulb temperature as the independent variables. The threshold of a residual was fixed at 2^{o}F. Therefore, if the computed residual value for a performance indicator was less than 2^{o}F, then the residual was reset to a default value of 0.l ^{o}F. This default value signified that the particular indicator was not affected by the occurring fault. Using specific sets of sensitivity ratio, a particular fault can be successfully detected and diagnosed. The authors presented a list of sensitivity ratio diagnostic rules, which was sufficient to diagnose the faults investigated in their study. A flow chart was also provided to explain the sequential of the proposed FDD technique. Apart from the sensitivity ratio diagnostic rule, the author presented another simple rule base diagnostic methodology using only four types of measurements. The heuristic based rules were only applicable to steady state operating conditions. A table was provided to outline the nominal and fault range of the five selected measurements (e.g sub-cooling temperature, difference between condensing temperature and ambient temperature, temperature difference across the liquid line restriction valve and difference between the air dry-bulb temperature and evaporating temperature). The thresholds for the parameters were given in a range rather than an absolute value. The authors concluded that both the sensitivity ration and simple rule methods yielded similar performance.

Reuda, Tassou and Grace (2005) reported a FDD analysis for liquid chillers using neural networks. The paper was specifically focused on the fault related to refrigerant undercharge and overcharge. The test unit comprised 25 kW R22 reciprocating chiller with

shell and tube water cooled condenser, shell and tube direct expansion evaporator and thermostatic expansion valve. Complete details of the instrumentations were provided in their report. The proposed on-line FDD scheme was developed on a Java 2 platform and consisted of the following module:- (i) data acquisition (ii) fault-free performance prediction (iii) residual calculation (iv) steady state detection (v) condition diagnosis and (f) user interfacing. Ten performance indicators (such as coolant outlet temperatures and eight refrigerant measurements) were used in this study where the fault free prediction model for each parameter was obtained using neural networks. Steady state data obtained during the fault free conditions were used to train the Multi Layer Perceptron (MLP) neural networks. However, for fault related to undercharge and overcharge, only the fault free model of condenser refrigerant outlet temperature and discharge pressure were used. It was shown that the MLP networks were capable of predicting the two parameters with a high accuracy. Steady state detectors were deployed in the proposed technique to ensure that the diagnostic routine was only activated during the steady state periods. The detectors tracked the compressor pressure and the discharge temperature to verify the steady state periods. During the steady state period, the diagnostic module would be activated to identify the charge level of the system as low, normal or high. To achieve this classification, an expert system was designed to evaluate the charge level. The expert system consisted of three rules that specified the thresholds for each residual of condenser refrigerant outlet temperature and discharge pressure. The successful diagnostic rates of the proposed FDD technique were more than 95% when the system was simulated with various charge levels.

Kim and Kim (2005) reported on the FDD analysis of variable speed compression system. Four type of common chiller faults namely (i) compressor fault (ii) evaporator fault (iii) condenser fault and (iv) refrigerant leakage were artificially simulated in this study. The experimental set up consisted of open type two cylinder R22 reciprocating compressor

complete with concentric condenser and evaporator. The throttling effect was achieved using PID controlled electronic expansion valve. An inverter assembly was utilized to maintain the evaporator outlet temperature at 16.7 ± 0.1 ^{o}C. A compressor fault was simulated using a by-pass line that connects the discharge and the suction ports of the compressor. Condenser and evaporator faults were simulated by reducing the heat exchanger areas. Leakage was simulated by undercharging the system. The operating set points for the analysis were obtained at three different cooling capacities in order to capture the part and full load performances of the system. The proposed FDD system in this report comprised two primary components, namely (i) Constant speed fault classification and (ii) variable speed classification. A routine would be executed to evaluate the speed of the compressor and the evaporator outlet temperature. If the evaporator outlet temperature did not meet the 16.7 ± 0.1 ^{o}C set point and the compressor was operated at full speed, then the constant speed fault classification would be triggered. Otherwise, the variable speed fault classifier was used if there was discrepancy in the measured and predicted compressor speed. Upon the detection of the fault, the diagnostic routine would be triggered where a set of performance indicators almost similar to previous studies were used to identify the faults. The authors concluded that COP degradation due to faults in the variable speed compressors was much more severe compared to that arising from fixed speed compressors.

Esbiri, Torrela and Cabello (2005) proposed an on-line refrigerant leakage detection using Kalman filter and dynamic threshold techniques. The technique was successfully applied in detecting faults related to leakage during the transient and steady state conditions. Compressor suction pressure was used as the performance indicator for the leakage detection and the fault free model of this parameter was developed using the Kalman Filter algorithm. Then, the residual between the measured and the predicted values was computed using the quadratic error model. The residual was later used to determine the dynamic threshold which

was particularly useful for transient fault detection. Details on the instrumentation used were clearly outlined in their report. From the experimental results, it can be seen that the proposed technique exhibited swift responses in detecting the leakage during both the steady and transient conditions. The proposed technique also worked well when being exposed to false alarm. The false alarm was artificially simulated by a sudden change in the cooling load. It is concluded that tuning of the forgetting factor used in Kaman Filter plays a critical role in developing a robust leakage detection tool that is insusceptible to false alarms resulting from cooling load variations. The forgetting factor is important in adjusting the memory of the model. The authors commented that a low forgetting factor will have less influenced from the previous data history, thus being too sensitive to the present conditions.

Cui and Wang (2005) demonstrated a model-based online fault detection and diagnosis strategy for centrifugal chillers. The FDD scheme employed six different performance indicators namely (i) log mean temperature difference (LMTD) of condenser (ii) LMTD of evaporator (iii) refrigerant mass flow rate (iv) compressor isentropic efficiency (v) drive motor efficiency and COP. Using cooling load, chilled water supply temperature and entering condensing water as independent variables, the fault free models for the performance indicators were built via polynomial regression method. An online threshold estimation scheme was developed on the basis of evaluating the modeling errors and the propagation of each measurement error through the mathematical formulations of the performance indexes, at a specific operating condition. 95% confidence level was used in the threshold determination. Upon detection of the fault, the diagnostic classifier would be used to determine the cause of the fault. The fault classifier was built using the thermo physical principle of chiller. The proposed FDD method was tested against a 1500 R-ton field centrifugal chiller and a lab based 90 R-ton centrifugal chiller. The authors reported that the occurrence of fouling was successfully diagnosed on the field chiller after 21 days of

commissioning. Significant deviations in the condenser LMTD, refrigerant mass flow rate and COP led to this classification. As for the lab based 90 R-ton chiller, five types of fault were analyzed. For fault related to reduction in evaporator water flow rate, the proposed model was able to diagnose fault from flow reduction of 30% and onwards. For leakage, the first diagnostic was made at the second severity level (20% leakage) while fouling and excess oil were diagnosed at the third and fourth level of severity respectively.

Agami (2007) has evaluated a simple model based automated FDD method suitable for large chillers. The proposed methodology used commonly available measurements and allowed the tuning of specific threshold to obtain a good balance between robustness and sensitivity. Details of the laboratory 90 R-ton centrifugal chiller test rig and test data used in this report can be obtained from research project report completed by Comstock and Braun (1999). The proposed FDD scheme was only applicable to process related fault such as fouling, leakage, overcharge and other. Faults related to control, instrumentations and electrical was not investigated in this report. Apart from that, the scheme was only valid for steady state processes and employed a quasi real-time approach. Of the total eight faults simulated by Comstack and Braun, only six were investigated by Agami. The faults are (i) reduced condenser water flow (ii) reduced evaporator water flow (iii) refrigerant leak (iv) refrigerant overcharge (v) condenser fouling and presence of non-condensable. Each fault described above was simulated at four different severity levels (e.g 10%, 20%, 30% and 40% from the nominal condition). All test data for both nominal and faulty conditions were obtained by varying the cooling load, condenser inlet water temperature and evaporator outlet water temperature. A total of 27 different operating steady state points were obtained by varying the three parameters for each test run. The condenser and evaporator water flow rates were fixed at the rated conditions for all the test runs except during the simulation of flow rates reductions. 15 characteristics features were discussed in this study. However, only five

most influential parameters were considered for FDD purposes. The selected five characteristic functions were (i) evaporator water temperature difference (ii) condenser water temperature difference (iii) condenser sub-cooling temperature (iv) condenser approach temperature and finally (v) overall condenser heat transfer coefficient. A fault diagnosis table were established to diagnose the six faults mentioned earlier with respect to the five characteristic functions. Fault detection was performed using the student t criterion ($t - statistic = \frac{(Y_{measured,i} - Y_{predicted,i})}{RMSE}$. Probability of a fault to occur exceeds three standard deviation of student t distribution if the t value is bigger than 3. As the computation of the student t requires the difference between the predicted and measured value of the characteristic function, fault free models were developed for each function. The models were generated using regression technique with cooling load as the only independent variable. However, only mean value was used as fault free model for overall condenser heat loss coefficient. The output of the FDD result were shown for two t thresholds, that is t = 3 and t = 4 respectively. Bigger threshold minimizes false alarms but might suffer from low sensitivity (missed alarm) where faults might only be detected at a later stage. It was demonstrated in the report that when the threshold was raised from 3 to 4 for fouling analysis, the number of detected faulty points reduced significantly. These missed alarms can lead to poor FDD capabilities. The author stated that the missed alarms can be offset using the proposed impact and frequency ratings. The author concluded that apart from process faults, a complete FDD scheme also needs to consider faults related to control, electrical, vibration and instrumentations.

2.3 Summary

Based on the extensive literature review carried out in this thesis work, it can be summarized that there is still a niche in developing a FDD model that is simple and reliable. Following are the some of the limitation identified in the existing FDD models:-

(i) The need for multiple thresholds to track the shift in the fault gradient

(ii) Lack of study on the time lag response between fault detection parameters

(iii) Development of a FDD model that is feasible for real time operation (not a quasi static model)

For soft faults, especially refrigerant leakage and condenser fouling, it is important to develop a model that is capable of detecting these faults at earliest possible time. As soft faults gradually increases over the time, a statistical method that is specifically built to detect minute deviation is required. Cumulative Sum (CUSUM) is one of the general statistical methods that are suitable for minute and gradual detection. The tunings of the general CUSUM to detect these faults are discussed in Chapter 3. Also discussed in the next chapter are the selection of the fault detection parameters and the development of the diagnostic model using Bayes probability.

Chapter 3: Vapor Compression (VC) Chiller Theories and Fault Detection and Diagnosis (FDD) Statistical Framework

Introduction

This chapter primarily focuses on two topics: - (i) Thermodynamics of vapour compression (VC) chiller and (ii) fault detection and diagnostic (FDD) statistical framework. The thermodynamic analysis describes the general aspects of irreversibilities of vapour-compression cycle and the derivation of entropy generation for key components of a VC chiller. Also encompassed in this section is a brief discussion on several established fault detection parameters such as the heat exchanger overall heat transfer coefficients, heat exchanger approach temperatures, suction superheat, condenser sub-cooling and other parameters associated to FDD of chillers. In addition, this chapter also emphasizes two statistical frameworks that are applicable to fault detection and diagnostics of chillers, namely, the (i) Cumulative Sum (CUSUM) approach and (ii) Bayes Theorem. The former can be effectively utilized as a fault detection tool while the Bayes probability theories prove to be one of the best tools for diagnostic purposes.

3.1 Thermodynamics of VC Chillers

Vapor compression chillers are widely used in the air conditioning and refrigeration industries. For VC chillers, the driving force for refrigeration is mechanically achieved using compressors. The four primary components of a standard VC chiller are: - (i) evaporator, (ii) compressor, (iii) condenser and (iv) expansion valve. The refrigerating effect is obtained by

absorbing heat from refrigerated space by the low quality, defined here as the ratio of vapour mass to the total mass, refrigerant in the evaporator. Consequently, the refrigerant boils off and enters the compressor suction as a superheated vapour where $T_{evap,out}$ is greater than T_{sat} corresponding to the evaporator pressure. Within the compressor, the refrigerant vapor is mechanically compressed and exits at a much higher pressure and temperature, i.e., higher enthalpy. The discharged vapor is channelled into a condenser where it is first de-superheated, condensed and eventually sub-cooled by rejecting heat to the ambient air or coolant. The high pressure sub-cooled liquid refrigerant, emanating from the condenser, finally passes through an expansion valve or a capillary tube. The refrigerant experiences a Joule-Thompson effect, i.e., a reduction in pressure and temperature due to the restrictions in the valve and re-enters the evaporator as low quality mixture to complete the refrigeration cycle. The schematic of a vapor compression chiller is shown in Figure 3.1.

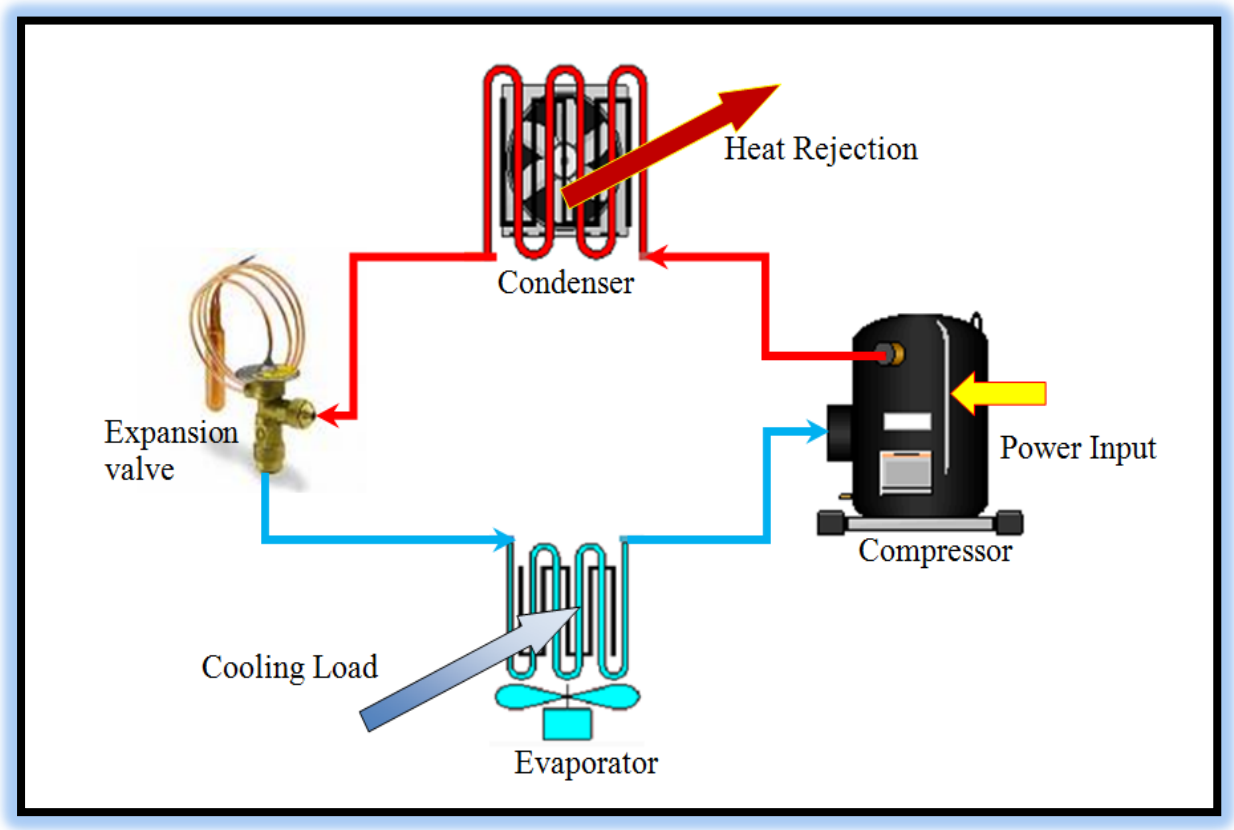

Figure 3.1: Key components of VC chiller

In contrast to the ideal vapor compression cycle that operates isothermally and isentropically, actual vapor compression suffers from several irreversibilities that are mainly governed by fluid friction (pressure drop), finite rate heat transfer and heat leaks to and from the surroundings. Pressure drops at the condenser and the evaporator as well as non-isentropic compression and expansion by the compressor and the expansion valve contribute to entropy generation in a VC system. The increase in entropy generation is further amplified during a faulty condition. In short, entropy generation can be employed as a fault detection tool.

3.1.1 First Law of Thermodynamics for a Control Volume

Using a control volume approach, the total internal energy per unit mass can be written as (Saad, 1993):-

$$\frac{\partial}{\partial t}\int_{cv} e\rho dV = \frac{dE}{dt} + \int_{cs} e(\rho \boldsymbol{V}.d\boldsymbol{A}) \tag{3.1}$$

where $\frac{dE}{dt}$ is the rate of energy change which is expressed as

$$\frac{dE}{dt} = \frac{\delta Q}{dt} + \frac{\delta W_{sys}}{dt}; \tag{3.2}$$

and W_{sys} is the work done and flow work.

From Equations (3.1) and (3.2), the First Law of Thermodynamics for a control volume can be expressed as:-

$$\frac{\delta Q}{dt} + \frac{\delta W}{dt} + \int_{cs}\left(h + \frac{V^2}{2} + gz\right)(\rho \boldsymbol{V}.d\boldsymbol{A}) = \frac{\partial}{\partial \mathrm{t}}\int_{\mathrm{cv}} e\rho\, dV \tag{3.3}$$

At steady state condition, Equation 3.3 reduces to

$$\dot{Q}_{in} + \dot{W}_{in} + \sum \dot{m}_{in}\theta_{in} = \dot{Q}_{out} + \dot{W}_{out} + \sum \dot{m}_{out}\theta_{out} \quad ; \ \theta = h + \frac{V^2}{2} + gz \qquad (3.4)$$

3.1.2 Second Law of Thermodynamics for a Control Volume

For a control volume, the total change of entropy, dS' during an interval of time can be expressed as:

$$dS' = dS + S_{in} - S_{out} \qquad (3.5)$$

The entropy change for a fix mass system, dS which is due to heat transfer, is expressed as:

$$dS \geq \frac{\delta Q}{T} \qquad (3.6)$$

Thus,

$$dS' \geq \frac{\delta Q}{T} + S_{in} - S_{out} \qquad (3.7)$$

where S_{in} and S_{out} are the respective positive inflow and negative outflow entropy.

By expressing the mass of control volume in terms of density and volume and the mass flow across the control surface in terms of density, velocity and area, Equation 3.7 can be redefined as:

$$\frac{\partial}{\partial \mathrm{t}} \int_{cv} s\rho \, dV \geq \frac{1}{T}\frac{\delta Q}{dt} + \int_{cs} s(\rho \boldsymbol{V}.d\boldsymbol{A}) \qquad (3.8)$$

At steady state condition, this can be simplified as:

$$\frac{1}{T}\frac{\delta Q}{dt} + \int_{cs} s(\rho \boldsymbol{V}.d\boldsymbol{A}) \leq 0 \qquad (3.9)$$

In a much simpler form, entropy of a system can be also written as:

$$\sum \frac{Q_k}{T_k} + \sum m_{in} s_{in} - \sum m_{out} s_{out} \leq \Delta S_{cv} \tag{3.10}$$

where T_k is the boundary temperature of the system and its surroundings. The inequality sign of this equation proves that entropy transfer due mass flow and heat transfer is always less than the entropy change in the control volume. This confirms the generation of entropy (due to the presence of irreversibilities). Therefore, the entropy generation, S_{gen} of a system during a steady state condition can be expressed as:

$$S_{gen} = \Delta S_{cv} - \left[\sum \frac{Q_k}{T_k} + \sum m_{in} s_{in} - \sum m_{out} s_{out}\right] \tag{3.11}$$

This entropy balance equation claims that the entropy change within a control volume is equivalent to the sum of net entropy transfer into the control volume (entropy due to heat and mass flow) and entropy generated within the control volume boundaries as a result of irreversibilities. During steady state, where $\Delta S_{cv} = 0$, the entropy generation rate can be formulated as following:-

$$\dot{S}_{gen} = \sum \dot{m}_{out} s_{out} - \sum \dot{m}_{in} s_{in} - \sum \frac{\dot{Q}_k}{T_k} \tag{3.12}$$

3.1.3 Entropy Generation and Lost Work

The general heat and entropy balance of an open system can be summarized as following:-

First Law:

$$\frac{dE}{dt} = \sum_{i=1}^{n} \dot{Q}_i + \dot{Q}_{ambient} - \dot{W} + \sum_{in} \dot{m}\, h^o - \sum_{out} \dot{m}\, h^o \qquad (3.13a)$$

where $h^o = h(P,T) + \frac{V^2}{2} + gz$

The entropy balance of a general system can be summarized as following

$$\dot{S}_{gen} = \frac{ds}{dt} - \sum_{i=1}^{n} \frac{\dot{Q}_i}{T_i} - \frac{\dot{Q}_{ambient}}{T_{ambient}} - \sum_{in} \dot{m}\, s(P,T) + \sum_{out} \dot{m}\, s\,(P,T) \qquad (3.13b)$$

In both equations, the ambient reservoir is separated from the other fixed reservoirs.

Equation 3.13b can be also rearranged as following:-

$$T_{ambient}\dot{S}_{gen} = T_{ambient}\frac{ds}{dt} - \sum_{i=1}^{n}\left(\frac{T_{ambient}}{T_i}\dot{Q}_i\right) - \dot{Q}_{ambient} - T_{ambient}\sum_{in}\dot{m}\, s(P,T) + T_{ambient}\sum_{out}\dot{m}\, s\,(P,T) \qquad (3.13c)$$

By adding 3.13a and 3.13c

$$\frac{dE}{dt} + T_{ambient}\dot{S}_{gen} = T_{ambient}\frac{ds}{dt} + \sum_{i=1}^{n}\dot{Q}_i - \sum_{i=1}^{n}\left(\frac{T_{ambient}}{T_i}\dot{Q}_i\right) + \sum_{in}\dot{m}\, h^o - T_{ambient}\sum_{in}\dot{m}\, s(P,T) - \sum_{out}\dot{m}\, h^o + T_{ambient}\sum_{out}\dot{m}\, s\,(P,T) - \dot{W} \qquad (3.13d)$$

Further simplification leads to:

$$\dot{W}_{open} = -\frac{d}{dt}(E - T_{ambient}s) + \sum_{i=1}^{n} \dot{Q}_i \left(1 - \frac{T_{ambient}}{T_i}\right)) + \sum_{in} \dot{m}\,(h^o - T_{ambient}s(P,T)) - \sum_{out} \dot{m}\,(h^o - T_{ambient}s(P,T)) - T_{ambient}\dot{S}_{gen} \quad (3.13e)$$

Equation 3.13e is the general expression for work done of an open system.

As for a closed system, Equation 3.13e is reduced to

$$\dot{W}_{close} = -\frac{d}{dt}(E - T_{ambient}s) + \sum_{i=1}^{n} \dot{Q}_i \left(1 - \frac{T_{ambient}}{T_i}\right)) - T_{ambient}\dot{S}_{gen} \quad (3.13f)$$

These equations can be used to obtain the maximum or reversible work of the system by setting $\dot{S}_{gen} = 0$. There is no possibility for the work to be more than the reversible work as $\dot{S}_{gen}$ cannot be negative in value. Therefore the reversible work, $\dot{W}_{reversible}$ of an open system can be expressed as:-

$$\dot{W}_{reverse\ open} = -\frac{d}{dt}(E - T_{ambient}s) + \sum_{i=1}^{n} \dot{Q}_i \left(1 - \frac{T_{ambient}}{T_i}\right)) + \sum_{in} \dot{m}\,(h^o - T_{ambient}s(P,T)) - \sum_{out} \dot{m}\,(h^o - T_{ambient}s(P,T) \quad (3.13g)$$

As for the close system, the reversible work is

$$\dot{W}_{reverse\ close} = -\frac{d}{dt}(E - T_{ambient}s) + \sum_{i=1}^{n} \dot{Q}_i \left(1 - \frac{T_{ambient}}{T_i}\right)) \quad (3.13h)$$

The actual work can be written as following;-

$$\dot{W}_{reversible} - \dot{W} = T_{ambient}\,\dot{S}_{gen} = \dot{W}_{Lost\ work}$$

$$\dot{W} = \dot{W}_{reversible} - \dot{W}_{Lost\ work} \quad (3.13i)$$

The general expression derived in Equation 3.13e is applied to the chiller system to evaluate the lost work and the entropy generation.

Figure 3.2 shows the sources of entropy generation in the chiller that stem from mass flow work and heat transfer from three main reservoirs, K1, K2, and K3. Reservoir K1 that operates at chilled water outlet temperature $T_{C,outlet}$ is associated with cooling load transfer from water to the refrigerant. On the other hand, the thermal reservoir, K2 receives heat rejected during condensation and operates at the cooling water inlet temperature, $T_{H,inlet}$. The last reservoir, K3 operates at ambient temperature and associated to both ambient positive and negative heat leaks. Using the concept of extended boundary, the reservoir temperatures are assumed as the boundary temperatures of the heat transfer processes. Figure 3.2 can be used to explain the entropy generation in each chiller component as well as the entire chiller system. For component analysis (e.g condenser, evaporator and etc), an open system approach is used while for the entire chiller, a close system analysis is applied.

Close System Analysis

For a closed system of a chiller during steady state, Equation 3.13f reduces to the following when the flow work term is reduced:-

$$\dot{W}_{close,steady} = \sum_{i=1}^{n} \dot{Q}_i \left(1 - \frac{T_{ambient}}{T_i}\right) - T_{ambient}\dot{S}_{gen} \qquad (3.13j)$$

$$\dot{W}_{close,steady} = \dot{Q}_{Evap}\left(1 - \frac{T_{ambient}}{T_{C,outlet}}\right) + \dot{Q}_{Cond}\left(1 - \frac{T_{ambient}}{T_{H,inlet}}\right) + \dot{Q}_{Leak}\left(1 - \frac{T_{ambient}}{T_{ambient}}\right) - T_{ambient}\dot{S}_{gen} \qquad (3.13k)$$

This reduces to

$$\dot{W}_{close,steady} = \dot{Q}_{Evap}\left(1 - \frac{T_{ambient}}{T_{C,outlet}}\right) + \dot{Q}_{Cond}\left(1 - \frac{T_{ambient}}{T_{H,inlet}}\right) - T_{ambient}\dot{S}_{gen} \quad (3.13l)$$

As outlined in Equation 3.13h, reversible work of a close steady system of chiller can be obtained when the entropy generation is zero. Thus,

$$\dot{W}_{reversible,closed\ steady} = \dot{Q}_{Evap}\left(1 - \frac{T_{ambient}}{T_{C,outlet}}\right) + \dot{Q}_{Cond}\left(1 - \frac{T_{ambient}}{T_{H,inlet}}\right) \quad (3.13m)$$

Entropy generation of the chiller (close system) during steady state can be computed directly from Equation 3.12 by dropping the flow work term. Thus, Equation 3.12 reduces to:-

$$\dot{S}_{gen,closed\ system} = -\frac{\dot{Q}_{Cond}}{T_{H,inlet}} - \frac{\dot{Q}_{Evap}}{T_{C,outlet}} - \frac{\dot{Q}_{Leak}}{T_{ambient}} \quad (3.13n)$$

The work of the close system can be computed using Equation 3.13l.

Open System Analysis

Open system analysis can be used to study sub-components of chiller namely, condenser and evaporator and etc. For instance, evaporator reversible and lost work can be obtained as follows:-

From Equation 3.13g, the reversible work during steady state can be computed as following

$$\dot{W}_{reversible\ open\ steady} = \dot{Q}_{Evap}\left(1 - \frac{T_{ambient}}{T_{C,outlet}}\right) + \dot{m}_{ref}(h_{in} - h_{out}) + \dot{m}_{ref}(s_{out} - s_{in})T_{ambient} \quad (3.13o)$$

Since $\dot{Q}_{evap} = \dot{m}_{ref}(h_{out} - h_{in})$

Thus

$$\dot{W}_{reversible\ open\ steady} = \dot{Q}_{Evap}\left(1 - \frac{T_{ambient}}{T_{C,outlet}}\right) - \dot{Q}_{Evap} + \dot{m}_{ref}(s_{out} - s_{in})T_{ambient} \quad (3.13p)$$

By simplifying

$$\dot{W}_{reversible\ open\ steady} = T_{ambient}\left[\dot{m}_{ref}(s_{out} - s_{in}) - \frac{\dot{Q}_{Evap}}{T_{C,outlet}}\right] \quad (3.13q)$$

Entropy generation of the evaporator during steady state can be obtained from Equation 3.12

$$\dot{S}_{gen} = \dot{m}_{ref}(s_{out} - s_{in}) - \frac{\dot{Q}_{Evap}}{T_{C,outlet}} \quad (3.13r)$$

For evaporator, it can be proved that the work produced is zero

$$\dot{W} = \dot{W}_{reversible} - \dot{W}_{Lost\ work} = \dot{W}_{reversible} - T_{ambient}\dot{S}_{gen}$$

$$\dot{W} = T_{ambient}\left[\dot{m}_{ref}(s_{out} - s_{in}) - \frac{\dot{Q}_{Evap}}{T_{C,outlet}}\right] - T_{ambient}\left[\dot{m}_{ref}(s_{out} - s_{in}) - \frac{\dot{Q}_{Evap}}{T_{C,outlet}}\right] \quad (3.13s)$$

$$\dot{W} = 0 \quad (3.13t)$$

Similar analysis for the other sub-components can be accomplished using the general expression Equation 3.13e and 3.12.

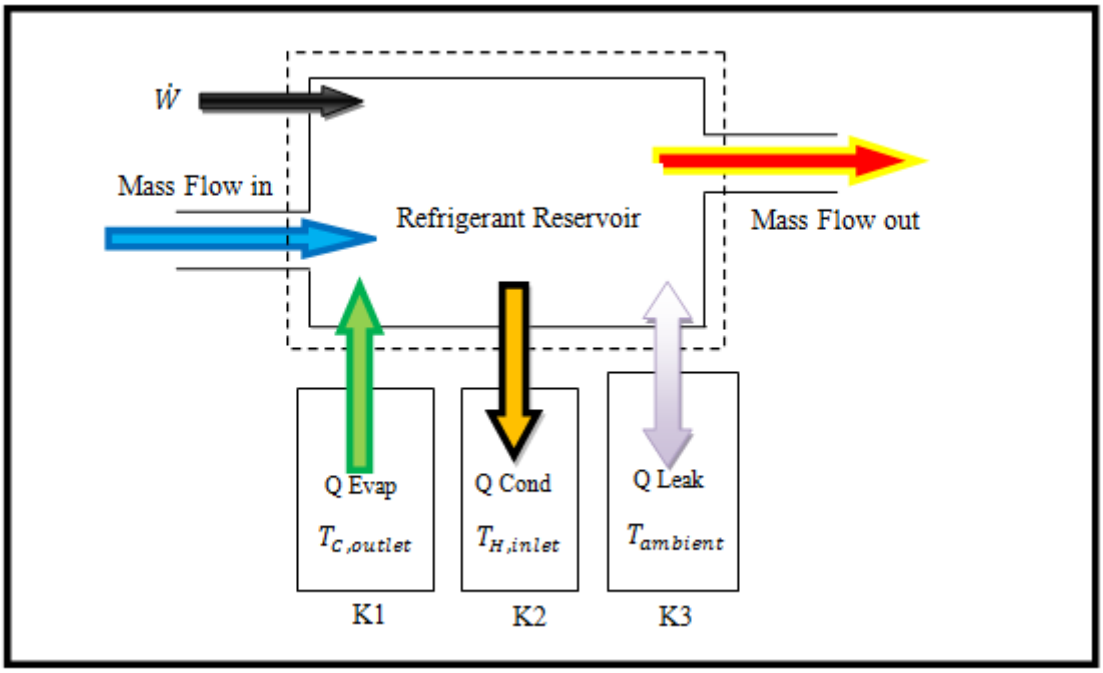

Figure 3.2: Sources of entropy generations in a chiller

3.1.4 Entropy Generation (Refrigerant system as a control volume) in Vapor Compression Chillers

For the calculation of entropy generation for each key component of a VC chiller at steady state condition, the refrigerant mass flow rate is assumed to be constant through out the cycle. Equations 3.4 and 3.12 are used to obtain the irreversibilities for each chiller component shown in Figure 3.3.

Evaporator:

1st law Energy Balance:

$$\dot{Q}_{evap}\,(kW) = \dot{Q}_{71} = \dot{m}_{ref}(h_1 - h_7) \tag{3.14}$$

2nd law Entropy Balance:

$$\dot{S}_{gen,71} = \left(\frac{kW}{K}\right) = \dot{m}_{ref}(s_1 - s_7) - \frac{\dot{Q}_{evap}}{T_R} \quad ; T_R = Refrigerated\ space\ area \qquad (3.15)$$

For water-cooled evaporator, T_R is taken as the chilled water outlet temperature, $T_{C,outlet}$ using the extended boundary concept. Since the chilled water outlet temperature is used as the chiller operating set point, it is reasonable to extend the system boundary until the set point temperature.

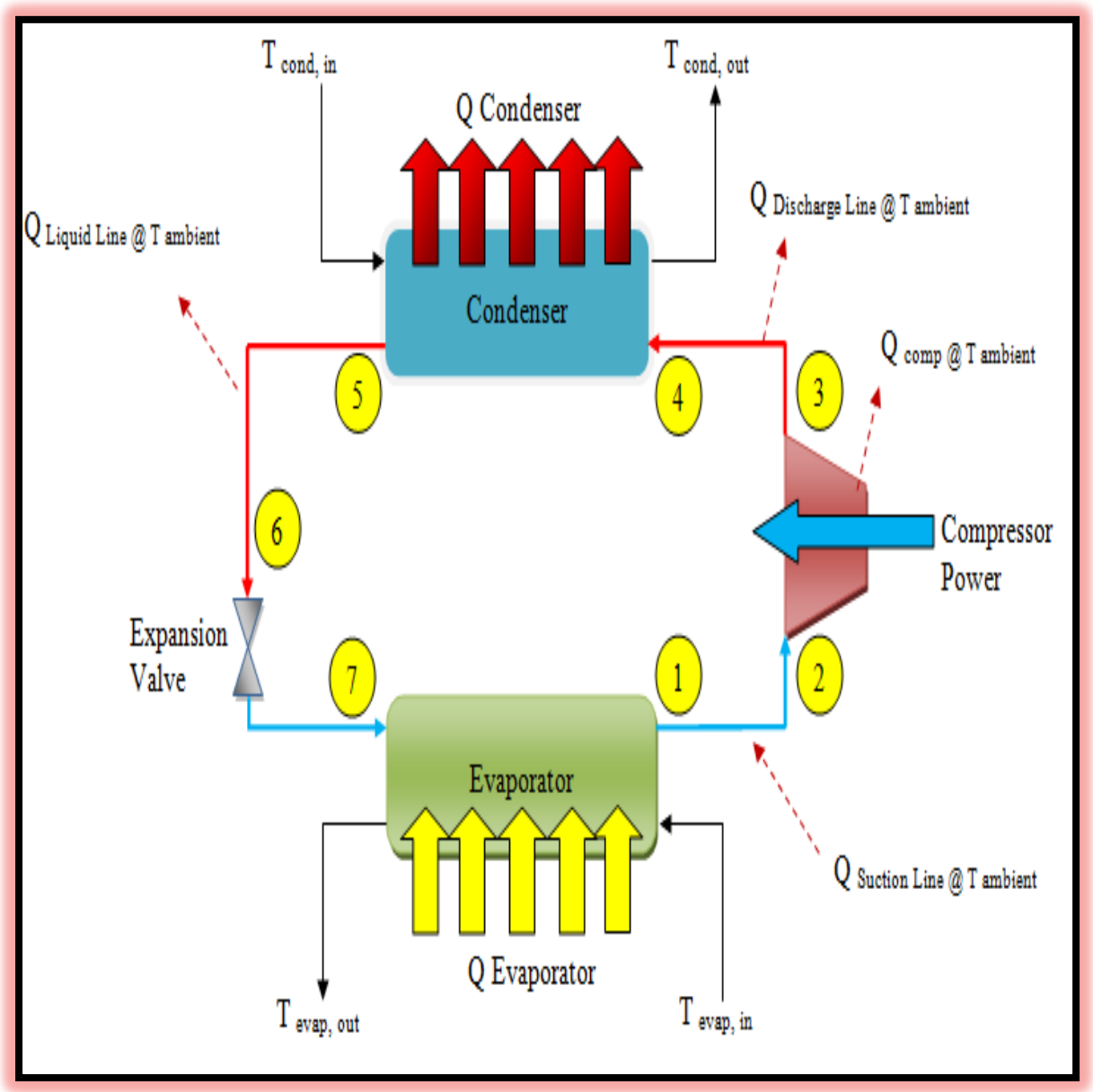

Figure 3.3: Required parameters for entropy generation calculation

Suction Line:

1st law Energy Balance:

$$\dot{Q}_{12}\,(kW) = \dot{m}_{ref}(h_2 - h_1) \tag{3.16}$$

2nd law Entropy Balance:

$$\dot{S}_{gen,12}\left(\frac{kW}{K}\right) = \dot{m}_{ref}(s_2 - s_1) - \frac{\dot{Q}_{12}}{T_{ambient}} \tag{3.17}$$

Compressor:

1st law Energy Balance:

$$\dot{Q}_{2\,3}(kW) = \dot{m}_{ref}(h_3 - h_2) + \dot{W}_{23} \tag{3.18}$$

2nd law Entropy Balance:

$$\dot{S}_{gen,23}\left(\frac{kW}{K}\right) = \dot{m}_{ref}(s_3 - s_2) - \frac{\dot{Q}_{23}}{T_{ambient}} \tag{3.19}$$

Discharge Line:

1st law Energy Balance:

$$\dot{Q}_{34}(kW) = \dot{m}_{ref}(h_4 - h_3) \tag{3.20}$$

2nd law Entropy Balance:

$$\dot{S}_{gen,34}\left(\frac{kW}{K}\right) = \dot{m}_{ref}(s_4 - s_3) - \frac{\dot{Q}_{34}}{T_{ambient}} \tag{3.21}$$

Condenser:

1st law Energy Balance:

$$\dot{Q}_{Cond} = \dot{Q}_{45}(kW) = \dot{m}_{ref}(h_5 - h_4) \tag{3.22}$$

2nd law Entropy Balance:

$$\dot{S}_{gen,45}\left(\frac{kW}{K}\right) = \dot{m}_{ref}(s_5 - s_4) - \frac{\dot{Q}_{45}}{T_{Cool}} \qquad ,T_{\ Cool} = Heat\ Sink\ Temperature \tag{3.23}$$

Using the concept of extended boundary, the heat sink temperature, $T_{\ Cool}$ is assumed as to be condenser inlet water temperature, $T_{H,inlet}$

Liquid Line:

1st law Energy Balance:

$$\dot{Q}_{56}(kW) = \dot{m}_{ref}(h_6 - h_5) \tag{3.24}$$

2nd law Entropy Balance:

$$\dot{S}_{gen,56}\left(\frac{kW}{K}\right) = \dot{m}_{ref}(s_6 - s_5) - \frac{\dot{Q}_{56}}{T_{ambient}} \tag{3.25}$$

Expansion Valve:

1st law Energy Balance:

$$\dot{Q}_{67}(kW) = \dot{m}_{ref}(h_6 - h_7) = 0\ (isenthalpic\ expansion) \tag{3.26}$$

2nd law Entropy Balance:

$$\dot{S}_{gen,67}\left(\frac{kW}{K}\right) = \dot{m}_{ref}(s_7 - s_6) \tag{3.27}$$

The total entropy generation, $\dot{S}_{gen,Total}$ of the refrigerant circuit can be obtained by summing the entropy generation of all the components.

$$\dot{S}_{gen,Total}\left(\frac{kW}{K}\right) = \dot{S}_{gen,Evaporator} + \dot{S}_{gen,Suction\ Line} + \dot{S}_{gen,Compressor} + \dot{S}_{gen,Discharge\ Line} + \dot{S}_{gen,Condenser} + \dot{S}_{gen,Liquid\ Line} + \dot{S}_{gen,Expansion\ valve} \quad (3.28a)$$

Alternatively, $\dot{S}_{gen,Total}\left(\frac{kW}{K}\right)$ can be obtained from Equation 3.13n

$$\dot{S}_{gen,Total} = -\frac{\dot{Q}_{45}}{T_{H,inlet}} - \frac{\dot{Q}_{71}}{T_{C,outlet}} - \frac{1}{T_{ambient}}\left(\dot{Q}_{12} + \dot{Q}_{23} + \dot{Q}_{34} + \dot{Q}_{56} + \dot{Q}_{67}\right) \quad (3.28b)$$

3.1.5 Carnot COP and Carnot Power

As shown in Figure 3.4, the energy and entropy balance for Reverse Carnot cycle can be expressed as follows:-

Energy Balance:

$$d\dot{Q}_{Cond} = d\dot{Q}_{Evap} + d\dot{W} \quad (3.29)$$

where

$$d\dot{Q}_{Cond} = \dot{m}_h Cp_h dT_H \quad (3.30)$$

$$d\dot{Q}_{Evap} = \dot{m}_c Cp_c dT_C \quad (3.31)$$

Entropy Balance:

$$dS = \frac{d\dot{Q}_{Cond}}{T_H} - \frac{d\dot{Q}_{Evap}}{T_C} = 0 \tag{3.32}$$

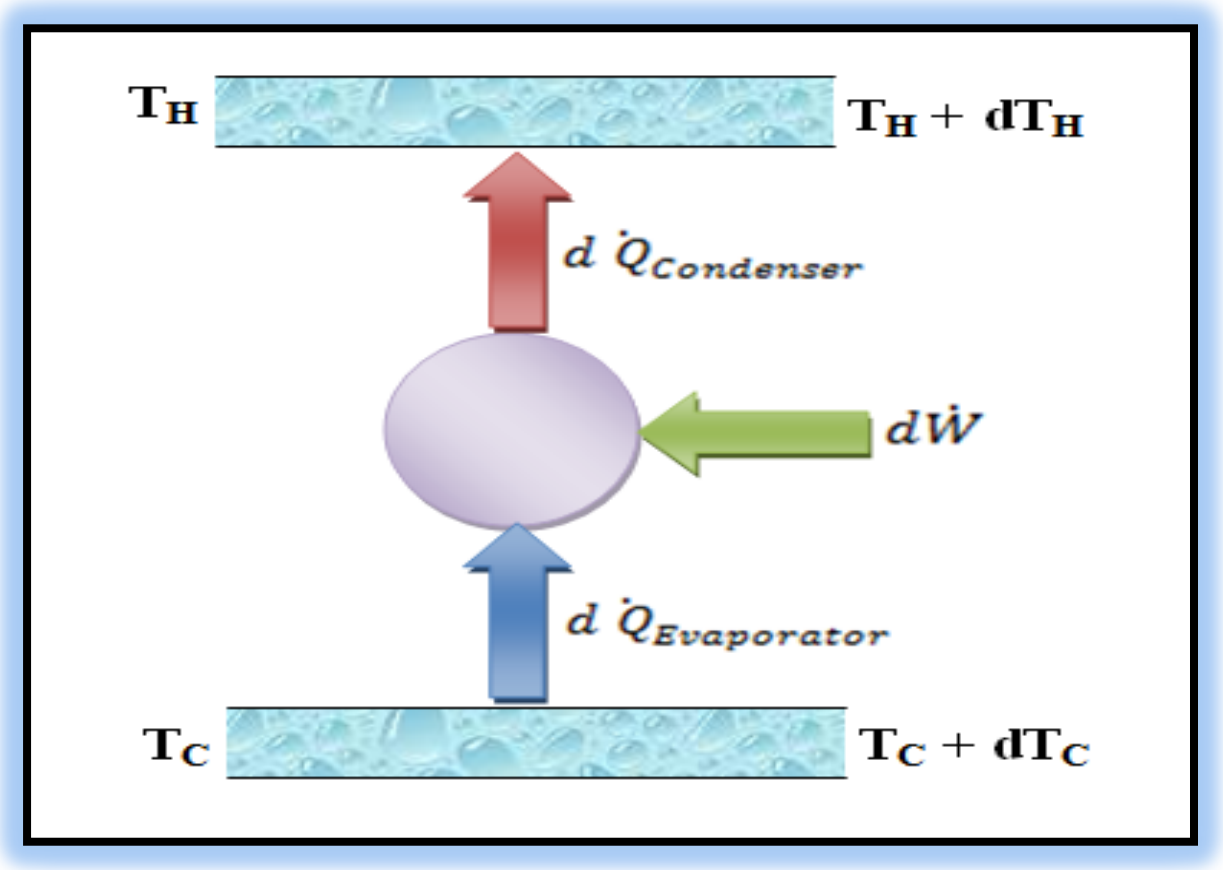

Figure 3.4: Reverse Carnot Cycle

From Equations 3.30 to 3.32,

$$(\dot{m}_h Cp_h)\frac{dT_H}{T_H} + (\dot{m}_c Cp_c)\frac{dT_C}{T_C} = 0 \tag{3.33}$$

Integrating this equation,

$$T_H{}^{(\dot{m}_h Cp_h)} T_C{}^{(\dot{m}_c Cp_c)} = Constant \tag{3.34}$$

Considering the inlet temperature conditions, the constant value of Equation 3.34 can be obtained. For a reverse Carnot cycle, the following equation can be used to determine the coolant temperatures:

$$T_H^{(\dot{m}_h Cp_h)} T_C^{(\dot{m}_c Cp_c)} = T_{H,inlet}^{(\dot{m}_h Cp_h)} T_{C,inlet}^{(\dot{m}_c Cp_c)} \tag{3.35}$$

For instance, at a specified TH Inlet, TC Inlet, and TC outlet, the condenser leaving water temperature (TH outlet) of a reverse Carnot cycle (Akau (1980) can be obtained:

$$T_{H,outlet\ Carnot} = \left[\left(\frac{T_{C,inlet}}{T_{C,outlet}} \right)^{\frac{\dot{m}_c Cp_c}{\dot{m}_h Cp_h}} \right] T_{H,inlet} \tag{3.36}$$

Therefore the Carnot Power (reversible work) can be obtained using the computed $T_{H,outlet}$ and other prescribed coolant temperatures. From Equation 3.29,

$$\dot{W}_{reversible} = \dot{m}_h Cp_h \left(T_{H,inlet} - T_{H,outlet\ Carnot} \right) + \dot{m}_c Cp_c \left(T_{C,inlet} - T_{C,outlet} \right) \tag{3.37}$$

Another alternative but simpler method to obtain $\dot{W}_{reversible}$ is by using the extended boundary concept where the condenser inlet water temperature, $T_{H,inlet}$ and the evaporator outlet water temperature, $T_{C,outlet}$ are used as the isothermal hot and cold reservoirs respectively. $\dot{W}_{reversible}$ can be obtained from the following equations:-

$$\dot{W}_{reversible} = \dot{Q}_{Evap} \left(1 - \frac{T_{ambient}}{T_{C,outlet}} \right) + \dot{Q}_{Cond} \left(1 - \frac{T_{ambient}}{T_{H,inlet}} \right) \tag{3.38}$$

Finally the actual power consumption of a vapor compression cycle can be predicted as following:

$$\dot{W} = \dot{W}_{reversible} - \dot{S}_{gen,Total}\, T_{ambient} \tag{3.13i}$$

The predictions of the compressor power from the lost work computation were presented in the Chapter 4. It was found that W_{Carnot} computed from both Equations 3.37 and 3.38 were capable of accurately predicting the actual compressor power.

3.2 Fault Detection Parameters

This section will be discussing several established fault detection parameters that can be effectively used to detect soft faults in chillers. In general, commercial chiller data acquisition mainly revolves around coolant properties such as the temperatures and flow rates of the chilled and cooling water circuits. As for the refrigerant circuits, the widely considered parameters are (i) evaporating pressure (ii) condensing pressure (iii) compressor suction pressure and discharge pressures (iv) superheat and (v) sub-cooling temperatures. Typically, data acquisition of a vapor compression chiller comprises the following measurements:-

i. Chilled water leaving temperature / Evaporator outlet water temperature
ii. Chilled water entering temperature/ Evaporator inlet water temperature
iii. Cooling water leaving temperature / Condenser outlet water temperature
iv. Cooling water entering temperature / Condenser inlet water temperature
v. Chilled water flow rate / Evaporator water flow rate
vi. Cooling water flow rate / Condenser water flow rate
vii. Chiller compressor power consumption
viii. Evaporator saturation pressure
ix. Condenser saturation pressure
x. Compressor suction and discharge pressures
xi. Refrigerant evaporator outlet temperature (for superheat computation)

xii. Refrigerant condenser outlet temperature (for sub-cooling computation)

In order to develop a generic fault detection and diagnosis tool, only the fault detection parameters that can be effortlessly computed from the above mentioned acquired data are considered in this thesis. The parameters are: - (i) Superheat (ii) Sub-cooling (iii) Effectiveness of condenser and evaporator (iv) Approach Temperature of condenser and evaporator (v) Overall heat transfer coefficient of condenser and evaporator and (vi) isentropic efficiency of the compressor.

3.2.1 Superheat

Superheat is the temperature difference between evaporator outlet temperature and the corresponding evaporator saturation temperature at the outlet point. In chillers, superheat is usually controlled at approximately 5K using thermostatic or electronic expansion valves. Refrigerant exiting the evaporator outlet need to be slightly superheated in order to prevent compressor sweating and slugging (liquid flood back). Nevertheless, too high superheat leads to capacity losses. Suction superheat calculation requires the following steps:-

i. Measure the evaporator outlet temperature,
ii. Measure the evaporator outlet pressure,
iii. Convert the evaporator outlet pressure to the equivalent saturation temperature using the refrigerant pressure - temperature saturation table
iv. Subtract the obtained saturation refrigerant temperature from the measured evaporator outlet temperature to obtain the superheat.

Superheat plays an important role as a fault detection parameter as it can be effectively used to detect refrigerant overcharge and leakage. Refrigerant overcharge reduces the

evaporation surface area and increases the risk of the excess refrigerant that travel through the evaporator in a liquid form rather than vapor state. This decreases superheat and leads to liquid flood back in the compressor. On the other hand, refrigerant leakage leads to less liquid refrigerant in the evaporator. Heat (cooling load) is partially removed by the evaporated vapor and this increases superheat. Higher superheat leads to lower specific volume at the compressor suction and effectively reduces its pumping capacity.

3.2.2 Sub-cooling

Similar to the suction superheat, sub-cooling is also a non-measured parameter. Mathematically, it is an arithmetic temperature difference between the condenser leaving saturation temperature and the measured refrigerant leaving temperature of the condenser. High sub-cooling is usually preferred to increase the cooling capacity of a chiller. Condenser sub-cooling computation requires the following steps:-

i. Measure the condenser outlet pressure,
ii. Measure the condenser outlet temperature,
iii. Convert the condenser outlet pressure to the equivalent saturation temperature using the refrigerant pressure - temperature saturation table
iv. Subtract the measured condenser outlet temperature from the obtained saturation condenser outlet temperature.

In contrast to superheat, sub-cooling increases due to refrigerant overcharge. Excessive liquid build up in the condenser due to overcharge reduces the effective condensation heat transfer area which in return increases the condensation pressure and temperature. As a result, higher sub-cooling can be observed. On the other hand, less sub-cooling is obtained during

the refrigerant leakage. Higher overall condenser heat transfer coefficient and larger exposed condensation surface area contributes to this observation.

3.2.3 Effectiveness of two phase heat exchangers

Effectiveness of a heat exchanger is defined as the ratio of the actual heat transfer to the maximum heat that could be transferred by an infinite size heat exchanger. The effectiveness value lies between 0 and 1. For an infinite counter flow heat exchanger, the maximum possible heat transfer is defined as:-

$$\dot{Q}_{max} = \left(\dot{m}\, c_p\right)_{min} (\Delta T_{\max}) \tag{3.39}$$

Where the minimum thermal mass and the maximum temperature difference are expressed as following:

$$\left(\dot{m}\, c_p\right)_{min} = min\left[\left(\dot{m}\, c_p\right)_{cold}\ ,\ \left(\dot{m}\, c_p\right)_{hot}\right] \tag{3.40}$$

$$(\Delta T_{\max}) = T_{H,inlet} - T_{C,inlet} \tag{3.41}$$

Therefore the effectiveness ε can be defined as:

$$\varepsilon = \frac{\dot{Q}}{\dot{Q}_{max}} = \frac{\left(\dot{m}\, c_p\right)_{cold}(T_{C,inlet} - T_{C,outlet})}{\left(\dot{m}\, c_p\right)_{min}(T_{H,inlet} - T_{C,inlet})} \tag{3.42}$$

If $\left(\dot{m}\, c_p\right)_{cold} < \left(\dot{m}\, c_p\right)_{hot}$, then $\left(\dot{m}\, c_p\right)_{min} = min\left[\left(\dot{m}\, c_p\right)_{cold}, \left(\dot{m}\, c_p\right)_{hot}\right] = \left(\dot{m}\, c_p\right)_{cold}$

Thus, the effectiveness can be written as a function of temperature only:

$$\varepsilon = \frac{\dot{Q}}{\dot{Q}_{max}} = \frac{(T_{C,inlet} - T_{C,outlet})}{(T_{H,inlet} - T_{C,inlet})} \tag{3.43}$$

For two phase flow heat exchangers, the effectiveness of the evaporator and condenser can be expressed as follows:

$$\varepsilon_{Evap} = \frac{(T_{C,inlet} - T_{C,outlet})}{(T_{C,inlet} - T_{Evap})} \; ; \; T_{evap} = Evap\ saturation\ temperature \tag{3.44}$$

$$\varepsilon_{Cond} = \frac{(T_{H,outlet} - T_{H,inlet})}{(T_{Cond} - T_{H,inlet})} ; \; T_{cond} = Cond\ saturation\ temperature \tag{3.45}$$

Heat exchanger effectiveness can be employed as a useful performance indicator for evaporator and condenser. The obvious reason is that its formulation captures all the working temperatures that enters and exits the heat exchanger. For instance, faults due to the presence of non-condensable or refrigerant overcharge tend to increase the condensation pressure and compressor discharge pressure. As a result, condenser effectiveness decreases due to the rise of the condenser saturation temperature.

3.2.4 Heat Exchanger Approach Temperatures

Similar to effectiveness, approach temperature is another powerful performance indicator of a heat exchanger. By definition, approach temperature for condenser is the temperature difference between condenser saturation and the leaving cooling water temperatures. Similarly, evaporator approach temperature is the difference between the leaving chilled water and evaporator saturation temperature. Approach temperatures in evaporator and condenser can be designed as low as 1 ^{o}C.

$$T_{Cond,appr} = T_{Cond} - T_{H,outlet} \tag{3.46}$$

$$T_{Evap,appr} = T_{C,outlet} - T_{Evap} \tag{3.47}$$

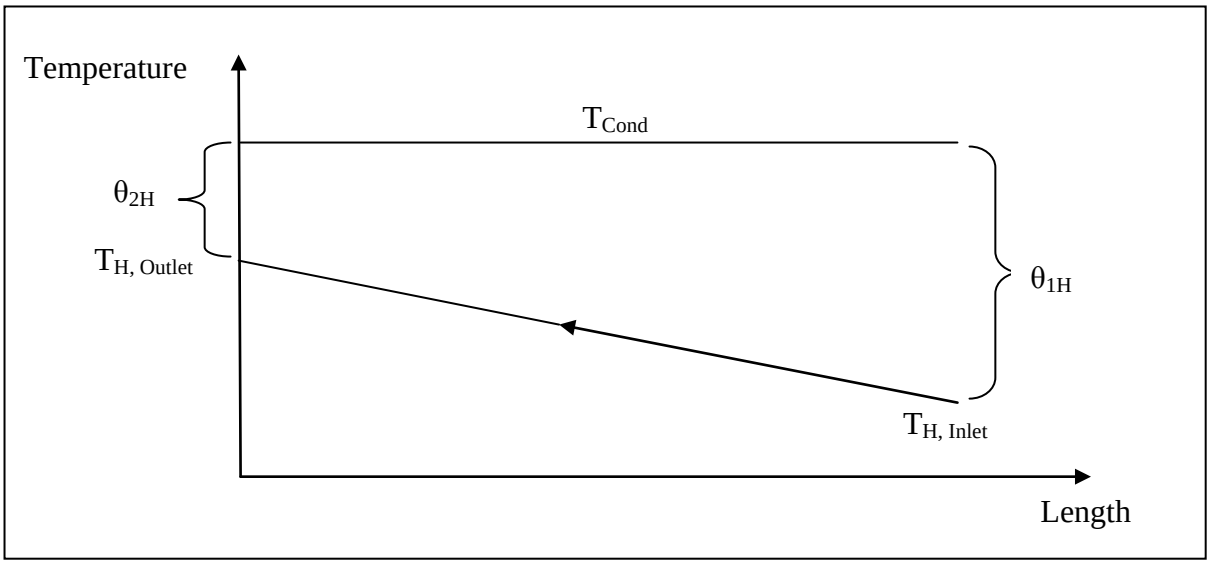

Figure 3.5: Working temperatures of a water cooled condenser

From Figure 3.5, it can be shown that for a condenser,

$$\theta_{2H} = T_{Cond,appr} = T_{cond} - T_{H,outlet} \tag{3.48}$$

$$\theta_{1H} = \Delta T_{max} = T_{cond} - T_{H,inlet} \tag{3.49}$$

$$\Delta T_{coolant} = T_{H,outlet} - T_{H,inlet} = \theta_{1H} - \theta_{2H} \tag{3.50}$$

Condenser effectiveness can also be expressed as a function of approach temperature

$$\varepsilon_{Cond} = \frac{(T_{H,outlet} - T_{H,inlet})}{(T_{Cond} - T_{H,inlet})} = \frac{\theta_{1H} - \theta_{2H}}{\theta_{1H}} = 1 - \frac{\theta_{2H}}{\theta_{1H}} = 1 - \left(\frac{T_{Cond,appr}}{\theta_{1H}}\right) \tag{3.51}$$

Similarly,

$$\varepsilon_{Evap} = \frac{(T_{C,inlet} - T_{C,outlet})}{(T_{C,inlet} - T_{Evap})} = \frac{\theta_{1C} - \theta_{2C}}{\theta_{1C}} = 1 - \frac{\theta_{2C}}{\theta_{1C}} = 1 - \left(\frac{T_{Evap,appr}}{\theta_{1C}}\right) \tag{3.52}$$

3.2.5 Heat Exchanger Overall Heat Transfer Coefficients

For un-finned tubular heat exchangers, the overall heat transfer coefficient, UA can be expressed as:-

$$\frac{1}{UA} = \frac{1}{U_{int}A_{int}} = \frac{1}{U_{ext}A_{ext}}$$

$$= \frac{1}{h_{int}A_{int}} + \frac{R_{f,int}}{A_{int}} + \frac{ln\left(D_{ext}/D_{int}\right)}{2\pi kL} + \frac{R_{f,ext}}{A_{ext}} + \frac{1}{h_{ext}A_{ext}} \quad (3.53)$$

Where *int* and *ext* refer to the inner and outer tube surface respectively; L is the tube length; R_f is the fouling factor; $A_{int} = (\pi D_{int} L)$; $A_{ext} = (\pi D_{ext} L)$

Apart from this definition, UA (e.g of condenser) can also be computed as follows:-

$$\dot{Q}_{Cond} = (UA)_{Cond}\,(LMTD)_{Cond}$$

$$(UA)_{Cond} = \frac{\dot{Q}_{Cond}}{\left(\frac{\theta_{1H} - \theta_{2H}}{\ln\left(\theta_{1H}/\theta_{2H}\right)}\right)}$$

$$(UA)_{Cond} = \left(\dot{m}\, c_p\right)_H \ln\left(\theta_{1H}/\theta_{2H}\right) \quad (3.54)$$

In term of effectiveness, UA condenser can be expressed as

$$(UA)_{Cond} = -\left(\dot{m}\, c_p\right)_H \ln\left(1 - \varepsilon_{Cond}\right) \quad (3.55)$$

Overall heat transfer coefficient is one of the popular and effective performance indicators used in chiller and heat exchanger fault detection. For instance, it can be used to diagnose faults stemming from:-

(i) Fouling - flagged by fouling factors, $R_{f,int}$ or $R_{f,ext}$

(ii) Refrigerant Over charge/Leak and non- condensable - flagged by $\frac{1}{h_{ext}A_{ext}}$ if the refrigerant is flowing around the outer tube

(iii) Reduction in cooling water flow rate - flagged by $\frac{1}{h_{int}A_{int}}$ if the refrigerant is flowing inside the tube.

3.2.6 Isentropic Efficiency of the Compressor

As all the fault detection indicators discussed earlier revolve around the two phase flow heat exchangers namely evaporator and condenser, it is also imperative to monitor the efficiency and condition of the chiller compressors. The compressor is the heart of a vapor compression chiller and is the most expensive component of a chiller. It is common to screen the performance of a compressor using isentropic efficiency, η_C which is defined as:-

$$\eta_C = \frac{\left(h_{Suction} - h_{Discharge@S\ Suction}\right)}{\left(h_{Suction} - h_{Discharge}\right)} \tag{3.56}$$

By computing the isentropic efficiency, η_C the actual performance can be compared with the ideal performance of the compressor with the same inlet and exit pressures.

3.3 FDD statistical framework

This section provides details on the two statistical frameworks that were employed in this thesis to detect and diagnose the occurrence of soft faults in vapor compression chillers. The statistical methods were: - (i) Cumulative Sum (CUSUM) and (ii) Bayes Theorem.

The Cumulative Sum chart was used to detect faults using the fault detection parameters described in Section 3.2 of this chapter. Two common techniques used in CUSUM are: - (i) V-Mask (a graphical model) and (ii) Decision Interval (a mathematical model). This study employed only the Decision Interval technique as it can be easily computed and coded as FDD software. CUSUM computed the running total deviation between the fault-free model and the on-line data. The fault-free models for each parameter were regressed using sets of fault-free data obtained during the normal test runs. The developments of the regressed fault-free model will be discussed in detail in Chapter 4. Once the accumulated difference between the model and the measured online data was above the decision limit, the diagnostic routine was then activated to correctly identify the root cause of the developing soft fault. The diagnostic routine was built using Bayes probability theory.

3.3.1 The Shewhart Chart

Before exploring the details of CUSUM charts, it is important to understand the Shewhart Chart, a common and powerful charting technique used in the Statistical Process Control field. Developed by Walter Shewhart, it mainly utilizes the subgroup mean, Xbar or XB (j) and subgroup range, R (j) chart to detect the shift of the mean and the spread of the monitored process variable respectively. For a group of sample that can be divided into a number of sub-groups of equal size, the XB(j) and R(j) can be obtained as following:-

$$\text{XB(j)} = \frac{\sum_{i=1}^{N} X(i,j)}{N}, \quad j = 1, \ldots\ldots, NS \tag{3.57}$$

$$\text{R(j)} = XMAX(j) - XMIN(j), \quad j = 1, \ldots\ldots, NS \tag{3.58}$$

The standard deviation, sigma of the subgroup can be expressed as:-

$$\text{S(j)} = \sqrt{\frac{\sum_{i=1}^{N}[X(i,j) - XB(j)]^2}{N-1}}, \quad j = 1, \ldots\ldots, NS \tag{3.59}$$

The Xbar mean, R mean and sigma mean are then computed as follows:

$$\text{XBB} = \frac{\sum_{j=1}^{NS} XB(j)}{NS}, \quad j = 1, \ldots\ldots, NS \tag{3.60}$$

$$\text{RB} = \frac{\sum_{j=1}^{NS} R(j)}{NS}, \quad j = 1, \ldots\ldots, NS \tag{3.61}$$

$$\text{SB} = \frac{\sum_{j=1}^{NS} S(j)}{NS}, \quad j = 1, \ldots\ldots, NS \tag{3.62}$$

Where

NS = number of subgroups,

N = subgroup size,

X (i,j) = ith value of the variable in subgroup j

XB (j) = jth subgroup mean

R (j) = jth subgroup range

XMAX (j) = jth subgroup maximum value

XMIN (j) = jth subgroup minimum value

S(j) = jth subgroup sigma

XBB = Xbar mean

RB = Range mean

SB = sigma mean

Shewhart chart is usually drawn with respect to sub groups, where the mean or the range values of the monitored variable occupying the Y-axis. Also usually presented on the chart are three horizontal lines that represent the following: - (I) Centre line (II) Upper control limit and (III) lower control limit. For Xbar chart (Badavas, 1993), the above mentioned horizontal lines are computed as follows:-

$$\text{Centre line of XBar} = XBB \tag{3.63}$$

$$\text{Upper control limit of XBar} = XBB + K1\ SIGXB \tag{3.64a}$$

$$\text{Lower control limit of XBar} = XBB - K1\ SIGXB \tag{3.64b}$$

Where

K1 = 3; denotes the deviation of 3 Sigma (99.73%) standard error from the centre line

SIGXB = standard deviation, sigma of the Xbar

Figure 3.6 shows the Xbar Shewhart chart with a 3 sigma control limits. It has to be emphasized that subgroup 10 has exceeded the upper control limit and thus requires corrective action from the operator. This demonstrates that Shewhart can be used to detect faults when the measured parameters surpass either of the control limits. Nevertheless, The

Shewhart chart is ineffective in detecting small shifts. This is a serious drawback from the perspective of this study as this thesis aims to detect and diagnose soft faults (e.g fouling, refrigerant leakage) as early as possible to minimize unscheduled breakdown or economic losses. Intuitively, one could argue that by reducing the width of control limits (e.g from 3 sigma to 2 sigma), the fault detection capability of Shewhart can be enhanced. It has to be cautioned that smaller control limits could lead to higher frequency of false alarms. Researchers have also proposed on the implementation of sequential control limits where 1-sigma, 2-sigma and 3-sigma are used to monitor the shift pattern from one control limit to another.

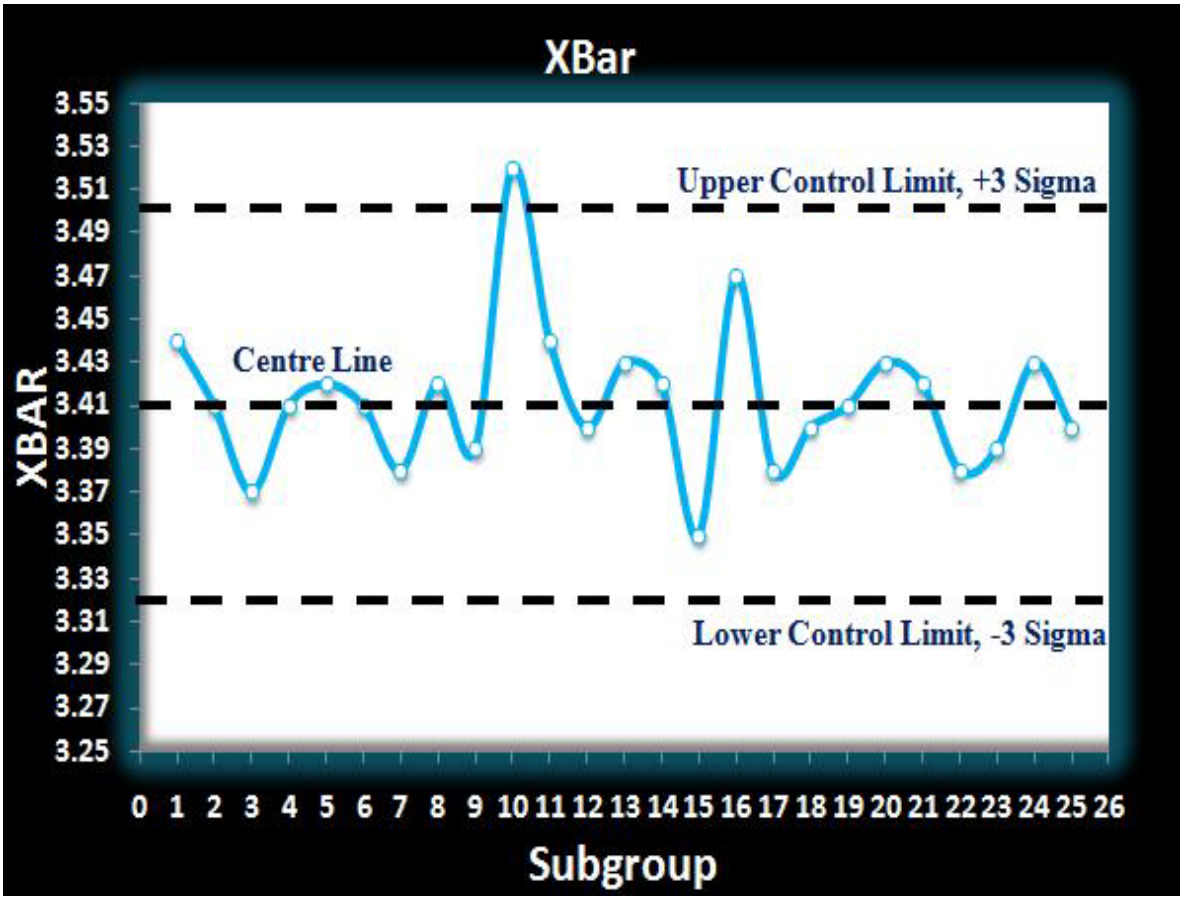

Figure 3.6: Xbar Shewhart with upper and lower control limit

3.3.2 The Cumulative Sum (CUSUM) Chart

The disadvantage of a Shewhart chart in detecting small persistent shifts can be effectively solved by using the Cumulative Sum (CUSUM) chart. CUSUM accumulates the running deviation of the incoming data with respect to an assigned benchmark. In mathematical form, it can be expressed as:-

$$\mathrm{C_n} = \sum_{j=1}^{n} (X_j - \mu) \tag{3.65}$$

Where X_j is the incoming data and μ is the benchmark value (mean value of the fault-free or nominal data). CUSUM can be also expressed in a non-dimensional form:-

$$\mathrm{S_n} = \sum_{j=1}^{n} \frac{(X_j - \mu)}{\sigma} \tag{3.66}$$

Where σ is the standard deviation of the nominal fault-free data.

By using the non-dimensional CUSUM, CUSUM charts of different units or types of measurements (pressure, temperature and etc) can be directly compared. In this study, all the presented CUSUM charts are in non-dimensional form. For a normal distribution, where the sum of the independent normal N (0, σ^2) is equivalent to $\mathrm{C_n}$, Equation 3.65 can be expanded as follows:-

$$\mathrm{C_0} = 0$$

$$\mathrm{C_n} = \mathrm{C_{n-1}} + (X_n - \mu) \tag{3.65 a}$$

Similarly, non dimensional CUSUM can be expressed as:

$$S_0 = 0$$

$$S_n = S_{n-1} + \left(\frac{X_n - \mu}{\sigma}\right) \tag{3.66b}$$

Conventional CUSUM charts require a substantial data to perform simple calibrations that mainly involve the computation of means and standard deviations of the fault-free data. Nevertheless, CUSUM can be tuned as "Self-Starting CUSUM" (Badavas, 1993) when there are limited historical data available. In this study, conventional CUSUM is deemed to be more than sufficient as a huge volume of fault free chiller data has been collected prior to the faulty test runs. It has be emphasized that conventional CUSUM is much simpler, efficient, straight forward and requires less computational memory.

3.3.3 Drift analysis using Cumulative Sum (CUSUM) Chart

As explained by Hawkins (1997), at a point m where there is a drift, δ in the mean value, μ, the normal distribution changes from N (μ, σ^2) to N $(\mu + \delta, \sigma^2)$. The CUSUM at any instance of scenario can be written as:

$$S_n = \sum_{j=1}^{n} \frac{(X_j - \mu)}{\sigma}$$

$$= \sum_{j=1}^{m} \frac{(X_j - \mu)}{\sigma} + \sum_{j=m+1}^{n} \frac{(X_j - \mu)}{\sigma} \tag{3.67}$$

The distribution of the second summation can be written as

$$\sum_{j=m+1}^{n} \frac{(X_j - \mu)}{\sigma} \sim N[(n-m)\delta, (n-m)\sigma^2 \tag{3.68}$$

This indicates that the average of the CUSUM after the point m is equivalent to$(n-m)\delta$. In other words, the average CUSUM will drift at a path centred on a line of slope,δ.

3.3.4 Fault Detection using Cumulative Sum (CUSUM) Chart

For the purpose of fault or drift detection, the basic CUSUM equations (3.65 and 3.66) can be further enhanced using the decision intervals (Ω), slack values (ζ), positive drift (ψ_H) and negative drift (ψ_L) functions. The decision intervals, Ω are the threshold limits that perform somehow similar to the control limits of the Shewhart charts. The slack value, ζ is one of the operating parameters of CUSUM that provides some allowance to the drift detection process. The positive and negative functions are other important elements in CUSUM drift detection. These functions indicate the direction of the occurring drifts where positive drift is captured by the $\psi_H$function while negative drift is tracked by the $\psi_L$function.

For each instance, the Positive Drift CUSUM $\psi_H(j)$ can be written as:

$$\psi_H(j) = \max\left[0, \psi_H(j-1) + \frac{(X_j - \mu)}{\sigma} - \zeta_1\right], \qquad j = 1, \ldots\ldots, NS \tag{3.69}$$

Similarly, the Negative Drift CUSUM $\psi_L(j)$ can be expresses as:

$$\psi_L(j) = \max\left[0, \psi_L(j-1) - \frac{(X_j - \mu)}{\sigma} - \zeta_2\right], \qquad j = 1, \ldots\ldots, NS \tag{3.70}$$

Positive and negative drifts were initialized at zero; e.g. $\psi_H(0) = \psi_L(0) = 0$

The slack parameter, ζ can be defined as following:-

$$\zeta = \frac{1}{2}\frac{(\text{acceptable change in mean})}{\sigma} \tag{3.71}$$

For instance, if a fault is anticipated to occur when the mean shifts beyond three standard deviations (3σ , 99.7% confidence level) from the mean value, ζ can be approximated as:

$$\zeta = \frac{1}{2}\frac{(3\ \sigma)}{\sigma} = 1.5 \tag{3.72}$$

It has to be emphasized that deviation of 3σ is unfavourable in certain circumstances as the large deviation gives excessive tolerance for CUSUM to react. Consequently, this leads to a classical hypothesis Type II error where CUSUM fails to flag the developing fault. In contrast, smaller threshold makes CUSUM vulnerable to classical hypothesis Type I error. High frequency of false alarm can be anticipated due to the smaller tolerance value. In this study, a slack value of 0.75 (where 1.5-sigma is used as acceptable change in mean) has been chosen to minimize the Type I and II errors.

$$\zeta = \frac{1}{2}\frac{\left(\frac{3}{2}\ \sigma\right)}{\sigma} = 0.75 \tag{3.73}$$

Badavas (1993) recommended the following useful rule of thumb that is helpful in determining the decision interval, Ω :-

$$\Omega + \zeta = 4.5 \tag{3.74}$$

Where $\zeta \geq 0$ and $\Omega \geq \zeta$

$$\Omega = 4.5 - \zeta = 4.5 - 0.75 = 3.75 \tag{3.75}$$

The decision interval, Ω can also be estimated using the CUSUM Average Run Length and the slack values as suggested by Hawkins (1997).

In conclusion, all the CUSUM analysis presented in this study employed the following values:-

Slack value, ζ = 0.75

Decision interval, Ω = 3.75

3.3.5 Post Fault Detection Analysis using CUSUM

In this study, the CUSUM analyses were performed in two different methods, namely (i) Reset CUSUM (ψ_R) and (ii) Non-Reset CUSUM (ψ_{NR}). Both techniques were applied in the proposed methodology to develop a reliable fault detection tool. The Non-Reset CUSUM (ψ_{NR}) can be computed directly using Equations 3.69 and 3.70 for both positive and negative drifts respectively. However, Reset CUSUM (ψ_R) works on a different principle where the CUSUM is reset and initialized to zero if the running total deviations exceed the decision interval. Since there were two types of CUSUM employed in this study, the decision limits for ψ_R were defined Ω_1 while the threshold for ψ_{NR} was assigned as Ω_2.

The following conditions were adopted by Schein (2003) for ψ_R CUSUM:-

Positive Drift

$$If\ \ \psi_H(j) > \Omega_1, then\ \ \psi_H(j) = 0$$

Negative Drift

$$If\ \ \psi_L(j) > \Omega_1, then\ \ \psi_L(j) = 0 \qquad (3.76a)$$

This technique enables us to monitor the reset frequencies which provide vital information on the developing fault. The reset frequencies indicate the severity of the developing fault. The severe the faults, the higher the reset frequencies are.

In this thesis, the Reset-CUSUM, ψ_R technique was modified to enhance CUSUM fault detection capabilities. Although the reset technique proposed by Schein (2003) yields fairly good results, it might not be suitable for detecting small shifts. For smaller drift/shift, the number of resets will be considerably less and the duration taken for the CUSUM to surpass the decision interval at every reset cycle will be longer. During this period, CUSUM suffers from classical hypothesis Type II error. It is proposed that CUSUM to be reset to one half of the decision interval value rather than zero.

$$If\ \ \psi_H(j) > \Omega, then\ \ \psi_H(j) = \frac{\Omega_1}{2} = \frac{3.75}{2}\ = 1.875$$

$$If\ \ \psi_L(j) > \Omega, then\ \ \psi_L(j) = \frac{\Omega_1}{2} = \frac{3.75}{2}\ = 1.875 \qquad (3.76b)$$

Through the proposed modification, higher reset frequencies can be observed for both small and large drift, thus minimizing the Type II errors.

As for the Non-Reset CUSUM, ψ_{NR}, the decision limit, Ω_2 is set to a slightly higher value than the Ω_1 to minimize false alarms. It is proposed that twice the Ω_1 is used.

$$\Omega_2 = \ 2\ \times\ \Omega_1 = 2\ \times 3.75 = 7.50 \qquad (3.77)$$

In this study, the diagnosis routine will be only activated if the ψ_{NR} exceeds the decision limit, Ω_2. On the other hand, ψ_R will provide visualization on the severity of the fault. Reset frequency increases as the severity of the fault rises. The input to the diagnostic routine will be in Boolean:- (i) "1" for positive CUSUM drift, ψ_H (ii) "-1" for negative CUSUM drift, ψ_L and (iii) "0" for zero CUSUM drift.

As the following fault detection parameters:

i. Superheat temperature (ϕ_1)

ii. Condenser Approach Temperature (ϕ_2)

iii. Condense sub-cooling temperature (ϕ_3)

iv. Condenser Heat Transfer coefficient (ϕ_4)

v. Condenser Entropy Generation (ϕ_5)

are used in the CUSUM as fault detection parameters, then the CUSUM output, $\boldsymbol{P}$ can be written as following:

$$\boldsymbol{P} = \begin{bmatrix} \phi_1 \\ \phi_2 \\ \phi_3 \\ \phi_4 \\ \phi_5 \end{bmatrix} = \begin{bmatrix} "1" \; or \; " -1" \; or \; "0" \\ "1" \; or \; " -1" \; or \; "0" \\ "1" \; or \; " -1" \; or \; "0" \\ "1" \; or \; " -1" \; or \; "0" \\ "1" \; or \; " -1" \; or \; "0" \end{bmatrix} \tag{3.78}$$

3.3.6 CUSUM Application in the Chiller Fault Detection

A typical CUSUM chart proposed in this thesis consists of 2 vertical axes. Primary Y-axis indicates the reset frequencies (ψ_R) for both positive, ψ_H and negative drift, ψ_L respectively. On the other hand, the secondary Y-axis represents the non-reset (ψ_{NR}) positive or negative drifts. As mentioned earlier, a fault is detected by a specific CUSUM if $\psi_{H\,NR}$ or $\psi_{L\,NR}$ exceeds the decision limit, Ω_2. From Figure 3.7, it can be seen that CUSUM ϕ_1 exhibited a single negative ($\psi_{L\,R}$) and positive ($\psi_{H\,R}$) reset at the Normal 2 and Normal 3 data sets respectively. These resets will not trigger the diagnostic routine as the non-reset positive ($\psi_{H\,NR}$) and negative ($\psi_{L\,NR}$) trend lines are below the decision limit, Ω_2. However, the diagnostic routine will be activated at the Fault 5% data set as $\psi_{H\,NR}$ increases beyond the Ω_2 threshold. The occurrence of the fault is further confirmed by the multiple positive reset ($\psi_{H\,R}$) trend line. At this time point, from Equation 3.78, $\phi_1$is assigned "1".

Similar processes can be repeated in other CUSUMs (e.g ϕ_2, ϕ_3, ϕ_4, ϕ_5) to complete the matrix, P of Equation 3.78. In short, it can be summarized as follows:-

a) If the non-reset drifts are above the Ω_2, then a fault is confirm detected

b) If the non-reset drifts are between the Ω_1 and Ω_2, then there are a possibility for a fault to occur.

c) If the non-reset drifts are below the Ω_1, then it is a fault-free operation

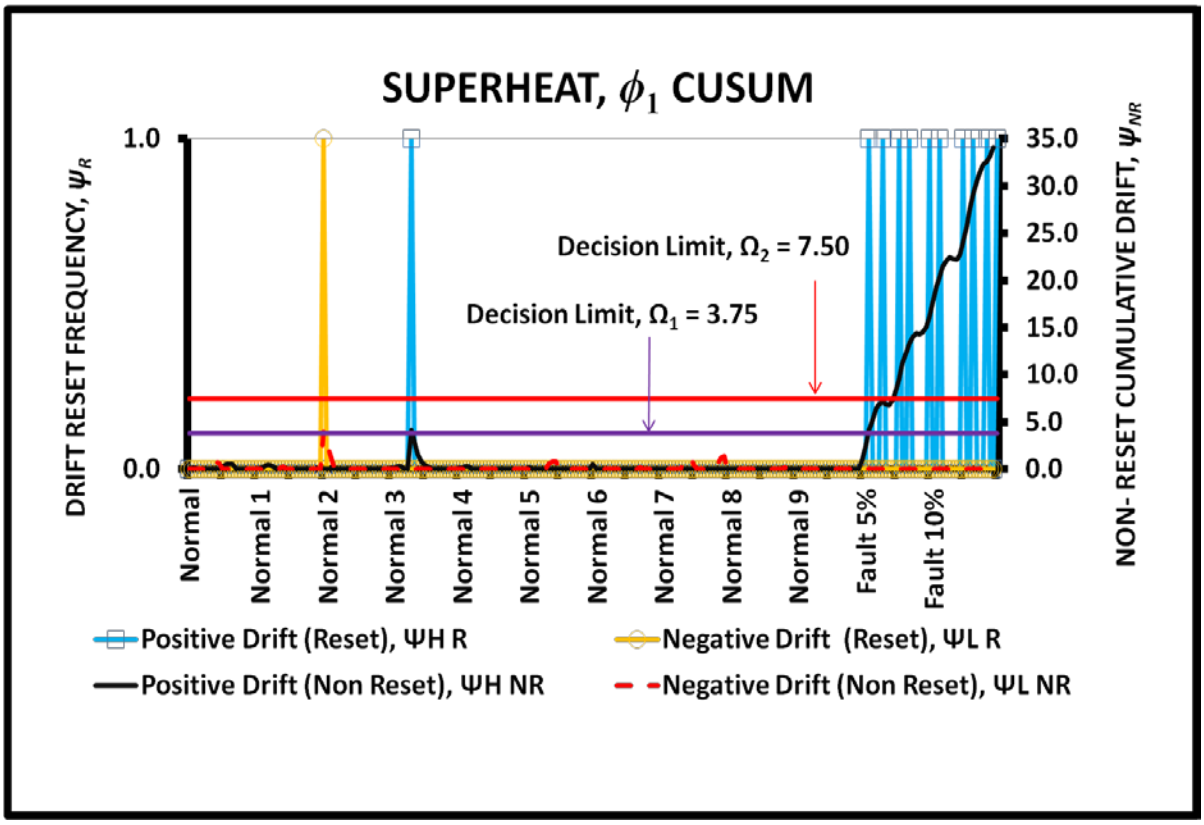

Figure 3.7: Working principle of one of the proposed CUSUM, ϕ_1

3.3.7 Bayes Probability Theory

Bayes Theorem was employed in diagnosing the faults detected using the five CUSUM parameters namely, ϕ_1, ϕ_2, ϕ_3, ϕ_4 and ϕ_5. The Bayes diagnosis analysis is activated if the non-reset drift (negative or positive) of any of the five CUSUM parameters surpasses the decision limit, $\Omega_2 = 7.50$.

Before establishing a suitable Bayes diagnosis routine for chiller fault detection and diagnosis, it is pertinent to understand some of the relevant fundamental probability theorems. The probability of an event A, a subset of the sample space event (A∈S), to occur is assigned as P (A). These probabilities must obey the following axioms.

Rule 1:

The probability of the sample space event, S to occur is certain and equivalent to one.

$$P(S) = 1 \tag{3.79}$$

Rule 2:

The probability of event A to occur is non-negative.

$$P(A) \gg 0 \tag{3.80}$$

Rule 3:

For disjoint and joint probabilities in a sample space, S as shown in Figures 3.8 and Figure 3.9 respectively, the union of event A (A∈S) and B (B∈S) can be expressed as:

Union (∪) of disjoint probability (mutually exclusive):

$$P(A \cup B) = P(A) + P(B) \tag{3.81}$$

Union of joint probability:

$$P(A \cup B) = P(A) + P(B) - P(A \cap B) \tag{3.82}$$

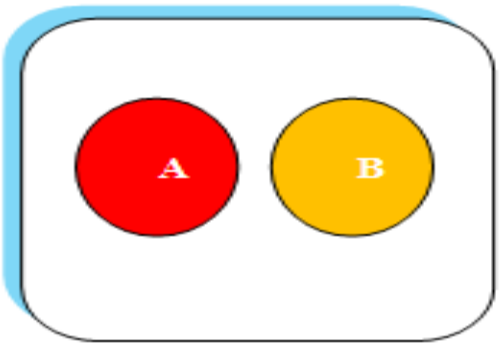

Figure 3.8: Event A and B are disjoint

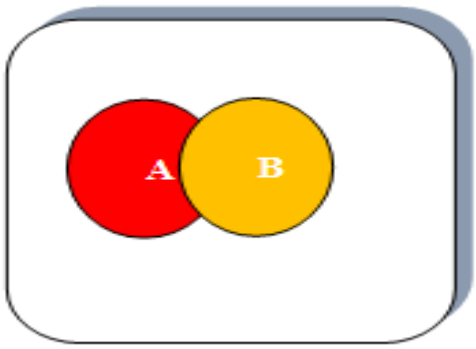

Figure 3.9: Joint probability of event A and B

Rule 4:

The intersection $(\cap)$ between event A and B can be expressed as follows if events A and B are independent:

$$P(A \cap B) = P(A)P(B) \tag{3.83a}$$

Similarly, for a large number of events that occur simultaneously, the intersection among them can be expressed as following:-

$$P(A \cap B \cap C \cap D \cap E \ldots) = P(A)P(B)P(BC)P(D)P(E) \ldots\ldots \quad (3.83b)$$

Another key probability rule that governs the proposed diagnostic routine in this study is the conditional probability. In lay terms, conditional probability may be stated as follows:

"Given event A, the probability of event B is p"

Mathematically, the conditional probability can be defined as:

$$P(B|A) = \frac{P(B \cap A)}{P(A)} \quad (3.84)$$

Where $P(B|A)$ is the conditional probability that states the probability of event B occurring given A.

Similarly, the probability of A to occur for a known event B can be defined as:

$$P(A|B) = \frac{P(A \cap B)}{P(B)} \quad (3.85)$$

Equations 3.84 and 3.85 can be rearranged as following:

$$P(B \cap A) = P(A)P(B|A) \quad (3.86)$$

$$P(A \cap B) = P(B)P(A|B) \quad (3.87)$$

Since $P(B \cap A) = P(A \cap B)$, the following can be proved:-

$$P(B|A) = \frac{P(B)P(A|B)}{P(A)} \quad (3.88)$$

This is known as the Bayes Rule (Berry (1996)). It provides a method for updating the user's belief about event B provided the information about the other event, A is known. The individual terms of Bayes Rule is defined as following:

i. $P(B)$ is the prior probability of B

ii. $P(B|A)$ is the posterior probability of B given A

iii. $P(A|B)$ is likelihood of B given A

3.3.8 Bayes Application in the Chiller Fault Diagnosis

Based on this important rule, it can now be easily elucidated on how the Bayes theorem fits into the proposed diagnostic routine of this study. The following expressions explain all:

What is the probability of event B to happen if event A is detected? The equivalent Bayes rule is: $P(B|A)$

What is the probability of refrigerant leakage if superheat decreases? The equivalent Bayes rule is: $P(\ Ref\text{rigerant}\ \ Leakage \mid Decrease\ in\ Superheat\ )$

What is the probability of refrigerant overcharge if superheat decreases? The equivalent Bayes rule is: $P(\ Ref\text{rigerant}\ \ overcharge \mid Decrease\ in\ Superheat)$

What is the probability of condenser fouling overcharge if superheat decreases? The equivalent Bayes rule is: $P(\ \text{condenser fouling} \mid Decrease\ in\ Superheat)$

Since event A is usually partitioned by sets of event B (B1, B2, B3… Bn), the probability of event A is the sum of the intersection of event A with each of the event B.

$$P(A) = P(A \cap B_1) + P(A \cap B_2) + P(A \cap B_3) + \ \ldots\ldots + P(A \cap B_n) \tag{3.89}$$

$$P(A) = \sum_{j=1}^{n} P\big(A \cap B_j\big) \tag{3.90}$$

Using Equation 3.87, it can be shown that $P(A \cap B) = P(B)P(A|B)$. Therefore $P(A)$ can be expressed as:

$$P(A) = \sum_{j=1}^{n} P(B_j)P(A|B_j) \tag{3.91}$$

Finally, using the Bayes theorem, it can be shown that the probability for each of event B to occur given A is:

$$P(B_i|A) = \frac{P(B_i)P(A|B_i)}{\sum_{j=1}^{n} P(B_j)P(A|B_j)} \tag{3.92}$$

Assuming B1= Refrigerant leakage (RL), B2=Refrigerant Overcharge (RO) and B3= Condenser fouling (CF) and A is the decrease in the superheat flagged by CUSUM, the following can be obtained:

Probability of Refrigerant Leakage due to decrease in superheat:

$$P(RL|\phi_{1=-1}) = \frac{P(RL)\ x\ P(\phi_{1=-1}|RL)}{P(RL)\ x\ P(\phi_{1=-1}|RL) + P(RO)\ x\ P(\phi_{1=-1}|RO) + P(CF)\ x\ P(\phi_{1=-1}|CF)}$$

**$\phi_1$respresents superheat parameter and " $= -1$" indicates decrement

Probability of Refrigerant Overcharge due to decrease in superheat:

$$P(RO|\phi_{1=-1}) = \frac{P(RO)\ x\ P(\phi_{1=-1}|RO)}{P(RL)\ x\ P(\phi_{1=-1}|RL) + P(RO)\ x\ P(\phi_{1=-1}|RO) + P(CF)\ x\ P(\phi_{1=-1}|CF)}$$

Probability of Condenser Fouling due to decrease in superheat:

$$P(CF|\phi_{1=-1}) = \frac{P(CF)\ x\ P(\phi_{1=-1}|CF)}{P(RL)\ x\ P(\phi_{1=-1}|RL) + P(RO)\ x\ P(\phi_{1=-1}|RO) + P(CF)\ x\ P(\phi_{1=-1}|CF)}$$

Using the above equations, the probabilities of refrigerant leakage, refrigerant overcharge and condenser fouling with respect to the decrement in superheat ($\phi_{1=-1}$) can be computed. However, there are many other fault detection parameters utilized in this study, besides superheat. The diagnostics capability of a FDD model can be significantly enhanced using multi fault detection parameters. Based on the CUSUM output matrix, $\boldsymbol{P}$ (Equation 3.78), the diagnostic routine for multiple parameters can be established as follows:

$$P(B_i|\boldsymbol{P}) = \frac{P(B_i)P(\boldsymbol{P}|B_i)}{\sum_{j=1}^{n} P(B_j)P(\boldsymbol{P}|B_j)} \tag{3.92}$$

The probability $P(B_i)$ and the likelihood probability $P(\boldsymbol{P}|B_i)$ are required in order to find the probability of a particular fault to occur with respect to the input matrix, $\boldsymbol{P}$. The computation and estimation of these probabilities can best and easily explained using numerical figures obtained from the experimental data sets. Hence, detail explanations of these probabilities are shown in the Chapter 5. Using these two probabilities, then the posterior probabilities $P(B_i|\boldsymbol{P})$ (e.g probability of condenser fouling to occur due to matrix, $\boldsymbol{P}$) can be easily computed for all the soft faults considered in the thesis. The diagnosis is accomplished once these posterior probabilities are computed.

3.4 Summary

It can be summarized that a minimum of five different fault detection parameters can be employed to detect faults related refrigerant leakage, condenser fouling and refrigerant overcharge. It was clearly demonstrated that CUSUM can be tuned using multiple thresholds to detect the deviation in faults whilst diagnosis of the faults can be computed using

probabilities. The next chapter will be mainly discussing on the development of the experimental test rig and the development of the fault free model.

Chapter 4: Experimental Test Facilities and Fault Free Data Analysis

Introduction

This chapter describes the experimental test facilities used in this study and the fault free analysis of the chiller. The experimental test facility consists of two primary systems, namely the coolant and the refrigerant system. The coolant system was developed to simulate artificial building loads by mixing the evaporator and condenser leaving water. Two mixing chambers with staggered internal baffles were designed to achieve this purpose. The temperature control mechanisms to obtain the desired set points (leaving chilled water temperature and entering cooling water temperature) were accomplished using four units of electric linear modulating valves. These valves were modulated using self developed PID controllers that maintained the coolant temperatures to within 0.15 K of the desired set points. On the other hand, the refrigerant system comprised of a 15kW R22 water-cooled Scroll chiller. The chiller was also fitted with a Pulse Width Modulating (PWM) electronic expansion valve and a variable speed drive. In this study, the chiller data were obtained by varying three operating test variables namely (i) leaving chilled water temperature (ii) entering cooling water temperature and (iii) compressor frequency. The coolant temperatures were controlled using the PID modulating globe valves while the compressor frequency was regulated using the variable speed drive. A steady state period of minimum 15 minutes was allowed before the data were extracted for fault free analysis. The filtered steady state data were then used to compute the following:- (i) entropy generation of the key chiller

components and (ii) fault detection parameters as described in the Chapter 3. Finally, the inputs for fault-free CUSUM data analysis were developed for each of these parameters.

4.1 Development of the Coolant System

The developed coolant system consisted of two mixing chambers, a cooling tower, a water tank, two flow meters, five resistance temperature detectors (RTDs), six positive displacement water pumps and associated valves, four modulating valves, strainers, air vents, flow switches and a network of water pipes. The desired set point of the leaving chilled water temperature, $T_{C,outlet}$ and the entering cooling water temperature, $T_{H,inlet}$ were obtained by mixing the water in respective cold and hot mixing chambers using four units of electric linear modulating valves (PID 1 - 4). The cold and hot chambers served the evaporator and condenser respectively. The chambers were designed with staggered internal baffles to enhance the mixing process. The hot and cold sources of the cold mixing chamber were supplied from the cooling tower return water (using pump 5) and the leaving chilled water from the evaporator respectively. These streams were controlled using PID 2 and PID 4. On the other hand, the PID 1 and PID 3 regulated the cold and hot streams of the hot mixing chamber. The cold stream for this chamber was supplied from the cooling tower return water using pump 3 while the hot stream was obtained from the leaving cooling water from the condenser. The PID 1-4 electric linear modulating globe valves were controlled using PID controllers that were developed using LabView 8.6. These controllers played a critical role in maintaining the coolant temperatures to within 0.15 K of the desired set points.

For the purpose of data acquisition and flow controls of the mixing chambers, five units of 4 wire RTD (±0.15K) were used to measure the following: - (i) Chilled water leaving

temperature / Evaporator outlet water temperature, $T_{C,outlet}$ (ii) Chilled water entering temperature/ Evaporator inlet water temperature $T_{C,inlet}$ (iii) Cooling water leaving temperature / Condenser outlet water temperature $T_{H,outlet}$ (iv) Cooling water entering temperature / Condenser inlet water temperature $T_{H,inlet}$ and (v) cooling tower return water temperature. These temperatures were data logged and used as inputs for the PID controllers. The outlet streams of the cold and hot mixing chambers supplied the coolants at the specified set point temperatures to the respective evaporator and condenser using pump 6 and 1. The flow rates of these feeds could be regulated using bypass valve 13 and 7. Two electromagnetic DANFOSS MAGFLO flow meters, model MAG 5000 and 6000 (accuracy of 0.25%) were used to measure the chilled and cooling water flow rates. The schematic and picture of the developed coolant system is shown in Figure 4.1 and 4.2.

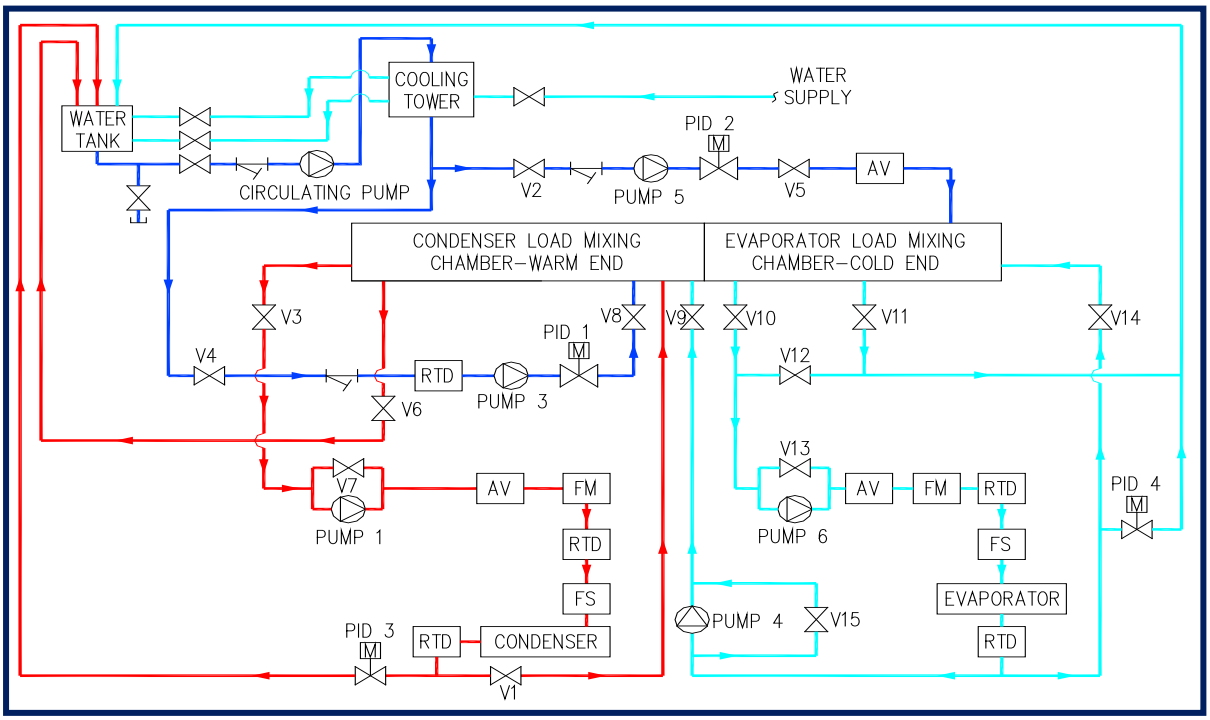

Figure 4.1: Schematic diagram of the coolant system

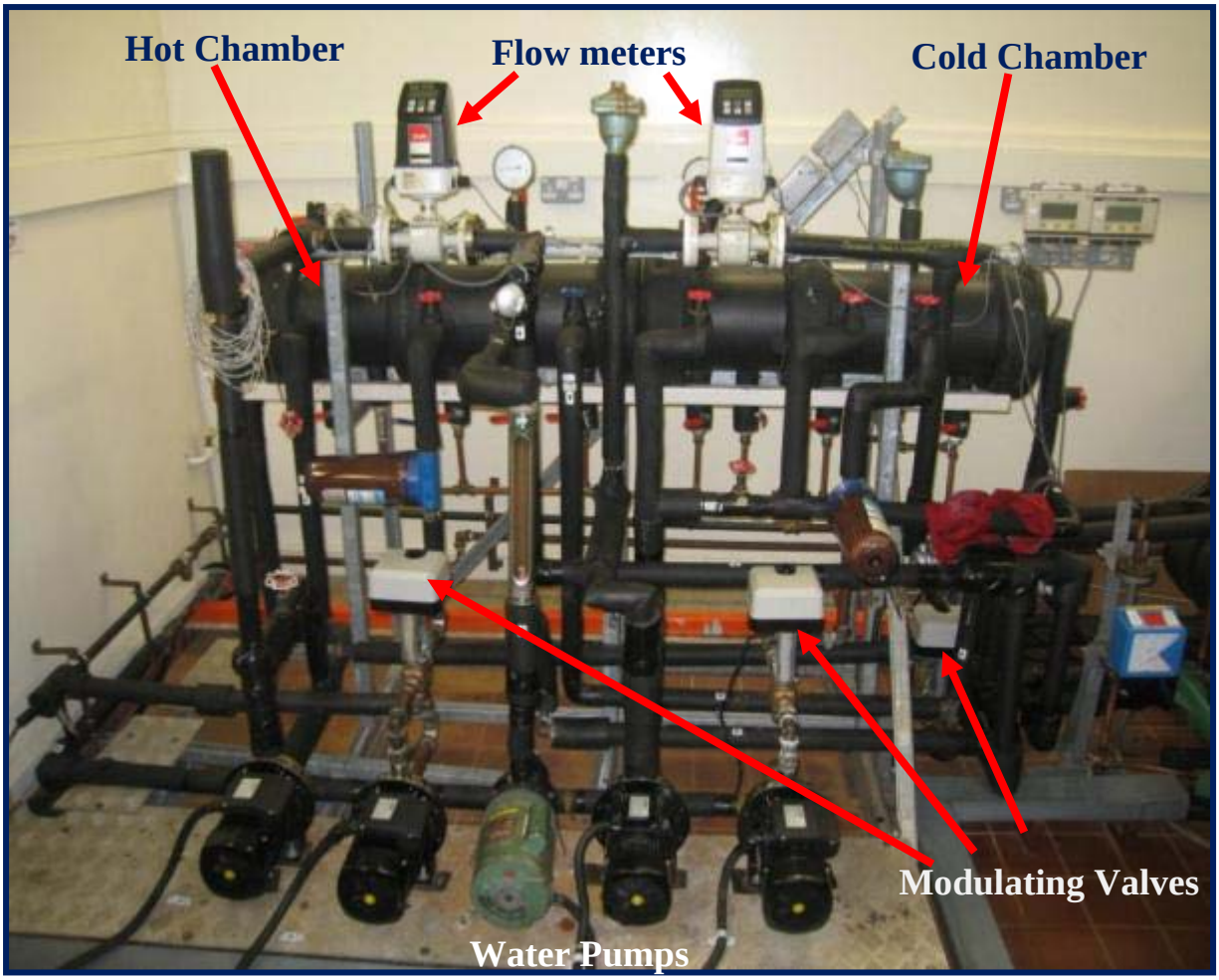

Figure 4.2: Developed coolant system

4.2 Development of the Refrigerant System

The refrigerant system consisted of a R22 scroll compressor, a water-cooled condenser, a direct-expansion water-cooled evaporator, an externally equalized thermostatic and electronic expansion valves, a variable speed drive, seven units of pressure transducers, seven units of 4 wire RTDs, a refrigerant flow meter, a liquid filter dryer unit, shut-off valves, a sight glass and solenoid valve. Extended details of this system are as following:-

i. Refrigerant:

R22 (Chlorodifluoromethane, CHClF2, Molecular mass: 86.5)

ii. Compressor:

COPELAND Scroll compressor, model ZR81 KC-TFD-522, with a nominal 6.8 horsepower.

iii. Evaporator

Direct expansion evaporator; Shell and tube type (with R22 in the tube and water on the shell), 4 passes (refrigerant) with Stainless steel 304 tubes.

iv. Condenser

Shell and tube type (with R22 on the shell and water inside the tube), 4 passes (water) with Stainless steel 304 tubes

v. Thermostatic Expansion Valve:

EMERSON TXV, model HFES 8HC (externally equalized)

vi. Electronic Expansion Valve:

EMERSON PWM EX-2 EXV with EC2-39 Controller. This Pulse Width Modulating (PWM) EXV is basically a slide type solenoid valve with an orifice for expansion. The life time of this EXV is approximately 80 million cycles (equivalent to 15 yr). The valve operates by either fully opening or closing the orifice where the period of this opening/closing sequence is precisely regulated by varying the width of the pulse. In this study, the width of the pulse is controlled using EC2-39 controller that operates with a fixed 6 second pulse width cycle. For example, if 50% of flow or cooling load is required then the EXV will only be held open for the first three seconds.

vii. Variable Speed Drive:

viii. VLT2875, 7.5 kW, 10 HP, 16 A, Three phases 380-460/380-480 VAC. This 3 phase variable speed drive is connected to the Copeland Scroll compressor to vary the compressor frequency. It is necessary to vary to the frequency to capture the part load performance of this chiller. In fact, frequency control is one of the operating test variables used this study

ix. Refrigerant Flow meter:

KROHNE , Model 29/RR/M9/es; Range: 36-360 L/hr; Accuracy: 1.6% F.S

x. Power Meter:

HIOKI, Model 3184, measures the electrical power consumption of the whole chiller system, with an accuracy of ±0.01kW.

xi. Pressure Transducers:

Low Pressure (Evaporator) measurements: Gems Sensors Pressure Transducer Model:1200BGB1001A3UA; Output : 4-20ma, two wire , Range : 0-10 barG , Accuracy: 0.5 % F.S

High Pressure (Condenser) measurements: Gems Sensors Pressure Transducer Model: 1200BGB2501A3UA; Output : 4-20ma, two wire , Range : 0-25 barG , Accuracy: 0.5 % F.S

xii. Temperature Compensated Pressure Gauges:

Low Pressure (Evaporator) measurements: ASHCROFT , Range : 0-200 psiG , Accuracy: 0.5 psi

High Pressure (Condenser) measurements: ASHCROFT , Range : 0-300 psiG , Accuracy: 1.0 psi

xiii. Temperature Probes:

4 wire RTD, PT100, 1/3 DIN (±0.15K)

The temperature and pressure transducers were installed at the following locations:- (i) compressor discharge line (TP1), (ii) condenser inlet (TP2), (iii) condenser outlet (TP3), (iv) liquid line before expansion valve (TP4), (v) evaporator inlet (TP5), (vi) evaporator outlet (TP6) , and (vii) compressor suction line (TP7). This schematic is shown in Figure 4.3. The major equipment of this refrigerant system is shown in the Figure 4.4 and 4.5.

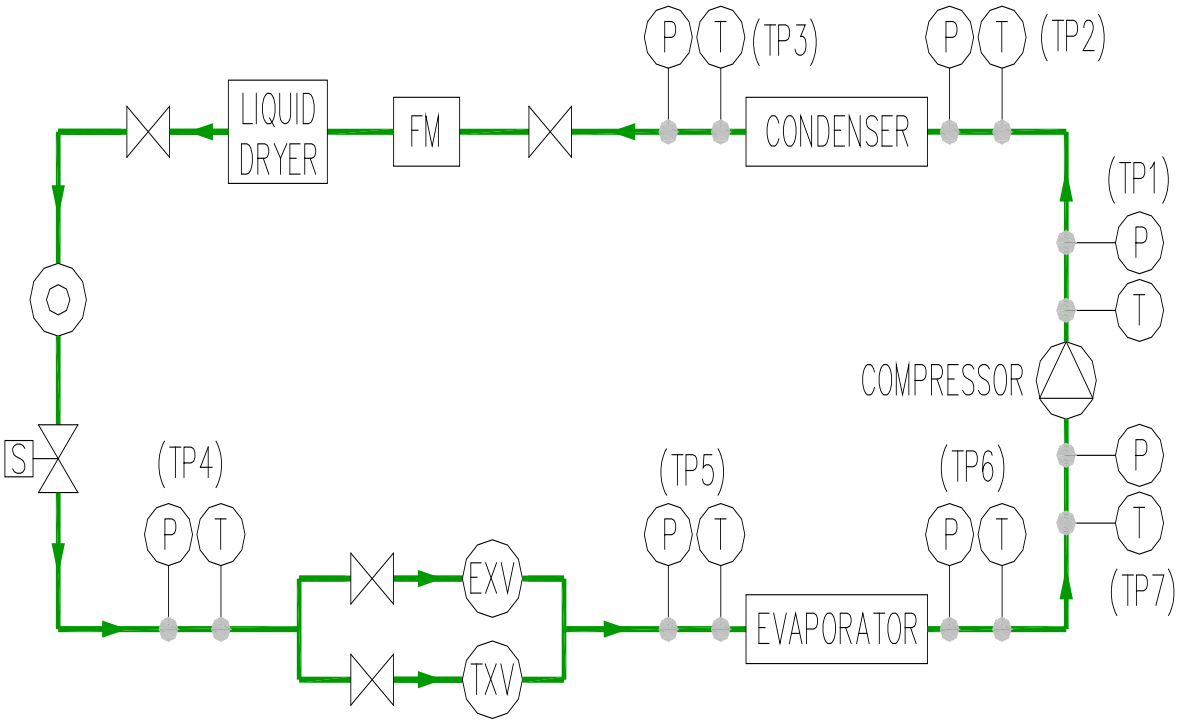

Figure 4.3: Location of the pressure (P) and temperature (T) sensors in the refrigerant system

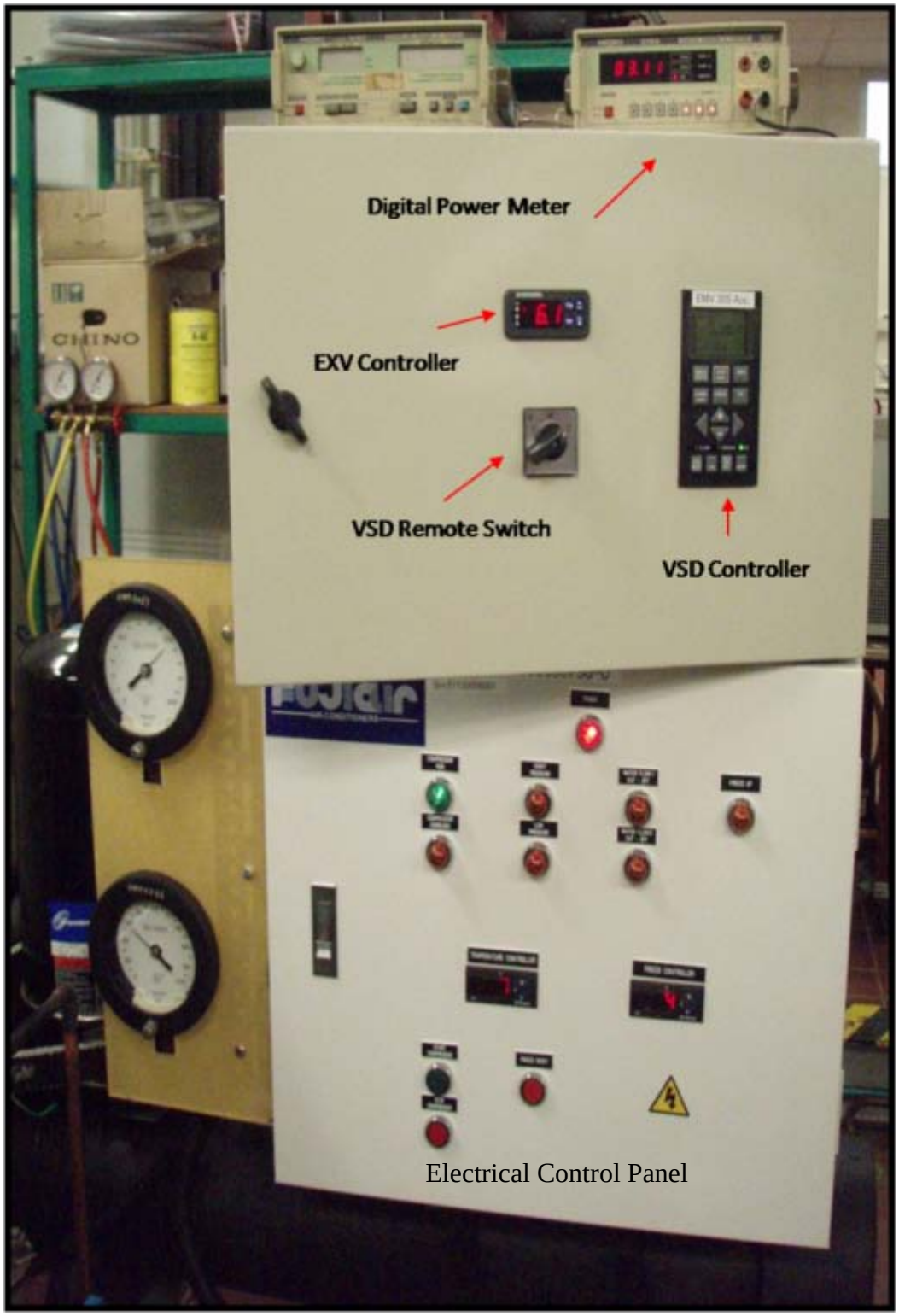

Figure 4.4: Front view of the refrigerant system

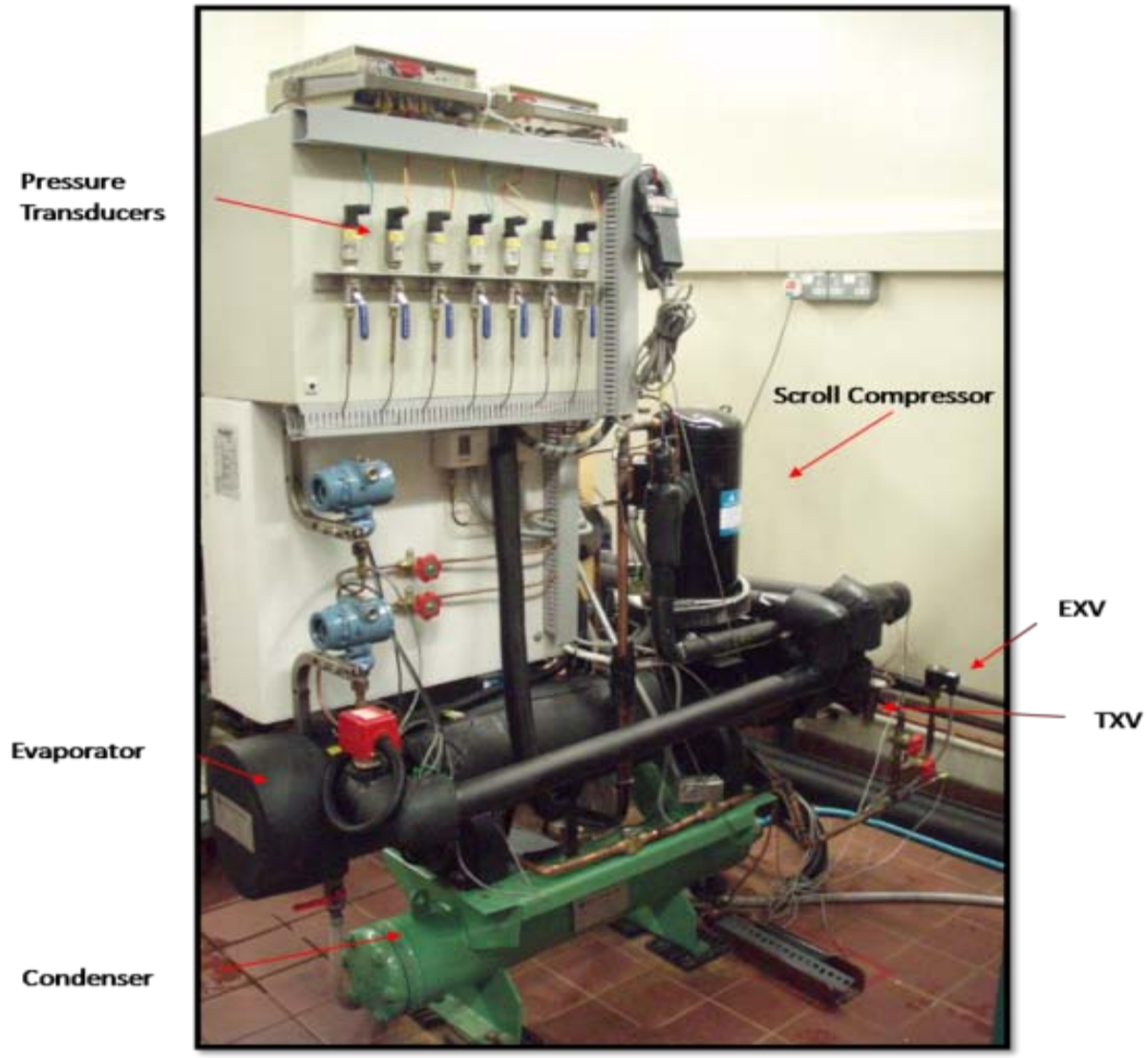

Figure 4.5: Rear view of the refrigerant system

4.3 Data Acquisition and PID control

A HP Agilent 34970A data logger was used to acquire the following data:

i. Refrigerant Pressures [kPa] and Temperatures [^{o}C] at the specified seven locations shown in Figure 4.3

ii. Refrigerant Flow rate [Lph]

iii. Compressor power [kW)]

iv. Coolant temperatures (inlet and outlet water temperatures of the evaporator and condenser) [^{o}C]

v. Cooling tower return water temperature (used in the mixing the chambers) [^{o}C]

vi. Coolant Flow rates (chilled and cooling water flow rates) [Lpm]

The above-mentioned data were sampled at 10 second intervals. The acquired data were then processed and analyzed using LabView 8.6. The incoming raw data were corrected to their respective calibration coefficients before being used to calculate useful parameters such as cooling load, energy balance, entropy generation etc. The developed LabView environment was also incorporated with R22 thermodynamic properties, where multiple interpolation routines were written to compute the enthalpy and entropy of the refrigerant using the measured pressure and corresponding temperature data. The developed data acquisition and flow control unit is shown in Figure 4.6.

For flow control purposes, a separate PID algorithm was developed using the similar LabView environment to operate the four PID valves (PID 1- 4). This PID loop was executed at an interval of five seconds (twice as fast as the data acquisition rate) in order to maintain the desired temperature set points at acceptable deviations of 0.15K. The inputs for this PID algorithm were the leaving chilled water temperature, entering cooling water temperature and cooling tower return temperature. Figures 4.7 and 4.8 demonstrates the efficacy of the developed PID routine in maintaining the set points at acceptable tolerance for both the leaving chilled water and entering cooling water temperatures during steady state.

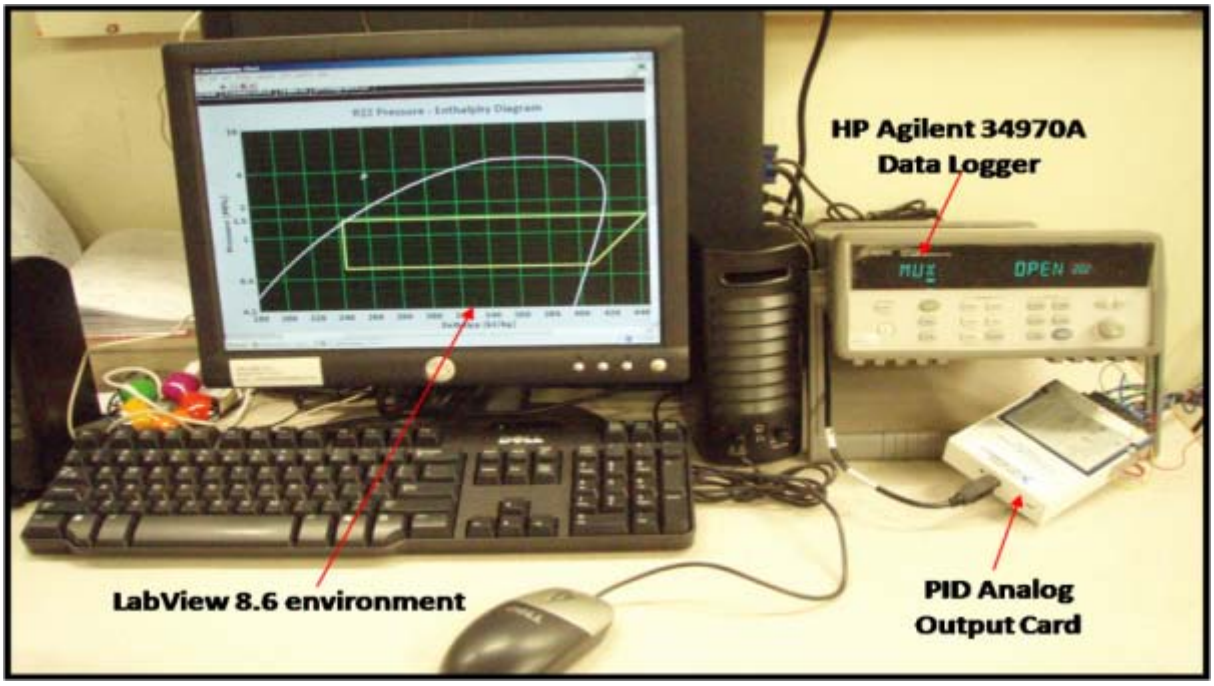

Figure 4.6: Data acquisition and flow control system (complete with pH diagram)

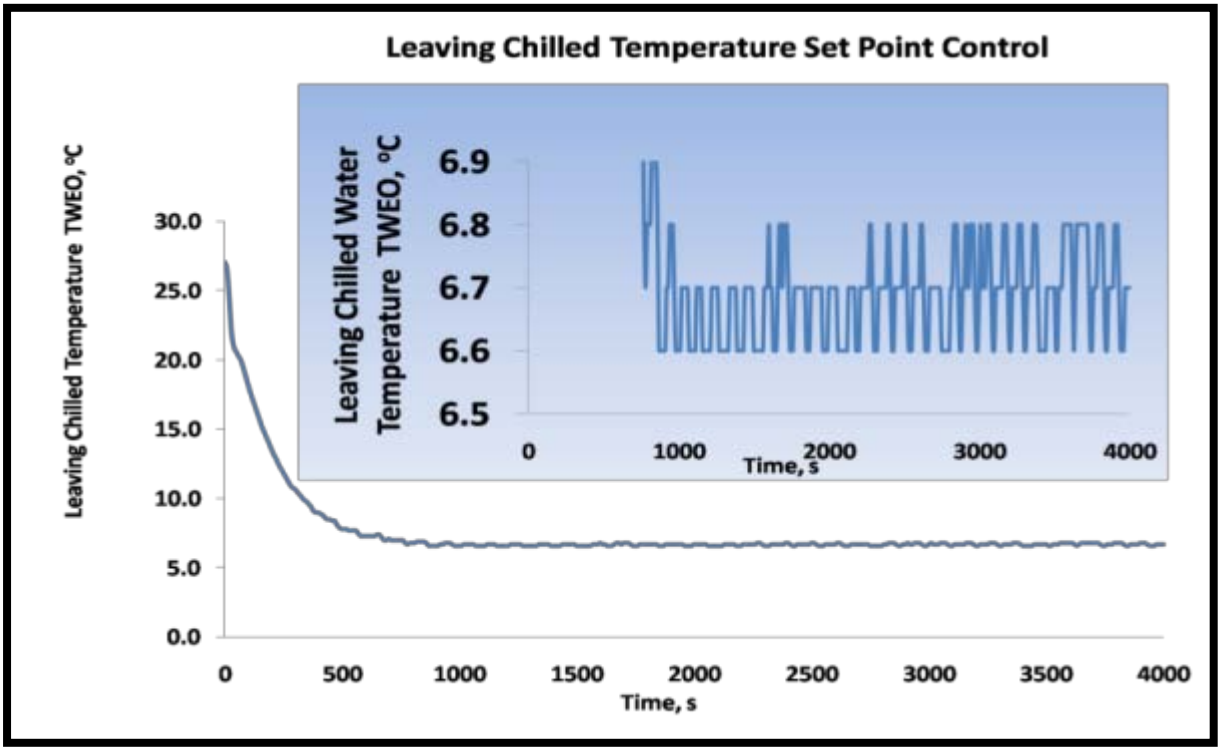

Figure 4.7: Good control of the leaving chilled water set point temperature (6.7oC). The deviation during steady state is less than 0.15 K (blue insert)

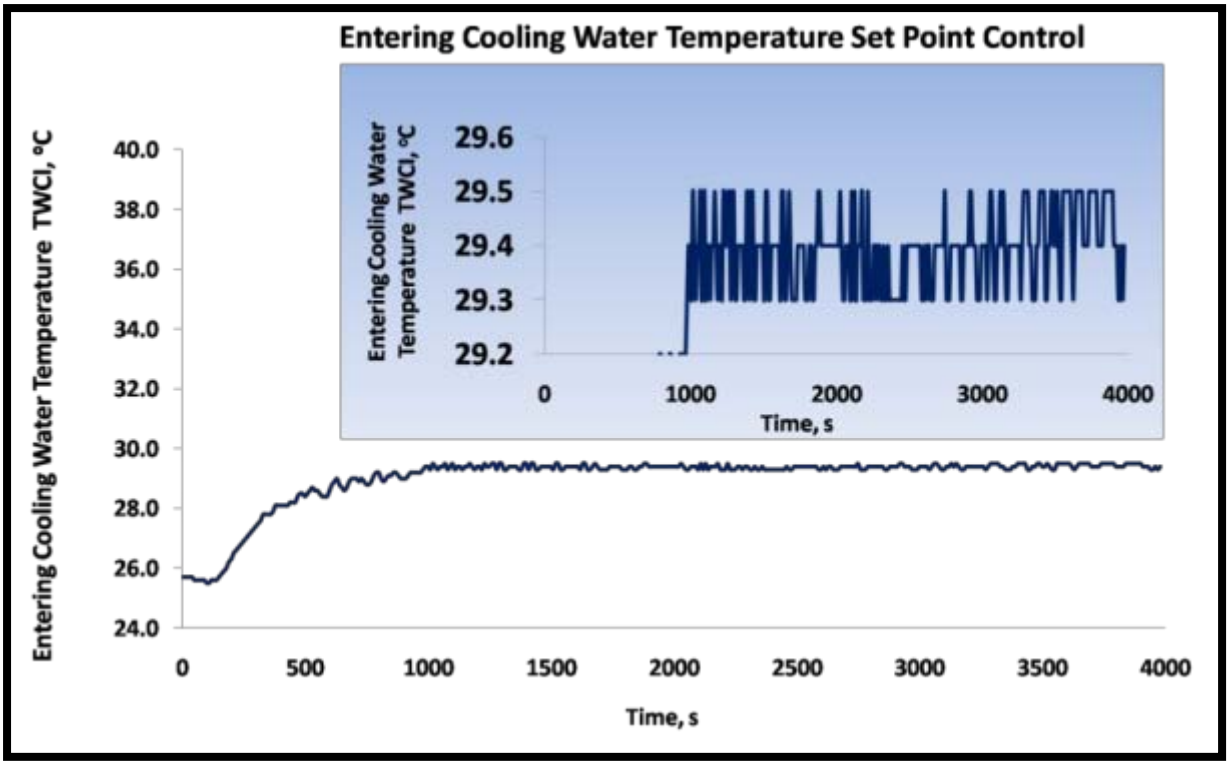

Figure 4.8: Good control of the entering cooling water set point temperature (29.4oC). The deviation during steady state is less than 0.15 K (blue insert)

4.4 Steady state Analysis

In this study, leaving chilled water temperature ($T_{C,outlet}$), entering cooling water temperature ($T_{H,inlet}$), and compressor frequency were used as operating test variables. These parameters were fixed as reference points for all the test runs (for both fault and fault-free chiller operations). For each test run, these set point parameters were varied as shown in Table 4.1. A total of 20 different set points were used to capture both the full and part load performance of the chiller. The coolant set points were controlled using the PID controlled valves while the compressor speed were regulated using the variable speed drive. Deviations in the set points were kept to minimal using these high accuracy devices.

Table 4.1: Test matrix used in this study for all the test runs

Set Point	Frequency (Hz)	$T_{C,outlet}$ (^{o}C)	$T_{H,inlet}$ (^{o}C)	Set Point	Frequency (Hz)	$T_{C,outlet}$ (^{o}C)	$T_{H,inlet}$ (^{o}C)
1	50	8.0	28.0	11	35	8.0	28.0
2	50	7.0	28.0	12	35	7.0	28.0
3	50	6.0	28.0	13	35	6.0	28.0
4	50	6.7	29.4	14	35	6.7	29.4
5	50	6.0	30.0	15	35	6.0	30.0
6	50	8.0	30.0	16	35	8.0	30.0
7	50	9.0	30.0	17	35	9.0	30.0
8	50	9.0	32.0	18	35	9.0	32.0
9	50	8.0	32.0	19	35	8.0	32.0
10	50	6.0	32.0	20	35	6.0	32.0

The specified set points along with cooling load and the overall system energy balance were used as steady state indicators of the chiller. The scroll chiller used in this study was assumed to be in a steady state if deviations in the steady indicators were below than their allowable tolerance for a minimum period of 15 minutes. The maximum allowable deviation for each steady indicator is as following:-

i. 0.15 K tolerance for the leaving chilled water temperature
ii. 0.15 K tolerance for the entering cooling water temperature
iii. 0.1 Hz tolerance for the compressor frequency
iv. 5% tolerance in the cooling load for full load data and 7.7% tolerance at a part load of 70%

v. 5% tolerance in the overall system energy balance for full load data and 7.7% tolerance at a part load of 70%

vi. 5% tolerance in both the rated cooling water and chilled water flow rate. The rated cooling water and the chilled water flow rates are 48.7 Lpm and 38.6 Lpm respectively.

The allowable tolerances for cooling load and overall system energy balance were obtained from the following (ARI 550/590):-

$$Allowable\ Tolerance(\%) = 10.5 + \frac{833.3}{DT_{FL}\ x\ \%\ FL} - 0.07x\ \%\ FL \quad (4.1)$$

Where DT_{FL} is the temperature between the entering and leaving chilled water at full load and $\%\ FL$ is the percentage of full load, i.e 75%, 60%

At full load, DT_{FL} is approximately 5.5 K and the full load tolerance can be obtained as following:-

$$Allowable\ Tolerance(\%) = 10.5 + \frac{833.3}{5.5\ x\ 100} - 0.07x\ 100 = 5.0\% \quad (4.2)$$

At part load, the compressor frequency was ramped down to 35Hz which equates to 70% part load. Thus, the tolerance at 35Hz part load can be computed as below:-

$$Allowable\ Tolerance(\%) = 10.5 + \frac{833.3}{5.5\ x\ 70} - 0.07x\ 70 = 7.7\ \% \quad (4.3)$$

This thesis also adopted the Chauvenet's criterion for a stricter secondary steady state filtration. This theorem is used to eliminate outliers in steady state data. It states that: For n number of points, a reading can be rejected if the probability of obtaining the particular deviation from the set point is less than ½ n. The simplified Chauvenet's theorem indicates

that a particular reading can be rejected if its ratio of deviation from the specified set point to the standard deviation ($|d_i|/S$) is larger than the maximum ratio, $(|d|/S)_{max}$ as shown in Table 4.2.

Table 4.2: Ratio of maximum acceptable deviation to standard deviation

Number of Readings, n	Ratio of maximum acceptable deviation to standard deviation, $(|d|/S)_{max}$
3	1.38
4	1.54
5	1.65
6	1.73
7	1.8
8	1.87
9	1.91
10	1.96
15	2.13
20	2.24
25	2.33
50	2.57
100	2.81
300	3.14
500	3.29
1,000	3.48

In our study, the minimum steady state period was 15 minutes and the data were logged at 10 seconds interval. Therefore, a total of 900 readings were collected during this period. From Chauvenet's theorem (Table 4.2), any of the 900 readings is considered as an outlier if its ($|d_i|/S$) is larger than 3.442.

4.5 Fault-Free Data Sets

A total of 10 fault-free test runs (hereinafter named as **Normal 0,Normal 1, Normal 2, Normal 3,…… and Normal 9**) were conducted in this study to demonstrate the consistency and repeatability of the obtained data. Some of the fault-free test run were used as reference points to ensure that the chiller system has attained its nominal condition and met the bench mark values before being simulated with other types of faults. For instance, after the simulation of refrigerant leakage, the chiller was recharged to its original capacity and tested against other fault-free bench mark data before being evaluated for different type of faults such as fouling and refrigerant overcharge. Table 4.3 shows the entire logged and computed steady state data obtained from one of the fault-free data sets, **Normal 0.** The data shown in Table 4.3 spanned across the twenty set points indicated in Table 4.1 and were filtered to meet the specified steady state criterions. Based on these acquired and computed data, the entropy generations and fault detection parameters described in chapter 3 were evaluated for each of the 10 fault-free data sets.

Table 4.3: Refrigerant system temperature of data set Normal 0

Point	T SUC ^{o}C	T DIS ^{o}C	T CONDI ^{o}C	T CONDO ^{o}C	T XVI ^{o}C	T EVAI ^{o}C	T EVAO ^{o}C	T EVAO WALL ^{o}C	T SUPERHEAT ^{o}C	T SUBCOOLING ^{o}C
1	4.9	79.0	77.7	40.3	39.4	1.1	4.3	5.0	5.4	1.2
2	3.9	79.3	78.0	40.0	39.3	0.1	3.4	4.4	5.5	1.1
3	2.7	80.4	79.1	39.4	38.6	-1.1	2.3	3.1	5.4	1.3
4	3.4	81.9	80.5	40.9	40.0	-0.4	3.0	3.8	5.4	1.3
5	2.6	83.5	82.0	41.1	40.2	-1.1	2.1	2.9	5.3	1.4
6	5.0	82.2	80.8	42.0	41.1	1.2	4.1	4.9	5.5	1.3
7	6.1	81.8	80.5	42.5	41.6	2.3	5.8	6.2	5.5	1.4
8	6.0	84.4	83.0	44.3	43.3	2.4	5.8	6.2	5.3	1.4
9	4.9	85.1	83.5	43.7	42.8	1.1	3.9	4.8	5.4	1.4
10	2.7	87.1	85.5	43.0	42.2	-1.1	2.0	2.9	5.3	1.4
11	5.5	69.0	67.8	36.9	36.2	1.8	5.3	5.9	4.3	0.9
12	4.5	69.3	68.0	36.6	35.9	0.8	4.1	4.8	4.2	1.0
13	3.4	69.7	68.5	36.3	35.6	-0.2	2.7	3.7	4.0	1.0
14	4.2	71.3	70.0	37.7	37.0	0.6	3.7	4.5	4.2	1.1
15	3.4	73.0	71.6	38.2	37.4	-0.1	2.5	3.7	4.0	1.0
16	5.5	72.2	70.9	38.8	38.1	1.9	4.8	5.9	4.2	1.1
17	6.5	71.8	70.5	39.1	38.3	2.9	6.1	6.8	4.1	1.1
18	6.6	74.6	73.2	40.7	40.0	2.9	6.2	6.9	4.0	1.2
19	5.5	75.2	73.8	40.5	39.7	1.9	4.9	5.8	4.3	1.2
20	3.4	76.0	74.5	39.9	39.1	-0.1	2.5	3.8	4.0	1.2

Table 4.3b: Coolant system temperature and flow rate of data set Normal 0

Point	T AMB ^{o}C	TWEI ^{o}C	TWEO ^{o}C	DEL T EVA ^{o}C	TWCI ^{o}C	TWCO ^{o}C	DEL T COND ^{o}C	TCT ^{o}C	Chilled Water Flow LPM	Cooling Water Flow LPM
1	22.2	13.7	8.0	5.7	28.0	33.9	5.9	25.5	38.5	48.7
2	22.8	12.5	7.0	5.5	28.0	33.8	5.7	26.1	38.7	48.5
3	22.0	11.4	6.0	5.4	28.0	33.5	5.5	25.9	38.3	48.7
4	22.1	12.1	6.7	5.4	29.4	35.0	5.6	25.7	38.5	48.7
5	22.0	11.2	6.0	5.2	30.0	35.5	5.5	25.4	38.6	48.6
6	22.0	13.7	8.0	5.6	30.0	35.8	5.9	25.4	38.6	48.6
7	22.0	14.8	9.0	5.8	30.0	36.0	6.0	25.1	38.9	48.7
8	22.1	14.7	9.0	5.7	32.0	38.0	6.0	25.1	38.8	48.7
9	22.0	13.4	7.9	5.5	32.0	37.8	5.8	25.1	38.7	48.8
10	24.6	11.1	5.9	5.2	32.0	37.5	5.5	25.3	38.3	48.7
11	22.7	12.3	8.0	4.3	28.0	32.2	4.3	25.4	38.7	48.6
12	22.8	11.2	7.0	4.2	28.0	32.1	4.1	25.2	38.5	48.4
13	22.7	10.0	6.0	4.0	28.0	32.0	4.0	25.3	38.5	48.6
14	22.5	10.8	6.7	4.1	29.4	33.5	4.1	25.2	38.4	48.4
15	26.1	9.9	6.0	3.9	30.0	34.0	4.0	25.5	38.7	48.9
16	27.3	12.2	8.0	4.2	30.1	34.3	4.2	25.2	38.6	48.9
17	27.2	13.3	9.0	4.3	30.0	34.3	4.3	25.2	38.7	48.9
18	27.0	13.2	9.0	4.2	32.0	36.2	4.3	25.1	39.1	48.8
19	26.8	12.0	8.0	4.1	32.0	36.2	4.2	25.1	38.9	48.7
20	26.4	9.8	6.0	3.8	32.0	35.9	3.9	25.3	38.8	48.8

Table 4.3c: Refrigerant flow rate and pressure of data set Normal 0

Point	R22 Flow Rate Lph	P SUC barg	P DIS barg	P CONDI barg	P CONDO barg	P VX IN barg	P EVAI barg	P EVAO barg
1	331.8	3.9	15.1	14.9	14.9	14.8	4.2	3.9
2	305.3	3.7	15.0	14.8	14.7	14.7	4.0	3.7
3	288.7	3.5	14.7	14.6	14.6	14.5	3.8	3.5
4	312.5	3.7	15.3	15.2	15.1	15.0	3.9	3.6
5	302.2	3.6	15.4	15.3	15.3	15.1	3.8	3.5
6	303.0	3.9	15.8	15.6	15.6	15.5	4.2	3.9
7	306.2	4.1	15.9	15.8	15.8	15.7	4.4	4.0
8	315.5	4.1	16.7	16.6	16.6	16.4	4.4	4.1
9	377.1	3.9	16.5	16.3	16.4	16.1	4.2	3.9
10	333.7	3.6	16.2	16.0	16.0	15.9	3.8	3.5
11	197.8	4.2	13.7	13.6	13.5	13.5	4.3	4.1
12	284.7	4.0	13.6	13.5	13.4	13.4	4.2	4.0
13	203.9	3.9	13.5	13.4	13.3	13.3	4.0	3.8
14	215.4	4.0	14.0	14.0	13.9	13.8	4.1	3.9
15	231.5	3.9	14.2	14.1	14.0	14.0	4.0	3.8
16	253.1	4.2	14.4	14.3	14.3	14.2	4.3	4.1
17	256.9	4.4	14.5	14.4	14.4	14.2	4.5	4.3
18	206.8	4.4	15.2	15.1	15.1	14.9	4.5	4.3
19	322.6	4.2	15.1	15.0	15.0	14.8	4.4	4.2
20	224.6	3.9	14.9	14.8	14.7	14.6	4.0	3.8

Table 4.3d: Computed heat loads, power, COP, energy balance and enthalpy of the refrigerant system of data set Normal 0

Point	Q EVA kW	POWER kW	Q COND kW	COP	EB %	H SUC kJ/kg	H DIS kJ/kg	H COND IN kJ/kg	H COND OUT kJ/kg	H XV IN kJ/kg	H EVA IN kJ/kg	H EVA OUT kJ/kg
1	15.5	4.6	20.0	3.4	1.3	408.8	450.4	449.4	250.0	248.9	248.9	408.4
2	15.0	4.6	19.5	3.3	1.2	408.5	450.8	449.8	249.6	248.7	248.7	408.1
3	14.4	4.5	18.8	3.2	1.5	407.9	452.0	451.0	248.8	247.7	247.7	407.7
4	14.6	4.7	19.1	3.1	2.2	408.3	452.5	451.5	250.8	249.6	249.6	407.9
5	14.2	4.7	18.7	3.0	2.0	407.9	453.8	452.7	251.1	249.9	249.9	407.6
6	15.2	4.8	19.9	3.2	1.5	408.9	452.3	451.3	252.3	251.1	251.1	408.3
7	15.8	4.9	20.5	3.2	1.3	409.3	451.7	450.7	253.0	251.8	251.8	409.2
8	15.5	5.1	20.4	3.0	1.2	409.2	453.0	451.9	255.4	254.1	254.1	409.1
9	15.0	5.0	19.8	3.0	1.6	408.8	453.9	452.7	254.6	253.3	253.3	408.1
10	13.8	4.9	18.7	2.8	1.6	407.9	456.0	454.8	253.7	252.6	252.6	407.5
11	11.6	3.0	14.5	3.9	1.4	408.7	443.5	442.6	245.6	244.6	244.6	408.7
12	11.2	2.9	14.0	3.9	1.7	408.2	443.9	443.0	245.2	244.2	244.2	408.1
13	10.8	2.9	13.6	3.7	1.9	407.8	444.4	443.5	244.8	243.9	243.9	407.4
14	11.0	3.0	13.9	3.7	1.5	408.1	445.1	444.0	246.6	245.6	245.6	407.9
15	10.6	3.1	13.6	3.5	2.1	407.8	446.3	445.3	247.2	246.2	246.2	407.2
16	11.3	3.1	14.4	3.6	1.2	408.6	445.3	444.3	248.1	247.1	247.1	408.2
17	11.7	3.1	14.7	3.7	1.3	409.0	444.9	443.9	248.4	247.4	247.4	408.9
18	11.5	3.2	14.6	3.6	1.3	409.0	446.5	445.4	250.6	249.6	249.6	408.9
19	11.0	3.2	14.2	3.5	1.3	408.7	447.1	446.0	250.3	249.2	249.2	408.3
20	10.4	3.2	13.4	3.2	2.4	407.8	448.0	446.9	249.5	248.4	248.4	407.2

Table 4.3e: Computed entropy, density and saturation temperature of the refrigerant system of data set Normal 0

Point	S SUC kJ/kgK	S DIS kJ/kgK	S COND IN kJ/kgK	S COND OUT kJ/kgK	S XV IN kJ/kgK	S EVA IN kJ/kgK	S EVA OUT kJ/kgK	DENSITY @ COND OUT kg/m^3	EVA SAT ^{o}C	COND SAT ^{o}C
1	1.766	1.797	1.795	1.168	1.164	1.178	1.764	1127.6	0.4	41.6
2	1.768	1.799	1.797	1.166	1.163	1.178	1.767	1128.8	-0.7	41.2
3	1.769	1.804	1.802	1.164	1.160	1.176	1.768	1131.6	-1.8	40.7
4	1.768	1.802	1.800	1.170	1.166	1.182	1.767	1125.2	-1.1	42.2
5	1.768	1.805	1.803	1.171	1.167	1.183	1.768	1124.2	-1.8	42.5
6	1.766	1.799	1.797	1.175	1.171	1.186	1.764	1120.0	0.3	43.3
7	1.765	1.797	1.795	1.177	1.173	1.188	1.764	1117.9	1.4	43.8
8	1.764	1.797	1.795	1.184	1.180	1.196	1.763	1109.7	1.6	45.7
9	1.766	1.801	1.798	1.182	1.178	1.194	1.763	1112.3	0.4	45.2
10	1.769	1.808	1.805	1.179	1.176	1.193	1.768	1115.5	-1.8	44.4
11	1.760	1.785	1.783	1.154	1.151	1.162	1.762	1142.2	1.3	38.0
12	1.761	1.787	1.785	1.152	1.149	1.161	1.762	1143.4	0.6	37.7
13	1.762	1.789	1.787	1.151	1.148	1.161	1.762	1144.7	-0.4	37.4
14	1.762	1.788	1.785	1.157	1.154	1.166	1.762	1138.7	0.3	38.9
15	1.762	1.791	1.788	1.158	1.156	1.169	1.761	1136.9	-0.4	39.3
16	1.760	1.786	1.784	1.161	1.158	1.171	1.759	1134.0	1.6	40.0
17	1.758	1.785	1.782	1.163	1.159	1.172	1.759	1133.0	2.5	40.2
18	1.758	1.786	1.783	1.169	1.166	1.179	1.759	1125.6	2.6	41.9
19	1.760	1.788	1.785	1.168	1.165	1.178	1.759	1126.8	1.8	41.7
20	1.762	1.792	1.789	1.166	1.162	1.177	1.761	1129.4	-0.3	41.1

4.6 Entropy Generation and Lost Work Analysis

Based on the Second Law of Thermodynamics derivations as described in Equation 3.12 of Chapter 3, the entropy generation of the key chiller components was computed based on refrigerant pressures and temperatures. The entropy and enthalpy values were obtained from NIST Refprop using these measured parameters. Table 4.5 shows the calculated entropy generation of the chiller components for all the 20 set points of data set Normal 0. Also shown in this subsection is the prediction of actual compressor power consumption using the computed total entropy generation. Using Equations 3.38 (or 3.37) and 3.13i as outlined in the Chapter 3, the compressor power were predicted by calculating the reversible and lost work of the system. For data set Normal 0, the details of compressor power prediction is shown in Table 4.4. The accuracy of the prediction can also be seen from Figure 4.9.

Table 4.4: Compressor power prediction from the lost work (data set Normal 0)

Point	$T_{ambient}$ K	$\dot{S}_{gen,Total}$ kW/K (E-02)	$T_{H,outlet\ Carnot}$ K	$\dot{W}_{reversible}$ kW	$\dot{W}_{Lost\ work}$ kW	Predicted Power kW	Actual Power kW	Diff %
1	295.3	1.172	306.0	1.16	3.46	4.62	4.61	0.2
2	296.0	1.160	305.9	1.18	3.43	4.61	4.59	0.4
3	295.2	1.134	305.7	1.19	3.35	4.53	4.53	0.1
4	295.3	1.170	307.1	1.24	3.46	4.70	4.69	0.1
5	295.2	1.163	307.6	1.29	3.43	4.73	4.71	0.3
6	295.2	1.202	308.0	1.27	3.55	4.81	4.80	0.3
7	295.2	1.242	308.1	1.25	3.67	4.92	4.90	0.4
8	295.3	1.263	310.1	1.36	3.73	5.09	5.08	0.2
9	295.2	1.227	309.9	1.38	3.62	5.00	5.00	0.0
10	297.8	1.199	309.6	1.36	3.57	4.93	4.90	0.6
11	295.9	0.744	304.8	0.85	2.20	3.05	3.00	1.8
12	295.9	0.706	304.7	0.87	2.09	2.95	2.91	1.5
13	295.8	0.700	304.6	0.88	2.07	2.95	2.90	1.6
14	295.6	0.716	306.0	0.92	2.12	3.04	3.00	1.3
15	299.3	0.724	306.5	0.93	2.17	3.10	3.05	1.5
16	300.5	0.738	306.8	0.90	2.22	3.12	3.10	0.6

17	300.4	0.760	306.8	0.89	2.28	3.17	3.10	2.2
18	300.1	0.776	308.7	0.96	2.33	3.29	3.24	1.7
19	299.9	0.745	308.6	0.97	2.23	3.20	3.20	0.1
20	299.5	0.748	308.5	1.00	2.24	3.24	3.20	1.2

The prediction accuracy of the compressor power from the lost work computations for all the other nine fault free data sets are shown in Figure 4.10. An accurate prediction for all the fault free data sets can be observed.

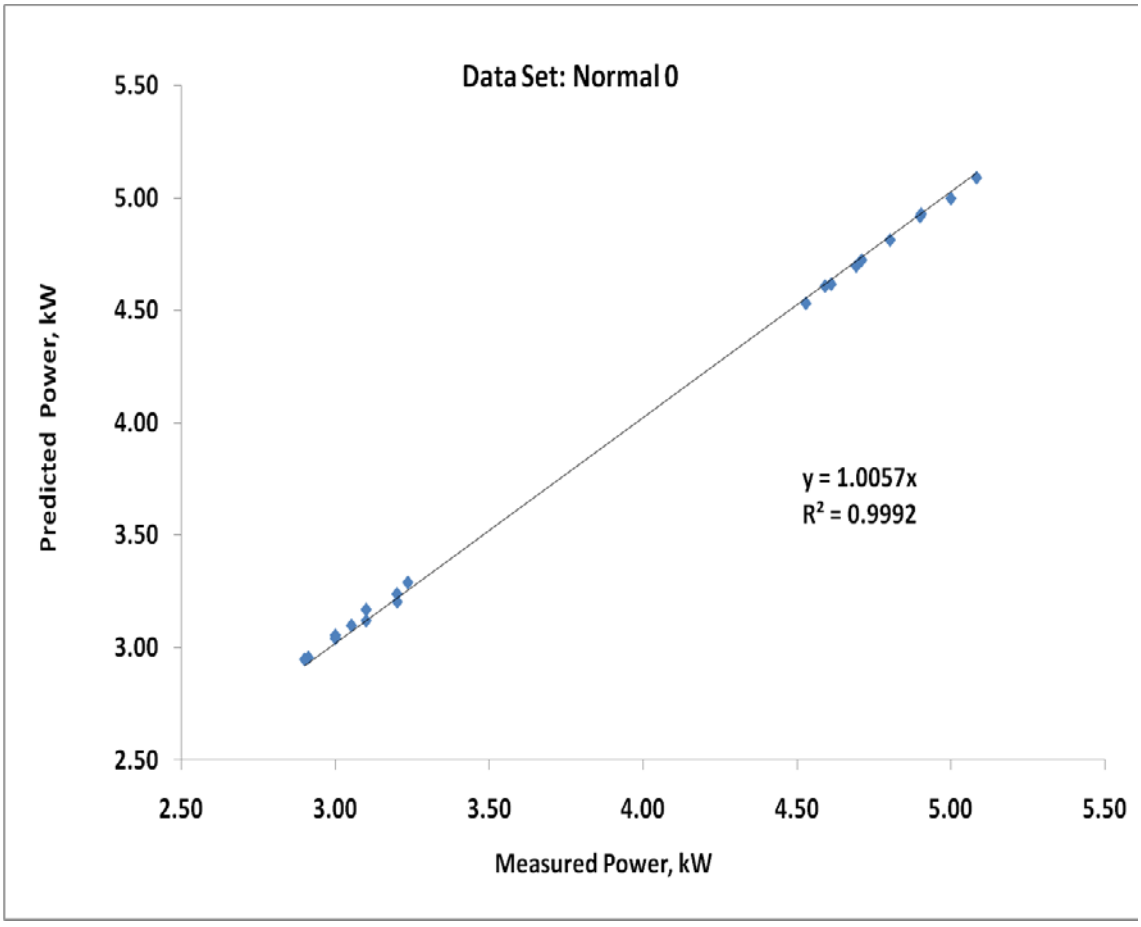

Figure 4.9: Predicted and measured compressor power (data set Normal 0)

Table 4.5: Entropy generation of the chiller components for all the 20 set points of data set Normal 0

Point	Ref Mass Flow, kg/s	$\dot{S}_{gen,71}$ Evaporator kW/K	$\dot{Q}_{12}$ Suction kW	$\dot{S}_{gen,12}$ Suction kW/K	$\dot{Q}_{23}$ Compressor kW	$\dot{S}_{gen,23}$ Compressor kW/K	$\dot{Q}_{34}$ Discharge kW	$\dot{S}_{gen,34}$ Discharge kW/K
1	0.097	1.844E-03	0.04	1.292E-05	-0.57	5.030E-03	-0.09	1.216E-04
2	0.094	1.820E-03	0.03	3.194E-05	-0.60	5.035E-03	-0.09	1.137E-04
3	0.090	1.761E-03	0.03	7.024E-06	-0.57	5.078E-03	-0.09	1.068E-04
4	0.092	1.786E-03	0.03	1.145E-05	-0.62	5.272E-03	-0.10	1.257E-04
5	0.090	1.730E-03	0.03	2.559E-05	-0.58	5.293E-03	-0.10	1.279E-04
6	0.097	1.822E-03	0.06	2.144E-05	-0.60	5.263E-03	-0.10	1.392E-04
7	0.100	1.859E-03	0.02	3.368E-05	-0.65	5.432E-03	-0.10	1.409E-04
8	0.100	1.769E-03	0.02	1.642E-05	-0.69	5.690E-03	-0.11	1.172E-04
9	0.097	1.781E-03	0.07	1.073E-05	-0.64	5.538E-03	-0.11	1.172E-04
10	0.089	1.731E-03	0.04	4.685E-05	-0.62	5.571E-03	-0.11	1.265E-04
11	0.071	1.134E-03	0.00	8.815E-05	-0.53	3.556E-03	-0.07	4.501E-05
12	0.068	1.069E-03	0.01	7.176E-05	-0.47	3.355E-03	-0.06	6.041E-05
13	0.066	1.038E-03	0.03	7.823E-05	-0.48	3.408E-03	-0.06	6.305E-05
14	0.068	1.062E-03	0.02	6.705E-05	-0.50	3.458E-03	-0.07	7.799E-05
15	0.066	1.020E-03	0.04	7.589E-05	-0.52	3.594E-03	-0.07	7.979E-05
16	0.070	1.054E-03	0.03	3.155E-05	-0.52	3.581E-03	-0.07	8.204E-05
17	0.072	1.073E-03	0.01	8.804E-05	-0.51	3.585E-03	-0.07	6.532E-05
18	0.072	1.068E-03	0.01	8.994E-05	-0.54	3.784E-03	-0.08	8.690E-05
19	0.069	1.023E-03	0.03	3.368E-06	-0.54	3.722E-03	-0.07	5.638E-05
20	0.066	9.833E-04	0.04	6.355E-05	-0.56	3.836E-03	-0.08	7.348E-05

Table 4.5 (continued) shows the entropy generation of the chiller components for all the 20 set points of data set Normal 0

Point	$\dot{Q}_{45}$ Condenser kW	$\dot{S}_{gen,45}$ Condenser kW/K	$\dot{Q}_{56}$ Liquid Line kW	$\dot{S}_{gen,56}$ Liquid Line kW/K	$\dot{S}_{gen,67}$ Exp Valve kW/K	$\dot{S}_{gen,Total}$ Chiller kW/K
1	-19.38	3.321E-03	-0.11	1.696E-05	1.374E-03	1.172E-02
2	-18.88	3.172E-03	-0.09	2.272E-05	1.407E-03	1.160E-02
3	-18.17	3.003E-03	-0.10	2.035E-05	1.365E-03	1.134E-02
4	-18.46	3.035E-03	-0.11	3.235E-05	1.441E-03	1.170E-02
5	-18.13	2.943E-03	-0.11	2.155E-05	1.489E-03	1.163E-02
6	-19.28	3.261E-03	-0.12	1.043E-05	1.509E-03	1.202E-02
7	-19.85	3.424E-03	-0.12	1.482E-05	1.519E-03	1.242E-02
8	-19.70	3.338E-03	-0.13	2.892E-05	1.670E-03	1.263E-02
9	-19.16	3.211E-03	-0.13	1.230E-05	1.598E-03	1.227E-02
10	-17.94	2.916E-03	-0.10	2.416E-05	1.579E-03	1.199E-02
11	-13.94	1.809E-03	-0.07	2.215E-06	8.091E-04	7.439E-03
12	-13.53	1.668E-03	-0.07	1.485E-05	8.217E-04	7.061E-03
13	-13.10	1.572E-03	-0.06	1.765E-05	8.214E-04	6.999E-03
14	-13.35	1.616E-03	-0.07	1.189E-05	8.650E-04	7.158E-03
15	-13.04	1.554E-03	-0.07	2.711E-05	8.903E-04	7.241E-03
16	-13.78	1.728E-03	-0.07	6.388E-06	8.946E-04	7.378E-03
17	-14.13	1.835E-03	-0.07	2.597E-05	9.284E-04	7.550E-03
18	-14.03	1.762E-03	-0.08	1.351E-05	9.568E-04	7.761E-03
19	-13.59	1.681E-03	-0.07	2.707E-05	9.328E-04	7.446E-03
20	-12.94	1.532E-03	-0.07	2.879E-05	9.584E-04	7.476E-03

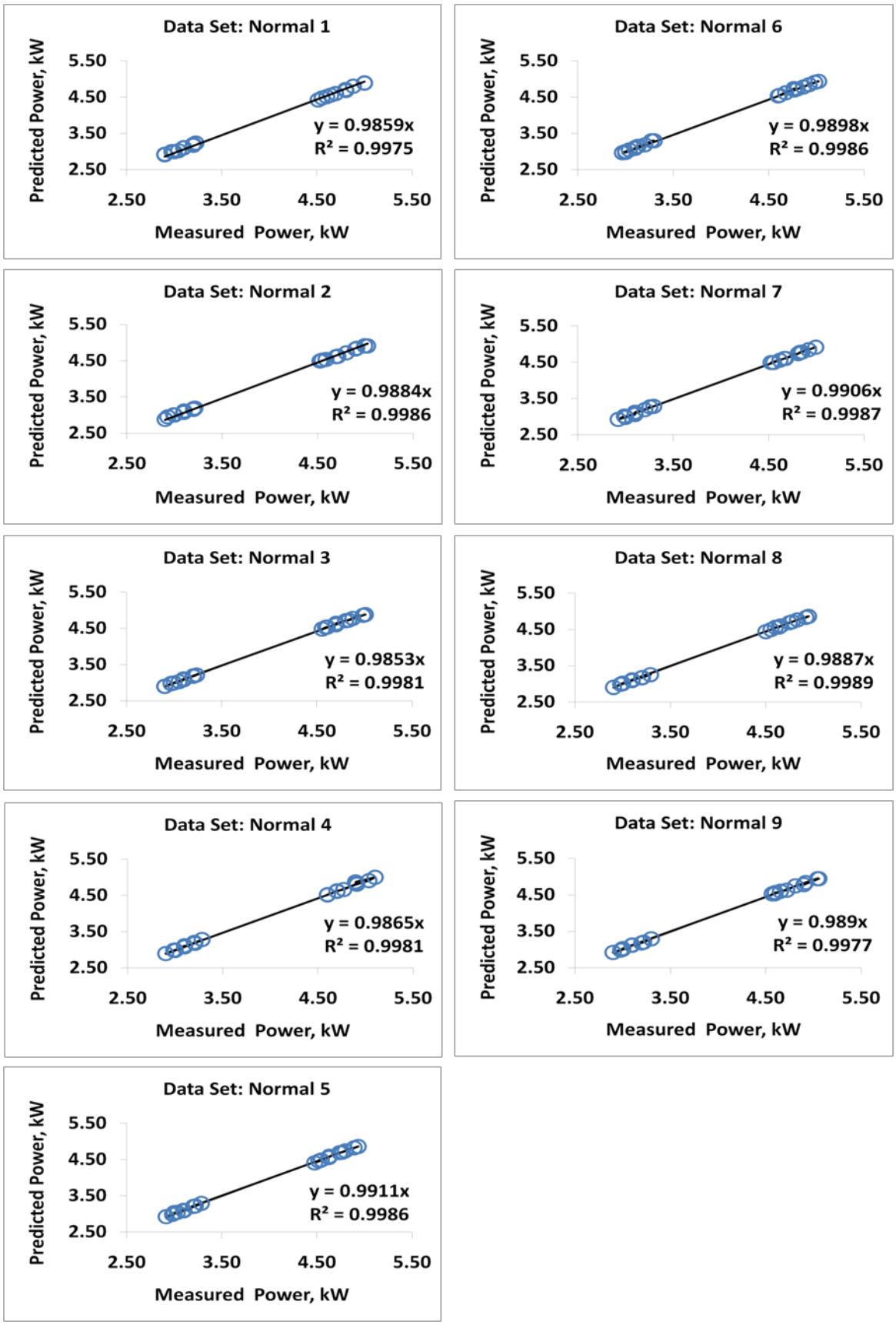

Figure 4.10: Good prediction of compressor power for all the fault free data sets

4.7 Fault Free Data Prediction

A fault is usually detected from the computed deviation between the present incoming data and the known fault free data. In this study, the fault free data was predicted using the multiple regression models. Multiple regression utilizes more than one independent variable to predict a dependent variable. The following independent parameters (i) leaving chilled water temperature, $T_{C,outlet}$ (ii) entering cooling water temperature, $T_{H,inlet}$ and (iii) compressor power, P_{in} were used in the regression models. A total of five fault-free models were developed in this thesis to predict the fault free conditions. The fault-free models were (i) suction superheat temperature, ϕ_1 (ii) condenser approach temperature, ϕ_2 (iii) condenser sub-cooling, ϕ_3 (iv) overall condenser heat transfer coefficient, ϕ_4 and (v) condenser entropy generation, ϕ_5. These models served as inputs for the CUSUM fault detection. It is vital to compute the accuracy of the predicted fault-free models. The accuracy of a regressed model is judged by comparing the original series of values with the forecasted values. The differences between the two values are known as residuals, e_t.

$$e_t = Y_{t-}\hat{Y}_t \tag{4.4}$$

Where

e_t = forecast error in time period t

Y_t = actual value in time period t

$\hat{Y}_t$ = forecast value for time period t

The prediction or forecasting accuracy of a model can be computed using four different techniques (Hanke and Wichern (2005)). The four techniques are (i) Mean absolute deviation,

MAD (ii) Mean squared error, MSE (iii) Mean absolute percentage error (MAPE) and (iv) Mean percentage error (MPE).

Mean absolute deviation, MAD

Mean absolute deviation, MAD computes the summation of the absolute error for each reading before averaging them. It is particularly useful when the predicted error is required to be in the same units of the original series. For n number of observations, the MAD is defined as:-

$$MAD = \frac{1}{n}\sum_{t=1}^{n}|e_t| \tag{4.5}$$

Mean squared error, MSE

For MSE, each residual is squared before being averaged over the number of observations. This technique penalizes large prediction errors as the errors are squared. MSE is defined as:-

$$MSE = \frac{1}{n}\sum_{t=1}^{n}{e_t}^2 \tag{4.6}$$

Mean absolute percentage error, MAPE

It is useful in certain occasions to express the forecasting accuracy in percentages. MAPE is computed by dividing the absolute residual with each actual value before averaging them over the total observations. MAPE signifies on how large the prediction errors compared to the actual observed values. It is defined as:-

$$MAPE = \frac{1}{n}\sum_{t=1}^{n}\frac{|e_t|}{Y_t} \tag{4.7}$$

Mean percentage error (MPE)

It is also important to ascertain whether a regressed model is biased in a particular direction (always over-predicting or vice versa). An unbiased model will have a MPE value which is close to zero. Large positive MPE indicates that the models will always under-predict. On the other hand, over-prediction of the regressed model will be reflected by large negative MPE values. MPE is defined as:-

$$MPE = \frac{1}{n}\sum_{t=1}^{n}\frac{e_t}{Y_t} \tag{4.8}$$

In this study, we have employed MAD to justify the prediction of the desired five fault-free parameters. The general multiple linear regression models utilized in this study is as following:-

$$\phi_i = \beta_0 + \beta_1 T_{C,outlet} + \beta_2 T_{H,Inlet} + \beta_3 P_{in} \tag{4.9}$$

where β represents the regressed coefficient for each independent variable and ϕ_i is the desired fault free parameters namely superheat, condenser approach temperature, sub-cooling, condenser overall heat transfer coefficient and condenser entropy generation.

The coefficients β_0, β_1, β_2, and $\beta_3$were regressed using data sets Normal 0, Normal 1 and Normal 5. The prediction accuracies were then justified using the remaining seven normal data sets that were not used in training the coefficients. The MAD values for each of the five forecasted fault free parameters are shown in Table 4.6, 4.7, 4.8, 4.9 and 4.10 respectively. All the tables indicate relatively small mean average deviations from the actual observed data. For instance, from Table 4.6 the maximum deviation in superheat prediction is 0.26 K as observed in the data set Normal 6.

Table 4.6: Regressed coefficients and the superheat, ϕ_1 prediction accuracy of the model for all the normal data sets.

Fault Free Superheat Prediction		
Data Sets	MAD (K)	$T_{superheat} = 0.01\,T_{C,outlet} + 0.03\,T_{H,Inlet} + 0.85\,P_{in}$
Normal 0	0.21	
Normal 1	0.21	
Normal 2	0.16	
Normal 3	0.18	
Normal 4	0.17	
Normal 5	0.19	
Normal 6	0.26	
Normal 7	0.14	
Normal 8	0.14	
Normal 9	0.18	
Maximum MAD	0.26	

Table 4.7: Regressed coefficients and the condenser approach temperature, ϕ_2 prediction accuracy of the model for all the normal data sets.

Fault Free Condenser Approach Temperature Prediction		
Data Sets	MAD (K)	$T_{Cond,appr} = 6.13 + 0.16\,T_{C,outlet} - 0.16\,T_{H,Inlet} + 1.06\,P_{in}$
Normal 0	0.09	
Normal 1	0.11	
Normal 2	0.10	
Normal 3	0.10	
Normal 4	0.10	
Normal 5	0.03	
Normal 6	0.28	
Normal 7	0.14	
Normal 8	0.20	
Normal 9	0.13	
Maximum MAD	0.28	

Table 4.8: Regressed coefficients and the condenser sub-cooling, ϕ_3 prediction accuracy of the model for all the normal data sets

Fault Free Condenser Sub-cooling Prediction		
Data Sets	MAD (kW/K)	$T_{subcool} = -0.58 - 0.021\,T_{C,outlet} - 0.05\,T_{H,Inlet} + 0.14\,P_{in}$
Normal 0	0.14	
Normal 1	0.22	
Normal 2	0.19	
Normal 3	0.23	
Normal 4	0.06	
Normal 5	0.06	
Normal 6	0.36	
Normal 7	0.11	
Normal 8	0.17	
Normal 9	0.36	
Maximum MAD	0.36	

Table 4.9: Regressed coefficients and the Condenser overall heat transfer coefficient, ϕ_4 prediction accuracy of the model for all the normal data sets.

Fault Free Condenser Overall Heat Transfer Coefficient Prediction		
Data Sets	MAD (kW/K)	$(UA)_{Cond} = 1.44 - 0.01\,T_{C,outlet} + 0.01\,T_{H,Inlet} + 0.04\,P_{in}$
Normal 0	0.03	
Normal 1	0.04	
Normal 2	0.03	
Normal 3	0.04	
Normal 4	0.02	
Normal 5	0.02	
Normal 6	0.07	
Normal 7	0.04	
Normal 8	0.05	
Normal 9	0.03	
Maximum MAD	0.07	

Table 4.10: Regressed coefficients and the condenser entropy generation, ϕ_5 prediction accuracy of the model for all the normal data sets

Fault Free Condenser Entropy Generation Prediction		
Data Sets	MAD (kW/K)	$S_{Gen,Cond} = 0.0012 - 8.43023\text{E}-05\, T_{C,outlet} - 9.13292E-05\, T_{H,Inlet} + 0.000861041\, P_{in}$
Normal 0	2.96E-05	
Normal 1	3.34E-05	
Normal 2	2.64E-05	
Normal 3	2.98E-05	
Normal 4	3.36E-05	
Normal 5	3.19E-05	
Normal 6	3.59E-05	
Normal 7	3.54E-05	
Normal 8	2.59E-05	
Normal 9	3.57E-05	
Maximum MAD	3.59E-05	

4.8 CUSUM Fault Free Data Analysis

As pointed out in Chapter 3, the fundamental equations in the CUSUM positive and negative drift detections are as following:-

Positive Drift, $\psi_H(j)$:

$$\psi_H(j) = \max\left[0, \psi_H(j-1) + \frac{(X_j - \mu)}{\sigma} - \zeta_1\right], \qquad j = 1, \ldots\ldots, NS \tag{3.69}$$

Negative Drift, $\psi_L(j)$:

$$\psi_L(j) = \max\left[0, \psi_L(j-1) - \frac{(X_j - \mu)}{\sigma} - \zeta_2\right], \qquad j = 1, \ldots\ldots, NS \tag{3.70}$$

The mean, μ and sigma, σ are to be obtained from the fault free data sets. The mean values at fault free conditions can be obtained from the regressed models as outlined in the

Section 4.7 of this chapter. The respective equations to obtain the mean values for each fault detection parameters namely (i) superheat, (ii) condenser approach temperature, (iii) sub-cooling, (iv) condenser overall heat transfer coefficient and (v) condenser entropy generation can be obtained from Tables 4.6 to 4.10 respectively. The sigma is mainly governed by the calibration error. The calibration error in our study stems from the maximum value of the mean absolute deviation, MAD of the fault free models. The maximum MAD value of each fault free model is augmented by a factor of 1.5 to offset uncertainties that might arise from other sources. These augmented values represented the CUSUM sigma of each fault detection parameter.

$$\sigma = 1.5\ x\ maximum[MAD] \tag{4.10}$$

4.9 Summary

In this study, an inverter driven scroll chiller test facility was designed and commissioned. The test facility consisted of two primary systems, namely the coolant and the refrigerant system. The coolant system was developed to simulate artificial building loads by mixing the evaporator and condenser leaving water. The temperature control mechanism to obtain the desired temperature set points was accomplished using four units of electric linear modulating valves. Using $T_{C,outlet}$, $T_{H,Inlet}$, and compressor power as independent variables, fault free models were developed using multiple linear regression technique for each of the fault detection parameters. σ for CUSUM chart were obtained from the mean average deviation of the models. The next chapter will be discussing on the efficacy of the proposed model in diagnosing soft faults.

Chapter 5: Fault Detection and Diagnosis Analysis of Vapor Compression Chiller

Introduction

This chapter describes the proposed fault detection and diagnosis techniques used in this study. The fault detection was carried out using the CUSUM analysis while the diagnosis routine employed the Bayesian probability theorem. Fault detection parameters such as (i) superheat, (ii) condenser approach temperature, (iii) sub-cooling, (iv) condenser overall heat transfer coefficient, and (v) condenser entropy generation were continuously monitored and compared against their respective fault free models developed in the chapter 4. The fault free models represented the nominal conditions of the scroll chiller and the required inputs for the models were:- (i) leaving chilled water temperature, $T_{C,outlet}$ (ii) entering cooling water temperature, $T_{H,Inlet}$ and (iii) compressor power, P_{in}. As outlined in the Chapter 3, CUSUM charts that monitor positive (ψ_H) and negative (ψ_L) drifts were specifically developed for each fault detection parameter. The required slack (ζ) and sigma (σ) values to execute CUSUM analyses were described in Chapters 3 and 4 respectively. Both the positive and negative drifts were simultaneously computed to corroborate the progressive gradient of the fault. Once the accumulated drift reached the predetermined decision interval (Ω), the CUSUM were reinitialized where the accumulated drift was reset to a zero value. The diagnosis analysis is activated if the non-reset drift (negative or positive) of any of the CUSUM parameters surpasses the decision limit, $\Omega_2 = 7.5$. The diagnostic routine employed the simple Bayes probability theorem to determine the root cause of the fault. Using Bayes

theory, the conditional probabilities of a particular soft fault to occur with respect to the fault detection parameters were then computed.

5.1 Fault Detection Parameters

The fault detection parameters used in this thesis mainly revolved around the condenser. Based on the previous study related to chiller fault detection, most of the practical models employed parameters related to condenser namely sub-cooling, condenser approach temperature and overall condenser heat transfer coefficient. Condensation is relatively a "quieter" process compared to boiling agitation in the evaporator. Therefore more stable and reliable readings and measurements can be obtained from the condenser. In this study, except for superheat, all the other fault detection parameters were obtained from the condenser.

Three common soft faults that plague chiller operations were investigated. The faults were (i) Refrigerant leakage (ii) Condenser fouling and (iii) Refrigerant overcharge. These faults were detected using the proposed fault detection parameters described in the chapter 4. The parameters were (i) superheat (ϕ_1), (ii) condenser approach temperature (ϕ_2), (iii) sub-cooling (ϕ_3), (iv) condenser overall heat transfer coefficient (ϕ_4), and (v) condenser entropy generation (ϕ_5). The responses of each fault detection parameter against the three common faults are shown in Table 5.1. One might question the uniqueness of the fault detection parameters in detecting the three faults. The diagnostic matrix proposed for leakage and fouling can be categorized as unique. This is not the case for refrigerant overcharge. Agami (2007) reported that overcharge and presence of non-condensable shared the same diagnostic symptoms. However, for high pressure chiller (e.g R22 scroll chiller as in our case) where the

evaporating pressure is higher that ambient, the probability for fault associated to non-condensable is virtually none.

It is very important to state that the proposed methodology is only valid for chillers that operate with constant cooling and chilled water flow rates. In other, simple interlock routines that monitor the coolant flow rates need to be incorporated into the FDD algorithm to ensure that the detection and diagnostics routines are only activated if constant water flow rates are detected.

Table 5.1: Fault detection and diagnosis matrix used in this study

	$T_{superheat}, \phi_1$	$T_{Cond,appr}, \phi_2$	$T_{subcool}, \phi_3$	$(UA)_{Cond}, \phi_4$	$S_{Gen,Cond}, \phi_5$
Ref Leakage	↑	↓	↓	↑	↓
Cond Fouling	—	↑	—	↓	↑
Ref Overcharge	↓	↑	↑	↓	↑

Refrigerant Leakage

When a vapor compression chiller experiences refrigerant leakage, suction superheat tend to rise as there is less boiling occurs in the evaporator. As a result of insufficient liquid for boiling, the refrigerant picks up us the heat in the form of vapor, thus leading to incremental superheat. As there is less refrigerant available in the system, the condenser appeared to be oversized for this particular fault. This explains the increase in the overall condensation heat transfer coefficient. This fictitious oversized condenser also leads to higher

heat exchanger effectiveness and smaller approach temperature. Decrease in the condenser entropy generation is also expected as there is less condensation activity. Less sub-cooling is required as there is less refrigerant available in the system.

Condenser fouling

In water cooled chillers, fouling is most likely to take place in the water circuits. The water tubes can be easily fouled due to the presence of bio slimes, organic and non-organic matters. Fouling increases the thermal resistance in the water tubes. This eventually leads to the decrement in the overall heat transfer coefficient of the condenser. This phenomenon also reduces the effectiveness of the condenser. This can be seen from the increment of the condenser approach temperature. The inefficient heat transfer also leads to increment of the entropy generation in the condenser. As for the superheat and sub-cooling temperatures, no significant change is expected as fouling on the water tubes does not affect the refrigerant flow.

Refrigerant Overcharge

The symptoms for an overcharged system are exactly opposite to those of leakage. Condensers appear undersized during overcharge. Less superheat is expected on the evaporator outlet or compressor suction as the latent heat removal from the loads is excessive. Higher sub-cooling is anticipated as more refrigerant need to be cooled down in the condenser. Condenser heat transfer coefficient and effectiveness deteriorate due to insufficient condensation area. These lead to a higher approach temperature and entropy generation in the condenser.

5.2 Fault Simulation

As outlined earlier, only three types of faults were considered in the current work. The soft faults were:- (i) refrigerant leakage (ii) condenser fouling and (iii) refrigerant overcharge. In order to obtain the faulty data, the scroll chiller was artificially altered to simulate the faulty conditions.

Refrigerant Leakage Simulation

The best possible option to simulate leakage problems in chillers was to reduce the nominal charged amount of the refrigeration system. In this study, the refrigerant, R22 was recovered into a recovery tank. The recovery tank was placed on a weighing scale to determine the amount refrigerant removed from the system. The initial charge of the system was 4.6 kg and the leakage simulation data were obtained at three different severity levels. The severity levels were (i) 5% leakage (ii) 10% Leakage and (iii) 20 % leakage. Some of the leakage data points were deliberately repeated to verify the consistency of the obtained data. In addition, upon the completion of 20% leakage test, the system was only topped up by 15% to ensure that the obtained data matched the 5% leakage data. Finally, the system was again tested at the nominal charge capacity to obtain the other fault free data sets. The discrepancies in all the redundancy testes were less than 5%, thus confirming the repeatability of the readings.

Condenser Fouling Simulation

In this study, condenser fouling was simulated by blocking the water tubes. As fouling increases the thermal resistance of heat transfer, the overall condenser heat transfer coefficient, $(UA)_{Cond,}$ is directly affected. Similar effect can be obtained by blocking the water tubes which affect the $(UA)_{Cond,}$ product. Fouling was simulated at three severity levels. The four pass water-cooled condenser used in this study consisted of 28 stainless tubes

where the tubes were blocked using the tapered bronze plugs. Table 5.2 shows the number of block tubes and the corresponding severity levels while Figure 5.1 shows the photos of the blocked tubes.

Table 5.2: Condenser fouling severity level

No of blocked tubes	Condenser Fouling Severity Level
3	≈ 10%
5	≈ 18%
7	25%

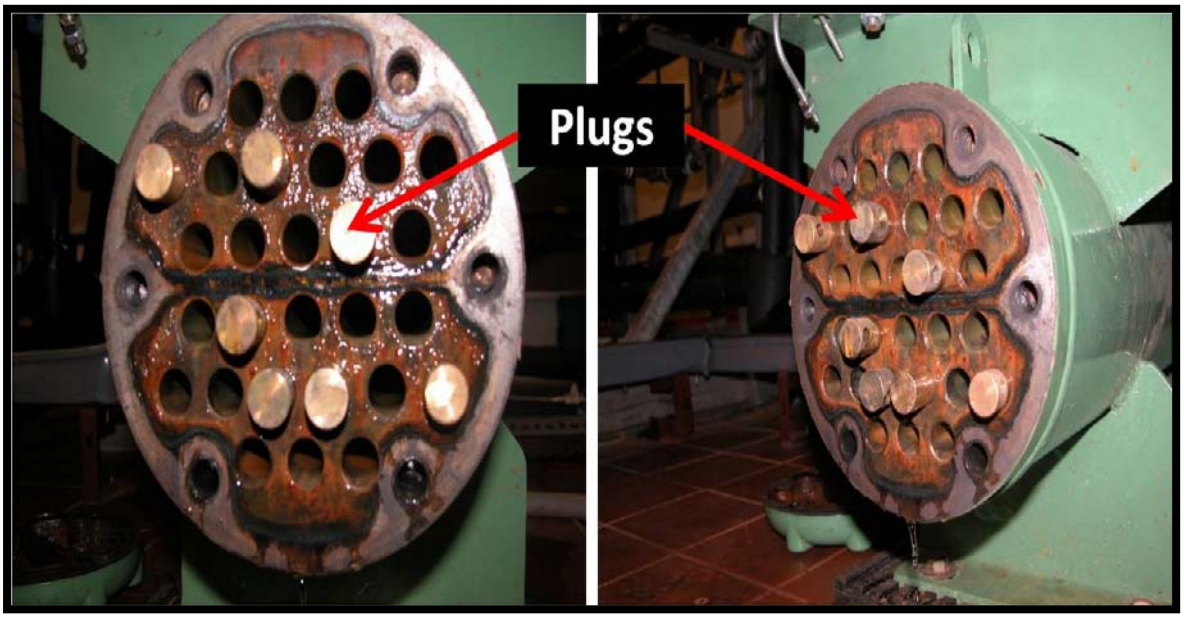

Figure 5.1: Fouling simulation by blocking the blocked water tubes

Refrigerant Overcharge Simulation

The fault simulation for the refrigerant overcharge was the easiest task amongst all. However, excessive overcharge can lead to serious damage to the scroll compressor due to the liquid flood-back or slugging. The compressor manufacturer specification allowed up to 15% of overcharge, was thus adopted as the maximum severity limit. Similar to other fault simulations, overcharge was performed at three severity levels with increments of 5% from the nominal charge of 4.6 kg.

5.3 CUSUM Fault-Free Data Analysis

As clearly explained in the Section 3.3 of Chapter 3, the CUSUM drifts (both positive and negative deviations) from the fault free conditions can be estimated as follows:-

Positive Drift, $\psi_H(j)$:

$$\psi_H(j) = \max\left[0, \psi_H(j-1) + \frac{(X_j - \mu)}{\sigma} - \zeta_1\right], \qquad j = 1, \ldots\ldots, NS \tag{3.69}$$

Negative Drift, $\psi_L(j)$:

$$\psi_L(j) = \max\left[0, \psi_L(j-1) - \frac{(X_j - \mu)}{\sigma} - \zeta_2\right], \qquad j = 1, \ldots\ldots, NS \tag{3.70}$$

It is important to emphasize at this point that the mean, μ and sigma, σ were obtained from the fault free prediction models. μ was the predicted value from the respective predictive models derived in the section 4.7 while the sigma can be computed from equation 4.10. X_j represents the online data. The slack values, ζ_1 and ζ_2 were also derived in Chapter 3. The CUSUM computations will only commence if constant cooling and chill water flow

rates are detected. In this thesis, five different CUSUM charts were simultaneously computed where each CUSUM was associated to fault detection parameters described earlier. Hereinafter, the CUSUM's are labelled as follows:

i. ϕ_1 *CUSUM* represents the superheat
ii. ϕ_2 *CUSUM* represents the condenser approach temperature
iii. ϕ_3 *CUSUM* represents condenser sub-cooling
iv. ϕ_4 *CUSUM* represents condenser overall heat transfer coefficient
v. ϕ_5 *CUSUM* represents condenser entropy generation

In this section, the efficacy of CUSUM in detecting the three soft faults mentioned earlier would be clearly demonstrated. The CUSUM technique was firstly tested against the fault free data sets to warrant that the CUSUM is insusceptible to false alarms. Figure 5.2 to 5.6 shows the CUSUM for the five detection parameters as described earlier. All the ten nominal fault-free data sets were validated. Each data set consists of 20 different operating set points as outlined in the chapter 4. A typical CUSUM chart proposed in this thesis consisted of 2 vertical axes. Primary Y-axis indicates the reset frequencies (ψ_R) for both positive, ψ_H and negative drift, ψ_L respectively. On the other hand, the secondary Y-axis represents the non-reset (ψ_{NR}) positive or negative drifts. As mentioned earlier, a fault is detected by a specific CUSUM if $\psi_{H\,NR}$ or $\psi_{L\,NR}$ exceeds the decision limit, Ω_2. Detail explanations on the development of CUSUM techniques can be found in Chapter 3.

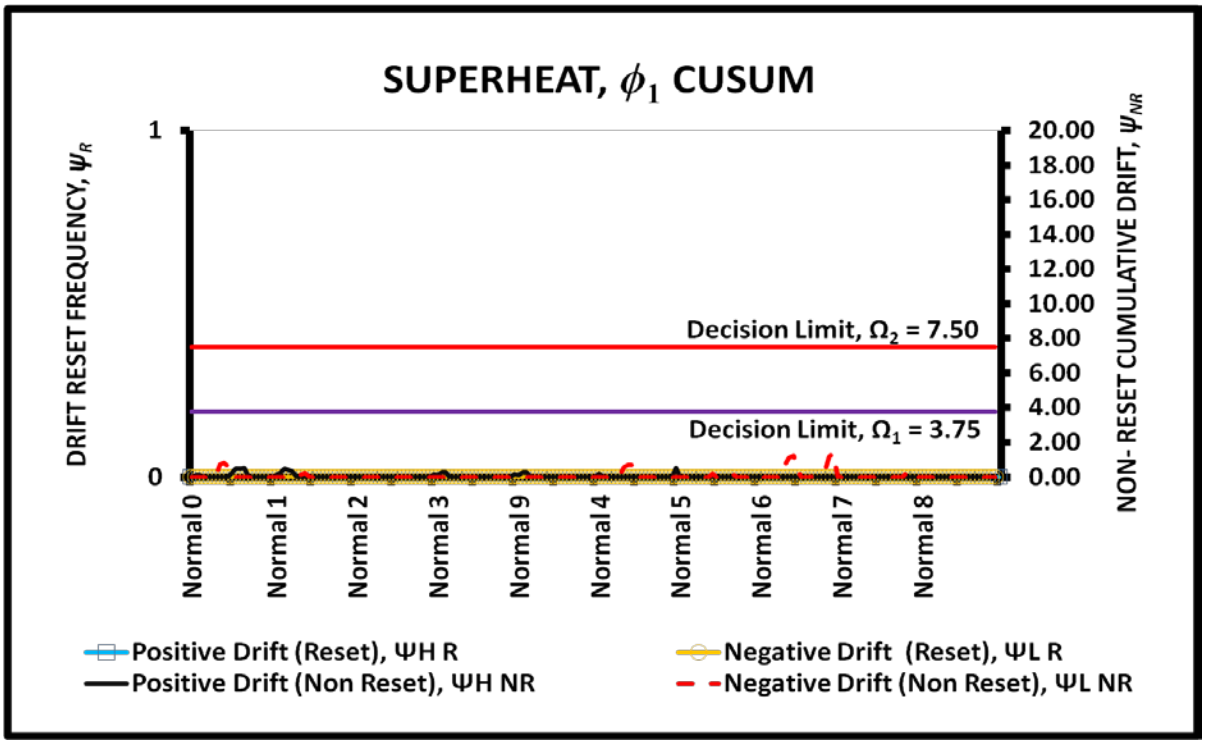

Figure 5.2: ϕ_1 CUSUM of the nominal data sets.

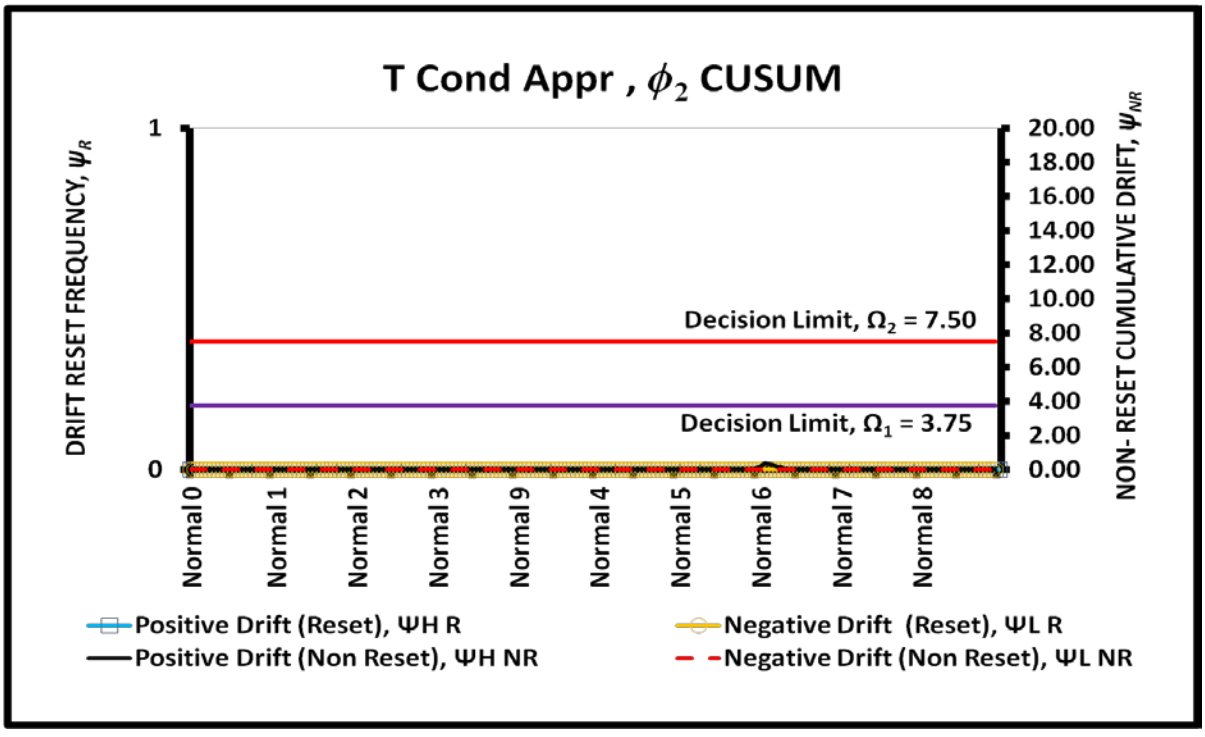

Figure 5.3: ϕ_2 CUSUM of the nominal data sets

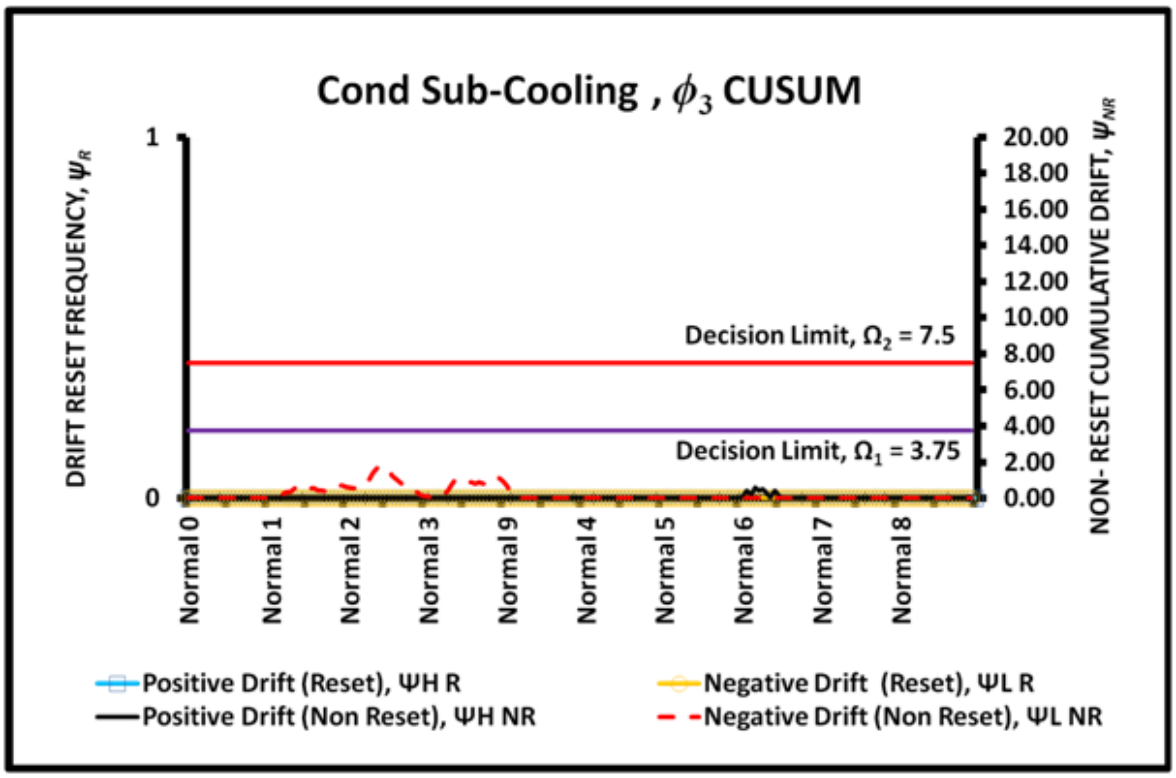

Figure 5.4: ϕ_3 CUSUM of the nominal data sets.

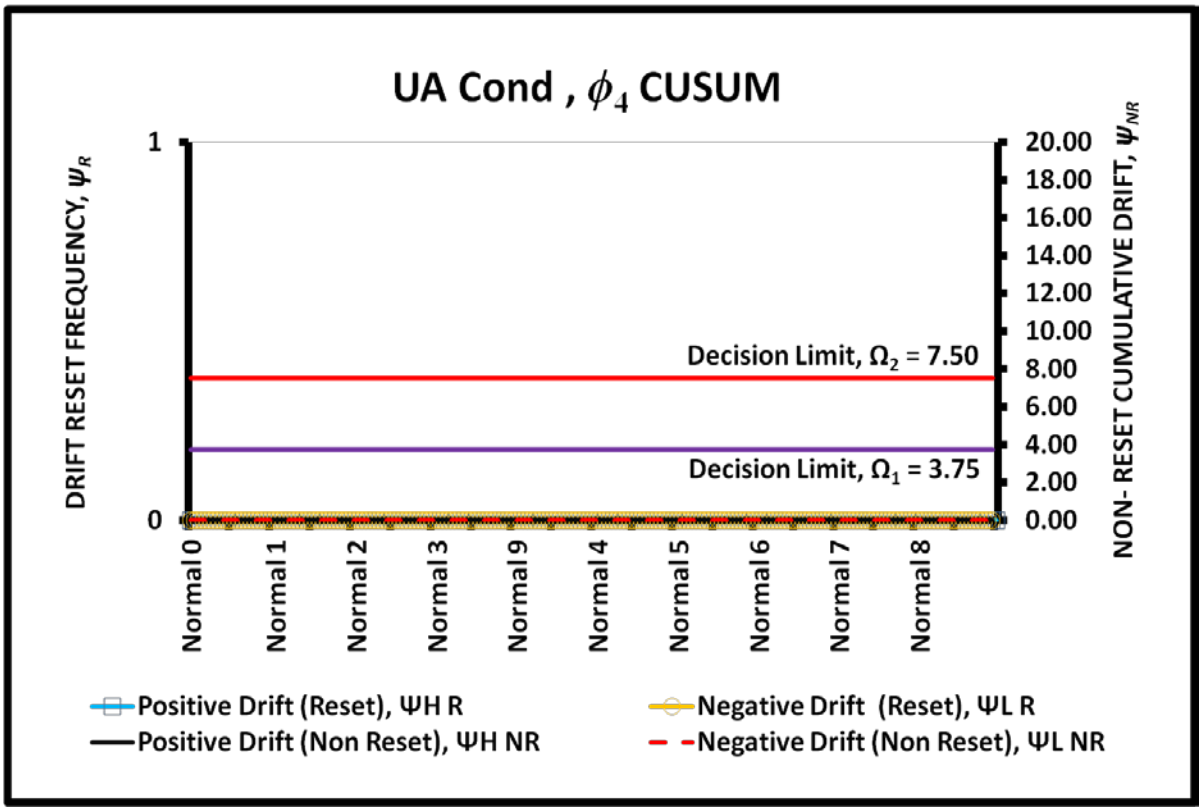

Figure 5.5: ϕ_4 CUSUM of the nominal data sets

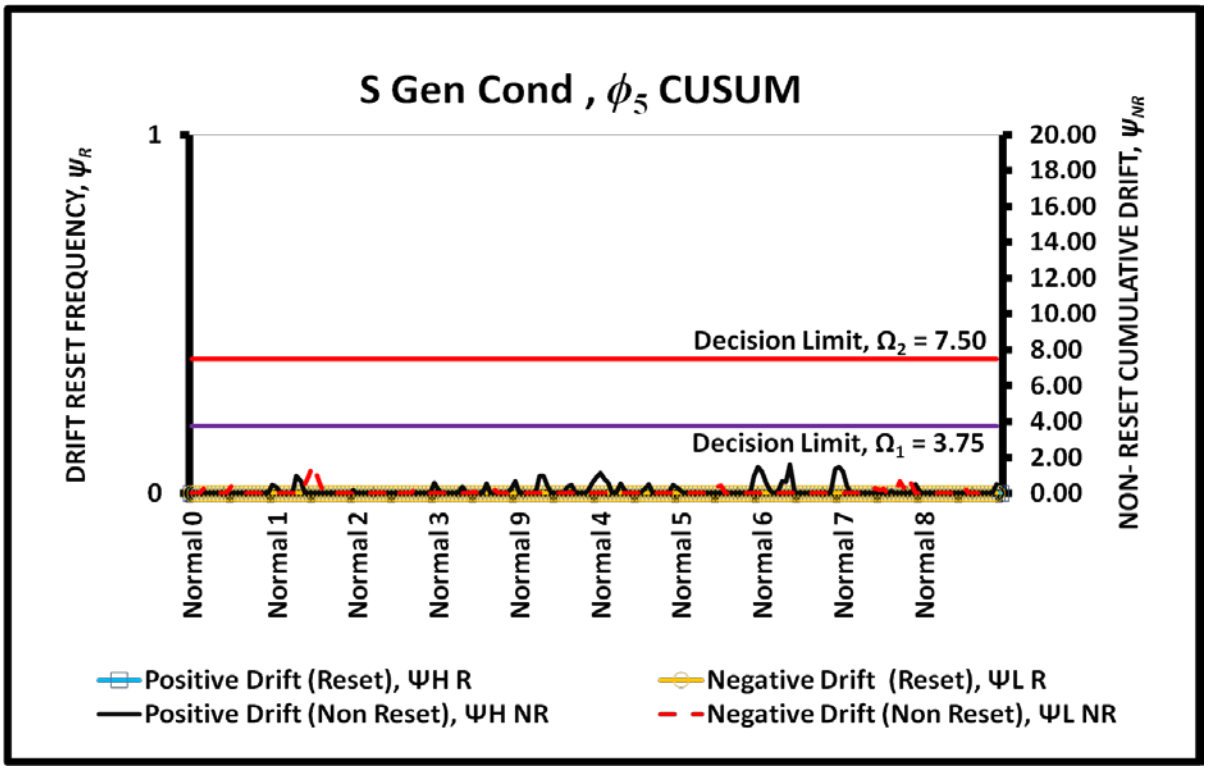

Figure 5.6: ϕ_5 CUSUM of the nominal data sets

From Figures 5.2 to 5.6, both $\psi_{H\,NR}$ or $\psi_{L\,NR}$ trend lines were lower than the non-reset decision limit, $\Omega_2 = 7.50$. Therefore, it can be concluded that the proposed CUSUM charts succinctly captured the fault-free operations. However, it can be argued that these CUSUM charts may be overly damped (in other words less sensitive) that it might not be able to detect the faults at the lowest possible severity level. This scenario is evaluated in the next section using the faulty data sets.

5.4 CUSUM Fault Detection

In this section, the five fault detection CUSUM charts would be demonstrated against the three types of soft faults investigated in this thesis. Each fault was simulated at three different severity levels. The difference in the severity level for each fault were kept at

minimum to demonstrate the efficacy of CUSUM technique in detecting faults at the lowest possible severity level. The fault matrix for the detection of refrigerant leakage, condenser fouling and refrigerant overcharge was based on Table 5.1. Similar to the nominal data sets, each faulty data set comprised of 20 different operating set points.

5.4.1 Refrigerant Leakage Fault Detection

Refrigerant leakage analyses were conducted in different severity levels namely (i) 5% leakage (ii) 10% leakage and finally (iii) 20% leakage. The entire leakage tests were carried out by removing the required amount of refrigerant into a recovery cylinder. Figure 5.7 to 5.12 shows the CUSUM charts of each fault detection parameter.

From Figure 5.7, it can be seen that positive non-reset ($\psi_{H\,NR}$) drift trend line (shown as solid black line) of ϕ_1 CUSUM crossed the non-reset decision limit $\Omega_2 = 7.50$ at the leakage severity level of 5%. The secondary Y axis, that represents the non-reset drifts, was assigned a minimum value of 5.5 to indicate the threshold of this decision limit. As mentioned before, a fault is detected by a CUSUM if the non-reset drift surpasses the decision limit. Therefore, it can be declared that the ϕ_1 CUSUM experienced a positive drift. This is further confirmed in the Figure 5.7 by the multiple positive resets ($\psi_{H\,R}$) trend line (solid blue with square). There was neither negative drift reset ($\psi_{L\,R}$) nor negative cumulative drift ($\psi_{L\,NR}$) can be observed. Higher positive reset frequencies can be clearly observed at the other ascending fault levels namely 10% and 20% leakage. However, from Figure 5.7 a void region can be observed between the second half of 5% leakage and the beginning of 10% leakage. At this region, no reset is detected and a slight drop in the $\psi_{H\,NR}$ can be observed. This pattern indicates that the superheat at this particular region is within the

nominal condition. A revisit to the Chapter 4 would explain this scenario. Of the total 20 different operating set points, the last ten set points were obtained at the lower compressor speed of 35 Hz. At lower compressor speed, the cooling load production drops and leads to liquid accumulation in the condenser shell. Thus, this excess refrigerant is sufficient to offset the small leakage effect. Thus 5% leakage at lower compressor speed has negligible impact on the overall system. Apart from that, the usually oversized expansion valve is capable of opening more to meet the demand and thus maintained the desired superheat set point.

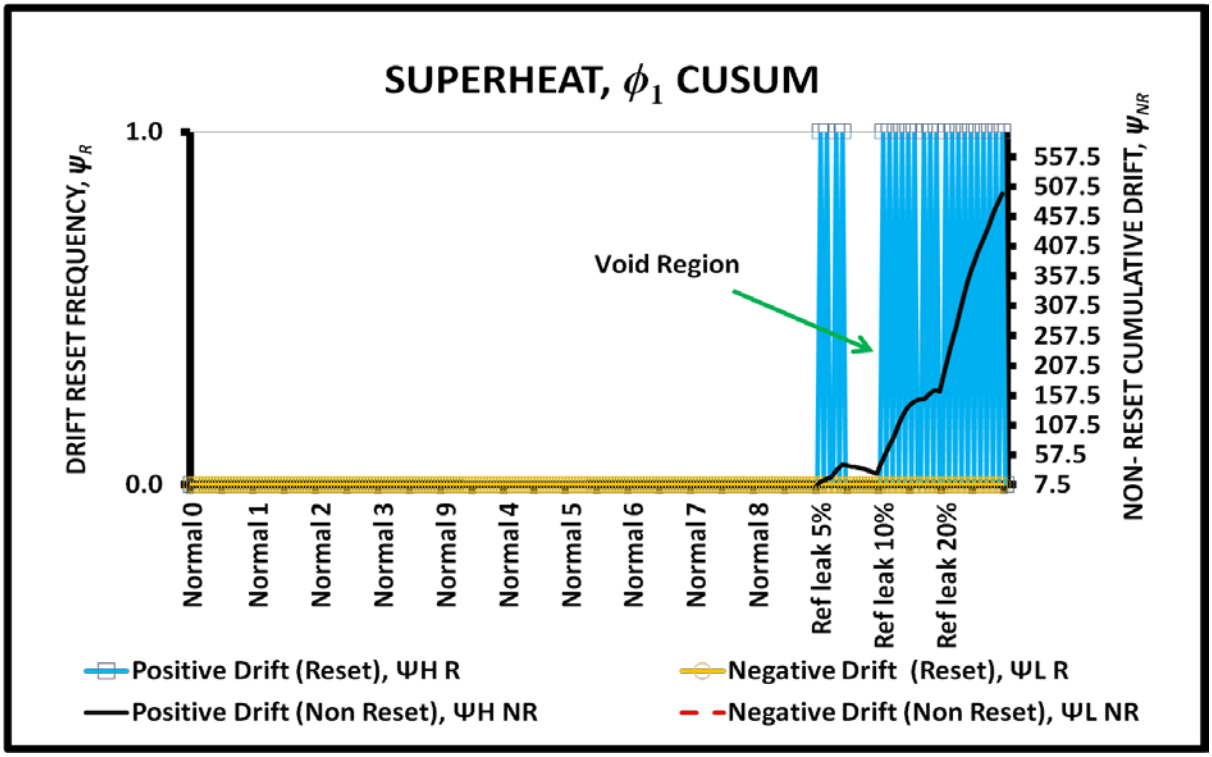

Figure 5.7: ϕ_1 CUSUM chart during refrigerant leakage

Condenser approach temperature, which is represented by ϕ_2 CUSUM chart, is shown in Figure 5.8. A negative drift can be observed. However, the fault was only captured by this specific ϕ_2 CUSUM at the severity level of 20% when the $\psi_{L\,NR}$ crossed the decision limit, Ω_2. The multiple negative drift reset $\psi_{L\,R}$ trend line authenticated the decrement in the

condenser approach temperature. Compared to ϕ_1 CUSUM result, one can argue that ϕ_2 CUSUM is less sensitive and overly damped as the fault was only detected at 20%. However, this is untrue as close inspection on the raw experimental data revealed that the maximum deviation between the 10% leakage and average of the fault-free data sets is less than 0.8K. Due to this small deviation, the ϕ_2CUSUM is unable to detect the shift at lower severity levels.

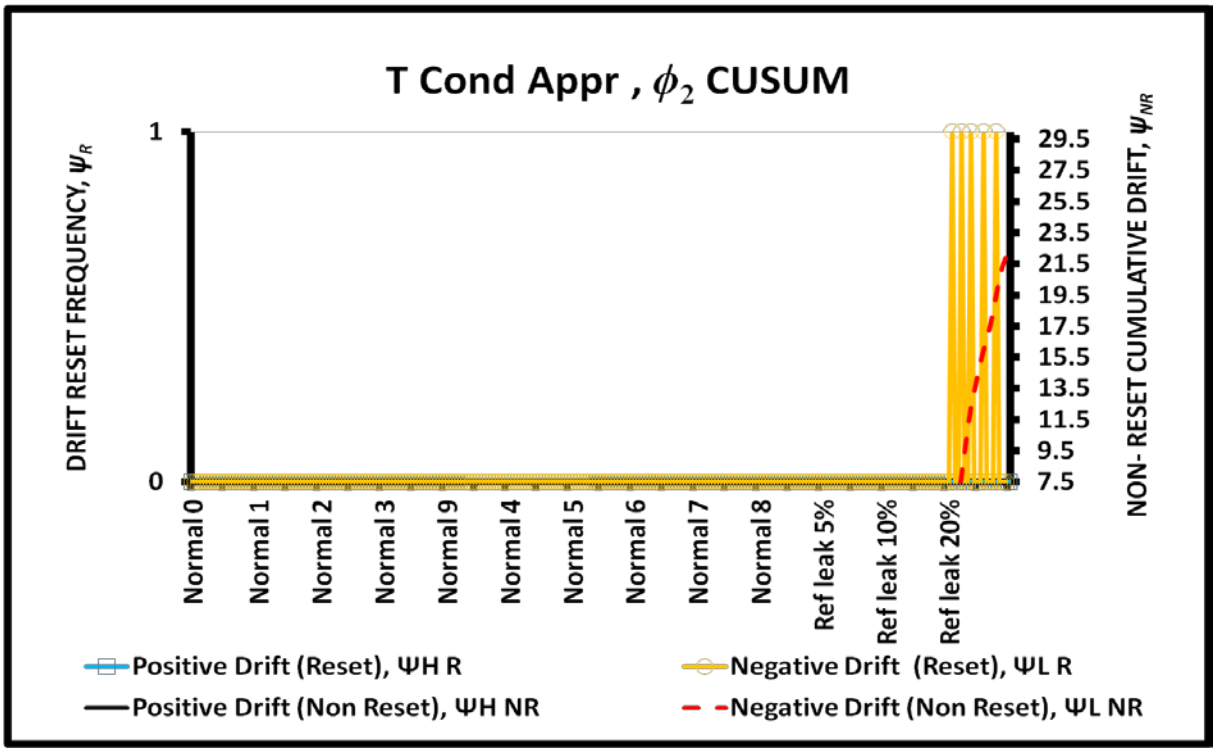

Figure 5.8: ϕ_2 CUSUM chart in the event of refrigerant leakage

In contrast to the diagnostic matrix established in Table 5.1, condenser sub-cooling, ϕ_3 CUSUM indicated zero drift for all the fault levels associate with leakage. This is shown in Figure 5.9. It is worth to mention that the nominal fault-free sub-cooling temperature of the scroll chiller studied in this thesis varies from 1.4 K to 1.7 K for all the 20 set points. During leakage of the 20%, the sub-cooling dropped to a minimum value of 0.7 K. Thus, the

change in the sub-cooling is relatively small and difficult to be detected using CUSUM or any other technique. This justifies the need for a more sensitive CUSUM.

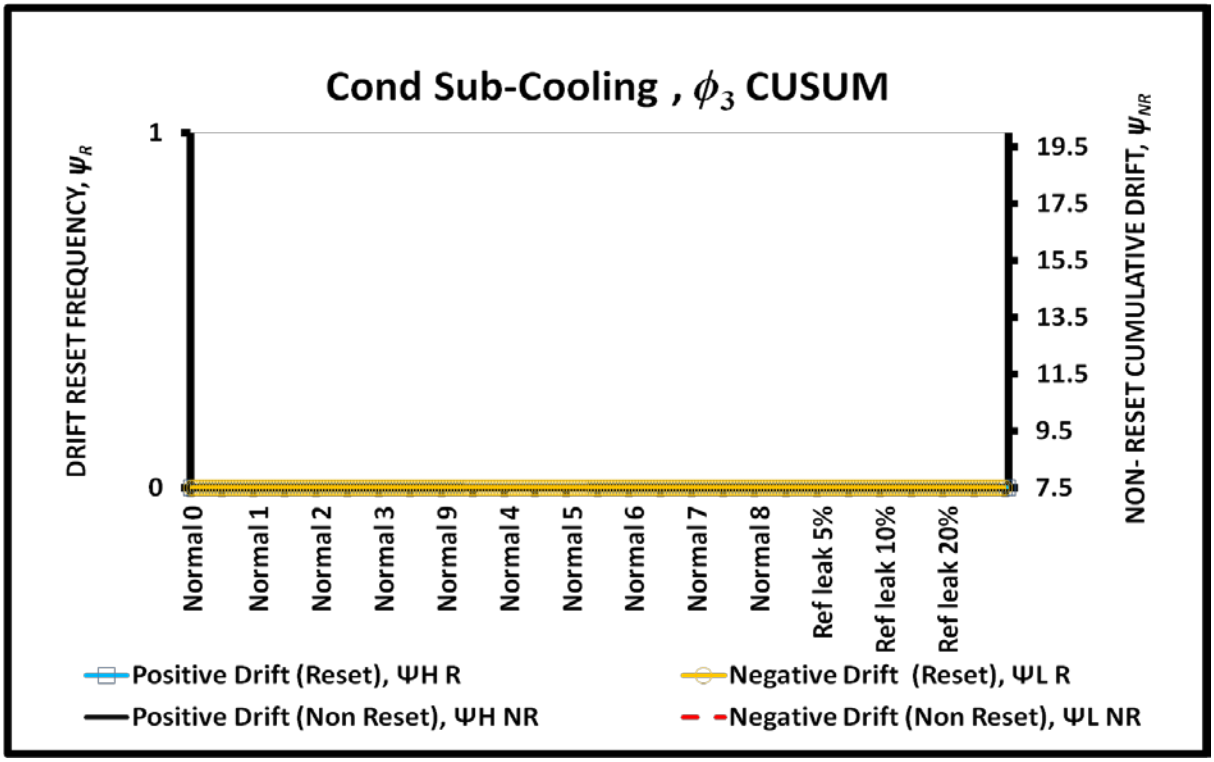

Figure 5.9: ϕ_3 CUSUM chart in the event of refrigerant leakage

A more sensitive CUSUM can be tuned by reducing the negative slack value, ζ_2. This tuning increases the sensitivity of the CUSUM. The new slack value was reduced by 50% from the previous analysis. Figure 5.10 shows the modified ϕ_3 CUSUM chart with a slack value ζ_2= 0.375 and the corresponding decision limits of Ω_1 = 4.125 and Ω_2 = 8.25. Estimation of these decision limits using the new slack value can be found in the Chapter 3. By increasing the sensitivity, it can be seen from Figure 5.10 that the $\psi_{L\,NR}$ crossed the decision limit at 10% leakage level. This confirms the detection of the fault. Apart from that, the negative reset drift trend $\psi_{L\,R}$ has already pre-signalled a decrement in the sub-cooling temperature at the 5% severity level. Although the diagnostic routine will only be activated based on the non reset drifts decision limit, the reset drift trend lines is capable of providing

earlier warnings or indications of the occurring fault. For the rest of analysis on negative drift of sub-cooling, the new set of CUSUM parameters were adopted.

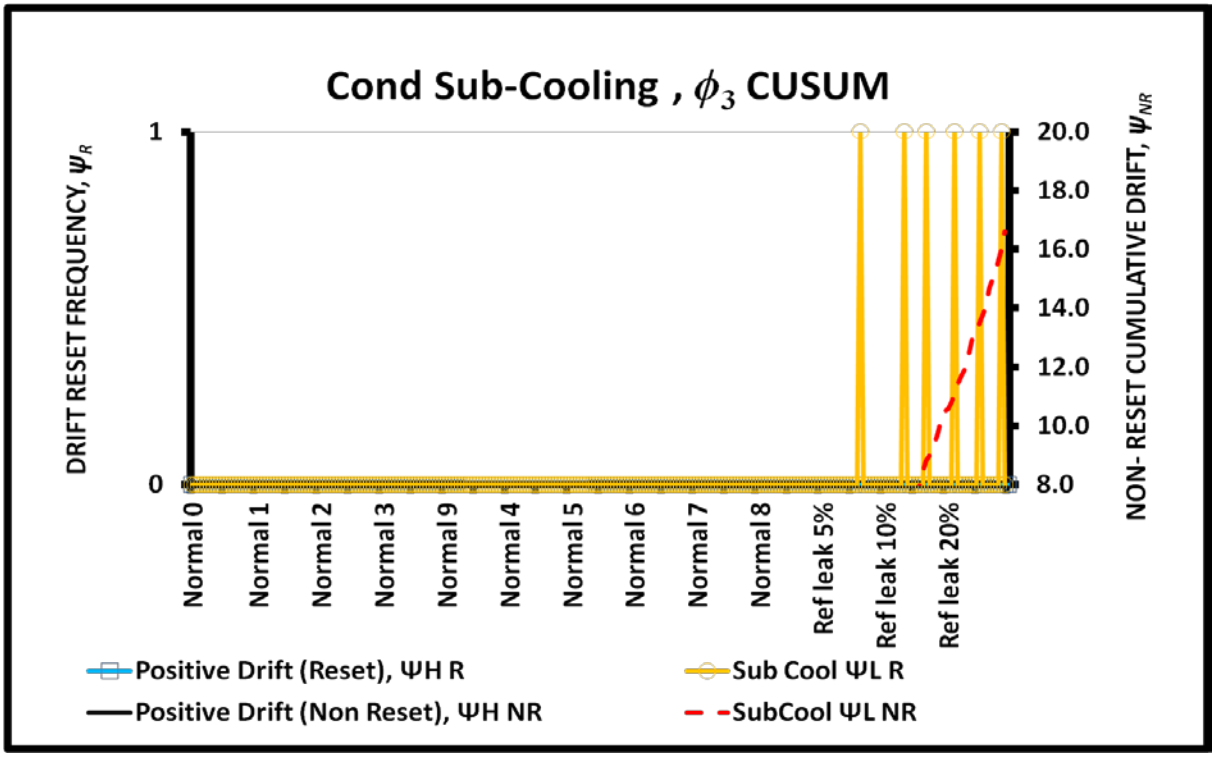

Figure 5.10: ϕ_3 CUSUM chart in the event of refrigerant leakage (ζ_2= 0.375 and Ω_2 = 8.25)

It has be to pointed out that the initial configuration of ϕ_3 CUSUM (ζ_2 = 0.75, Ω_1 =3.75 and Ω_2=7.50) can be used without qualms for machines that operate at high nominal sub-cooling of 5K. During leakage, the sub-cooling may deteriorate to a much lower values rather than a mere 0.7K as in our case. The large deviation can be succinctly captured by this initial configuration.

Similar to ϕ_3CUSUM, ϕ_4 does not vary significantly from the nominal data sets. As shown by the Figure 5.11, there was no drift flagged by the CUSUM during the leakage simulation. A closer look on the raw data of the leakage data sets confirmed the CUSUM findings as there were no significant change in $(UA)_{Cond}$. It is believed a significant increase in condenser heat transfer could be observed at a higher leakage level. Increase in $(UA)_{Cond}$

is definite during leakage as the condenser is virtually oversized when there are less refrigerant in the system.

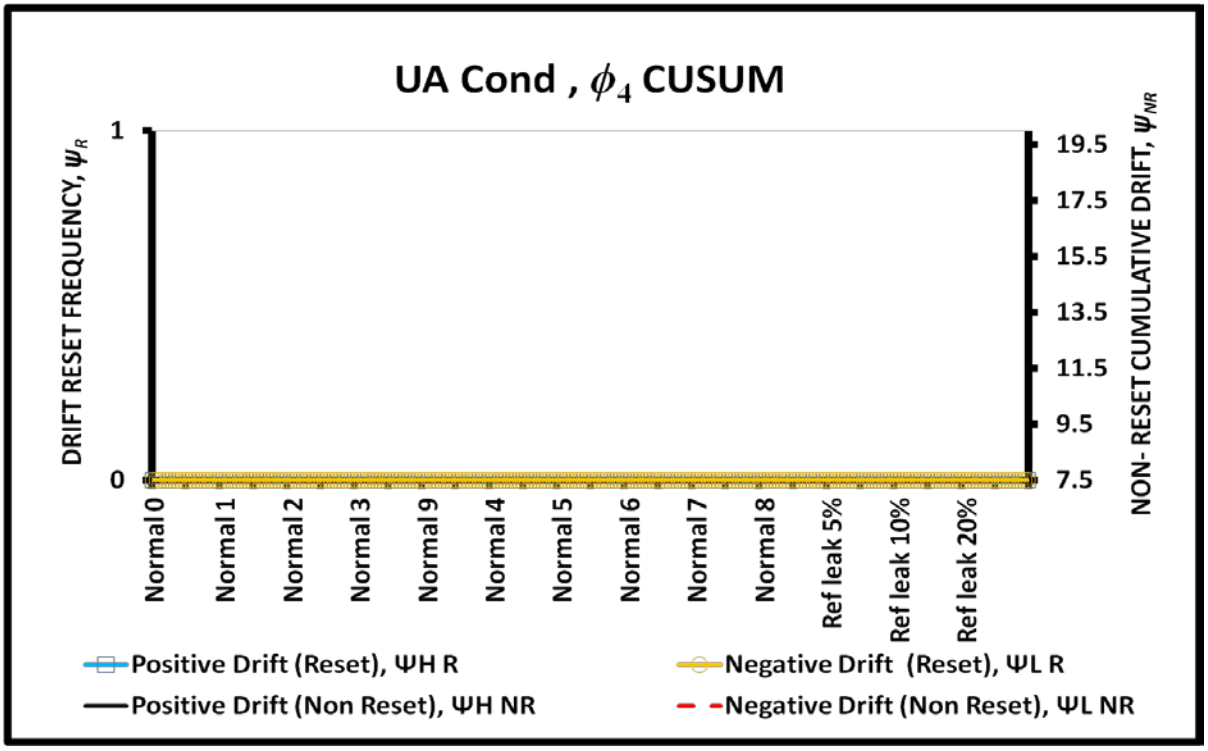

Figure 5.11: ϕ_4 CUSUM chart in the event of refrigerant leakage

As for the condenser entropy generation (ϕ_5), there was no sign of drift at the 5% leakage level. However, more rapid negative drift reset can be observed beyond the 5% leakage. This can be seen in the Figure 5.11. The fault is confirmed by ϕ_5CUSUM at the severity of 10%. The multiple resets as indicated by the negative drift reset trend line, $\psi_{L\,R}$ further support the findings.

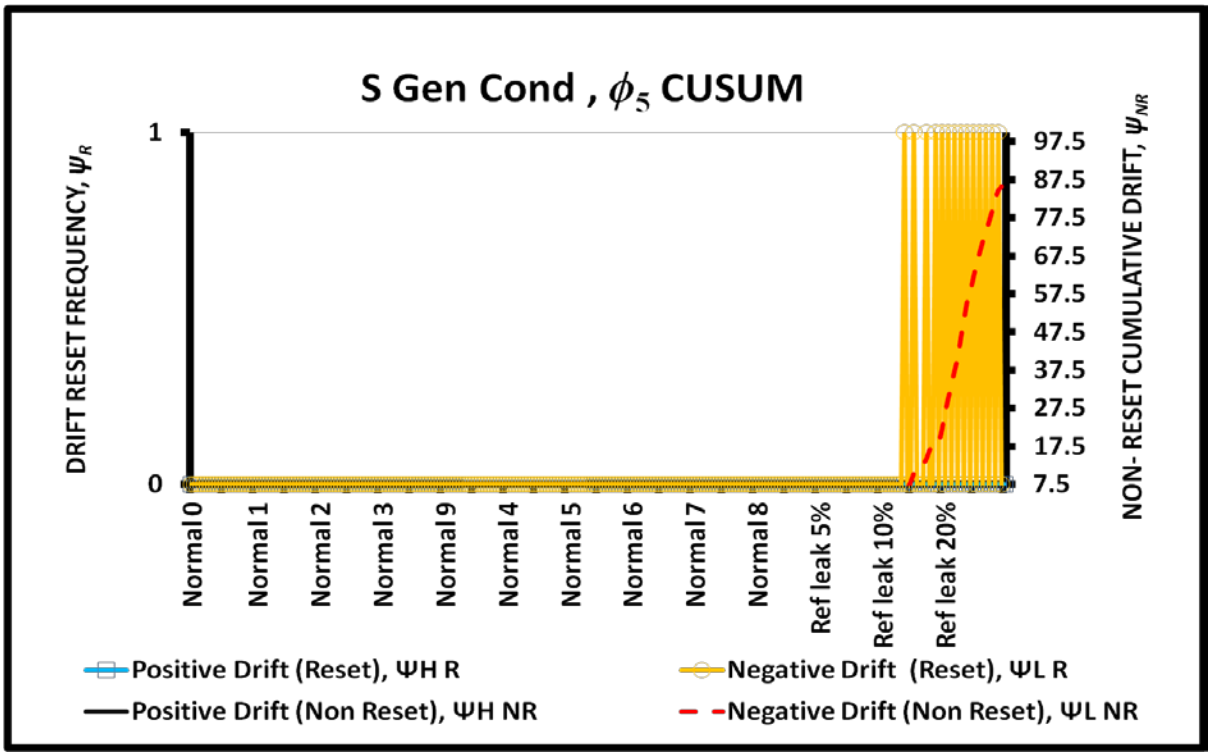

Figure 5.12: ϕ_5 CUSUM chart in the event of refrigerant leakage

5.4.2 Condenser Fouling Fault Detection

The simulation of the fouling conditions was clearly described in the earlier section. The condenser water tubes were plugged accordingly to achieve fouling level of 10%, 18% and 25%. The simulations were carried out in the ascending severity level. The obtained fouling data were then tested against the CUSUM charts to verify the diagnostic matrix outlined in Table 5.1.

From Figures 5.13 and 5.15 that represent the superheat and condenser sub-cooling, it can be observed that both charts indicated zero drift during the fouling simulation. Both parameters were insignificantly affected during the initial development of fouling. These

trends are expected as fouling on the water tubes does not affect the refrigerant flow. These profiles corroborate with the fouling diagnostic matrix outlined in the Table 5.1.

On the other hand, as shown in Figures 5.14 and 5.17, positive drifts with several reset ($\psi_{H\,R}$) frequencies can be observed for ϕ_2 and ϕ_5. Both condenser approach temperature and entropy generation parameters were successfully flagged positive for all the severity levels associated with fouling as the positive non-reset drift trend line ($\psi_{H\,NR}$) (indicated as solid black line) surpassed the decision limit, Ω_2=7.50 (the minimum value of the secondary Y axis). However, the entropy generation parameter is found to be less sensitive during the 10% fouling level especially when the system operates at part load. As for the $(UA)_{Cond}$, the associated ϕ_4 CUSUM chart clearly indicated multiple negative reset drift for all the fault levels. The continuous increment in the $\psi_{L\,NR}$ trend line (shown as dashed red line) further confirmed the decrement of $(UA)_{Cond}$ during the fouling condition. This is clearly depicted in Figure 5.16.

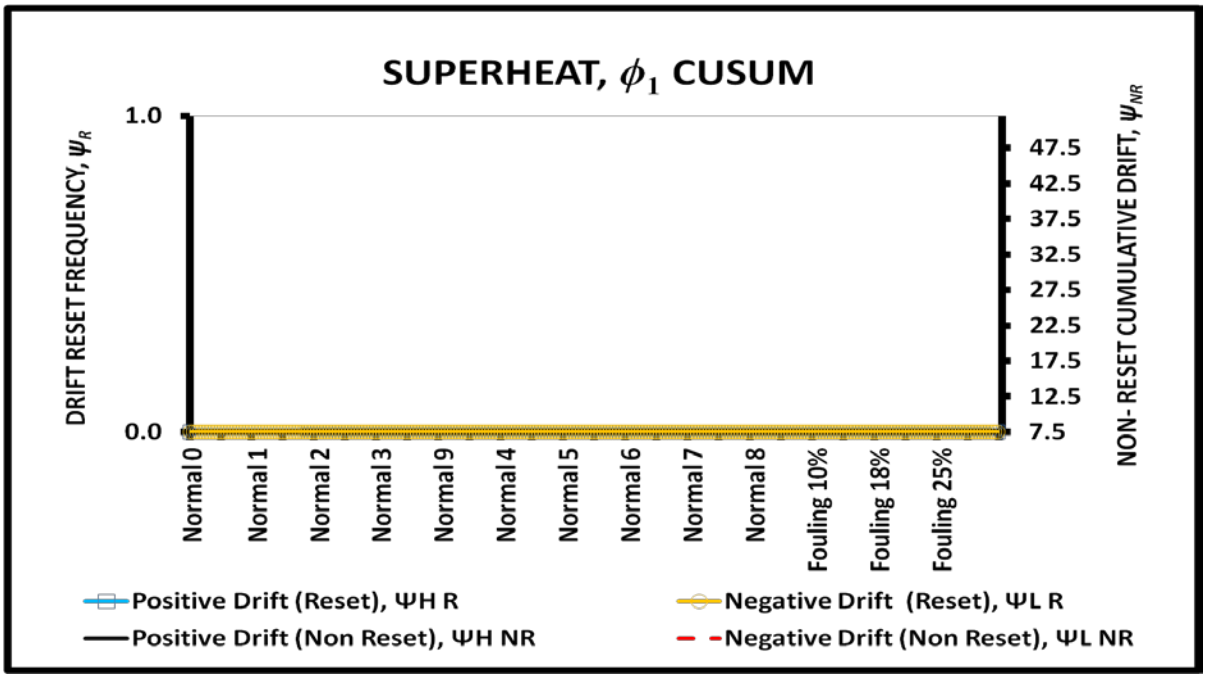

Figure 5.13: ϕ_1 CUSUM during condenser fouling

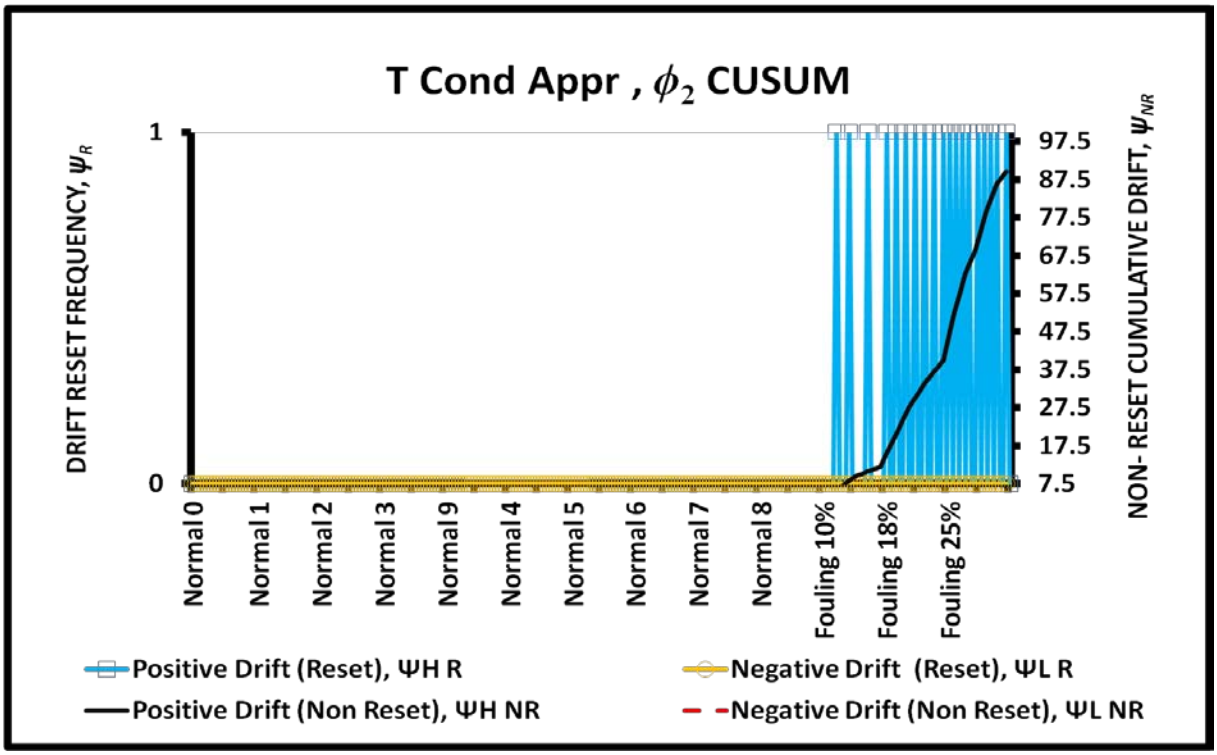

Figure 5.14: ϕ_2 CUSUM during condenser fouling

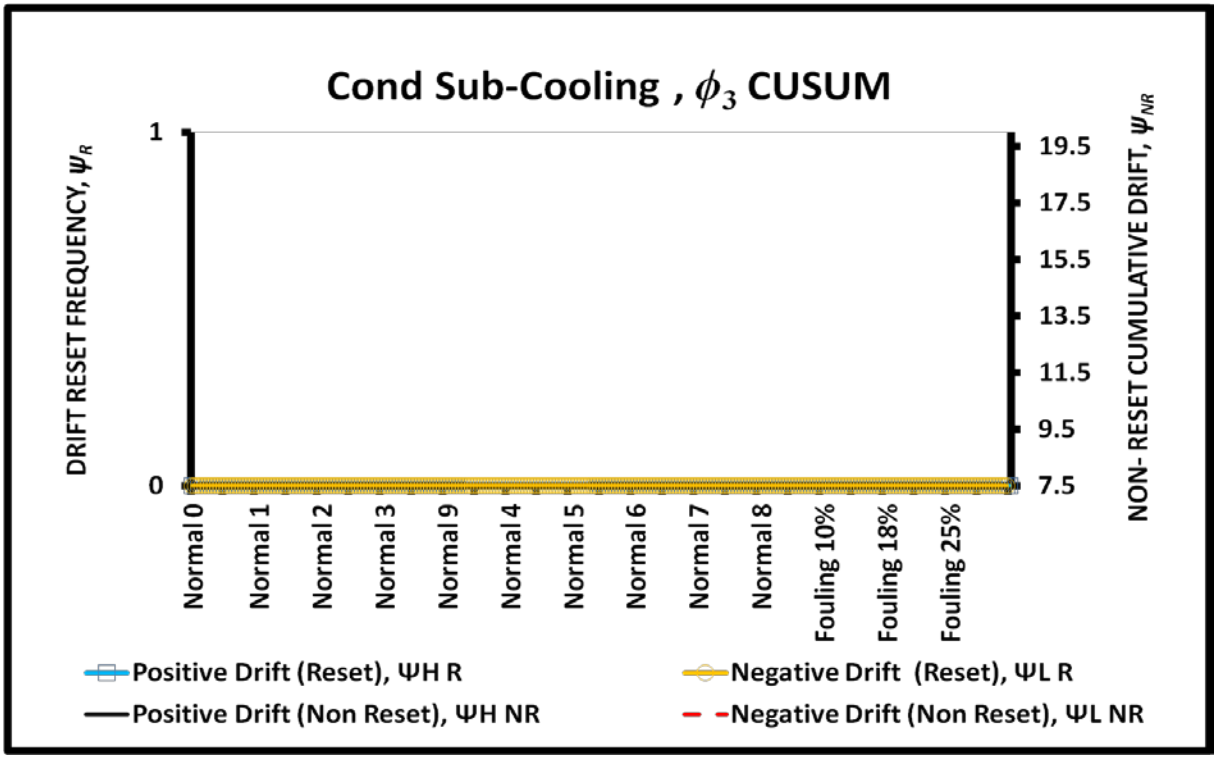

Figure 5.15: ϕ_3 CUSUM during condenser fouling

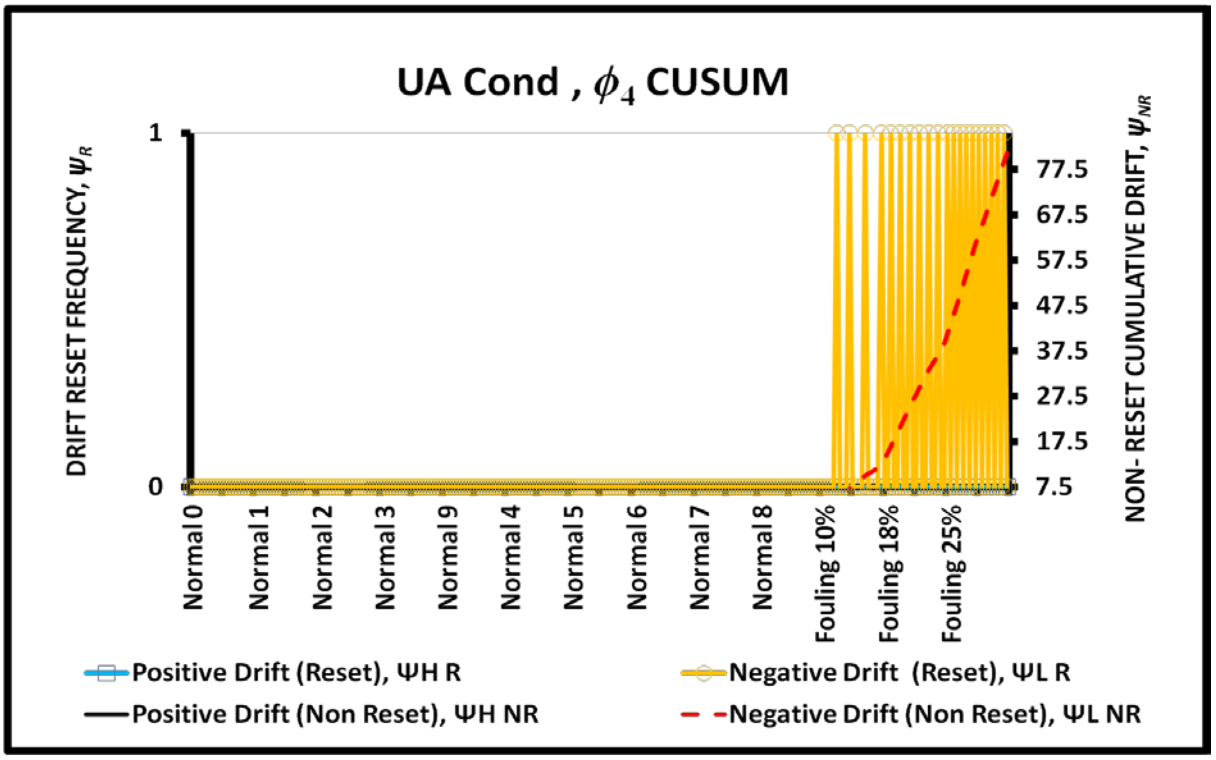

Figure 5.16: ϕ_4 CUSUM during condenser fouling

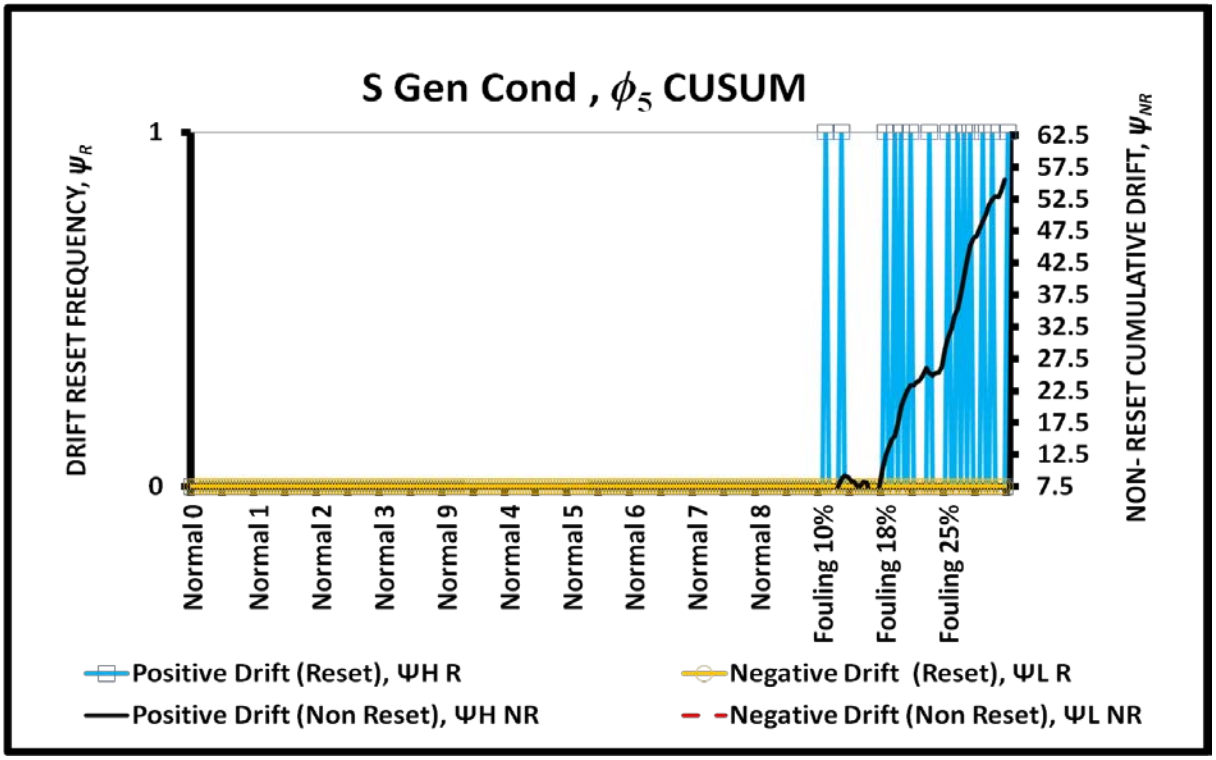

Figure 5.17: ϕ_5 CUSUM during condenser fouling

5.4.3 Refrigerant Overcharge Fault Detection

Similar to the other soft fault simulations, the overcharge procedure was carried out at three different severity levels. The initial overcharge was performed at 5% and then followed by a step increase of 5% for the other severity levels. The maximum overcharge simulation was limited to 15%. Based on the logged data, the CUSUM technique was then utilized to flag the appropriate fault detection parameters associated to refrigerant overcharge.

The results flagged by the CUSUM charts during the overcharge were opposite to the results obtained during the leakage simulations. However, the earliest detections were only captured at 10% overcharge. Significant number of resets and increase in the non-reset drifts can be seen for all the fault detection parameters except for superheat. This is due to the larger closing allowance available in the expansion valve and the good ability of the electronic expansion valve in maintaining the superheat. By closing the orifice to maintain the superheat during overcharge, bulk amount of liquid is trapped in the condenser. Therefore, the increment in the sub-cooling can be clearly detected by the CUSUM. As the liquid amount increases due to the increase in the severity level, there is a high possibility for the accumulated liquid to reduce the condensation heat transfer area by submerging the outer wall of the water tubes. Apart from that, liquid build-up in the condenser elevates the condenser pressure, thus resulting in higher condensing saturation temperature and approach temperatures. These phenomena contribute to the increment in condenser entropy generation. The drifts in the fault detection parameters as explained above were correctly flagged by their respective CUSUM charts as shown from Figures 5.18 to 5.22.

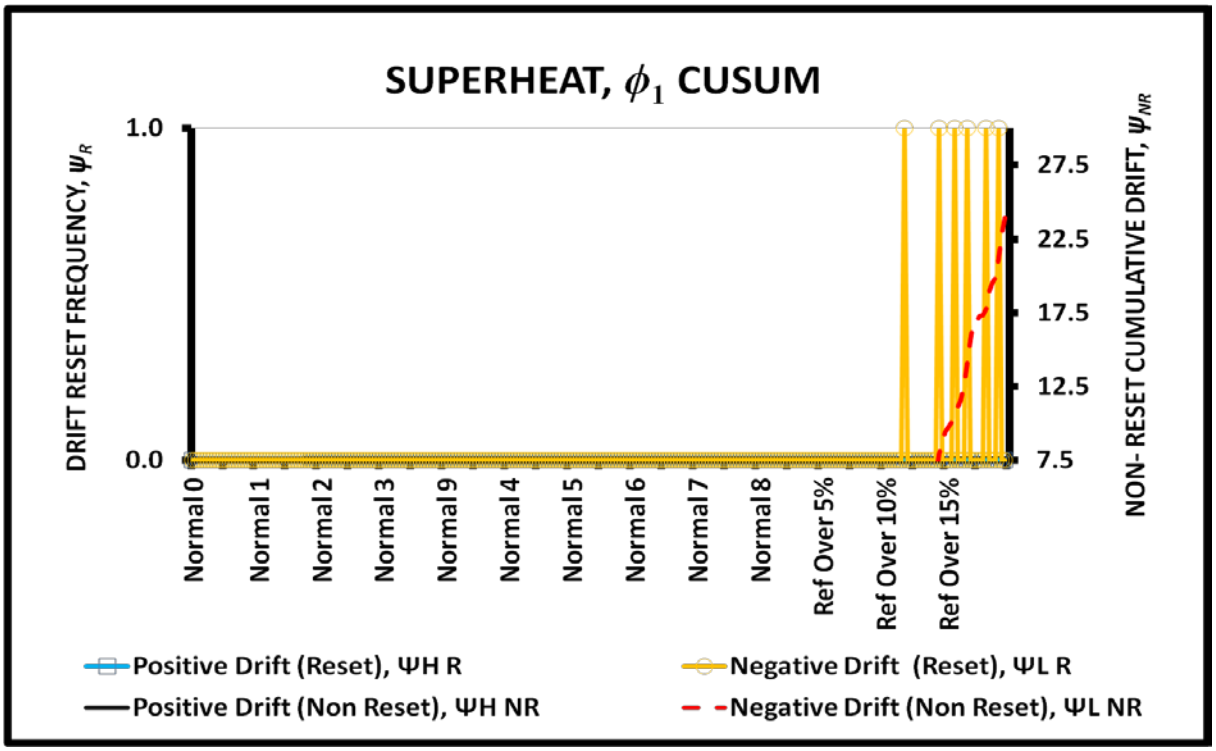

Figure 5.18: ϕ_1 CUSUM during refrigerant overcharge

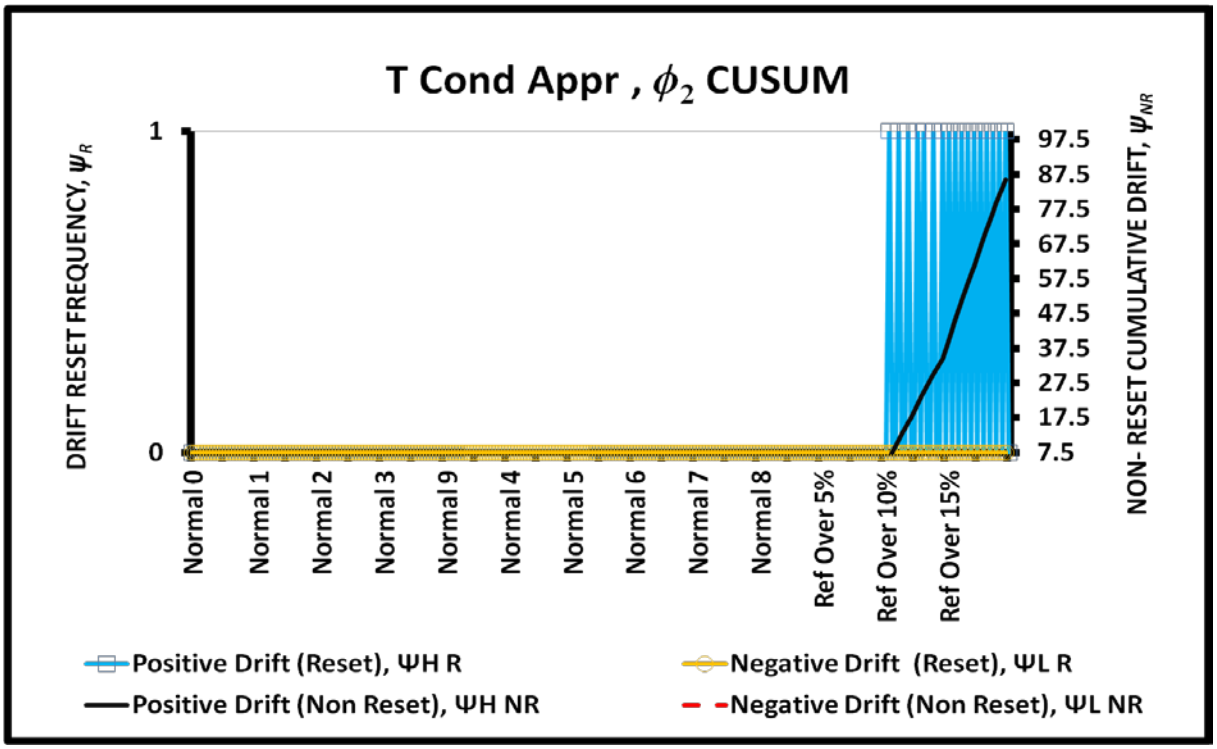

Figure 5.19: ϕ_2 CUSUM during refrigerant overcharge

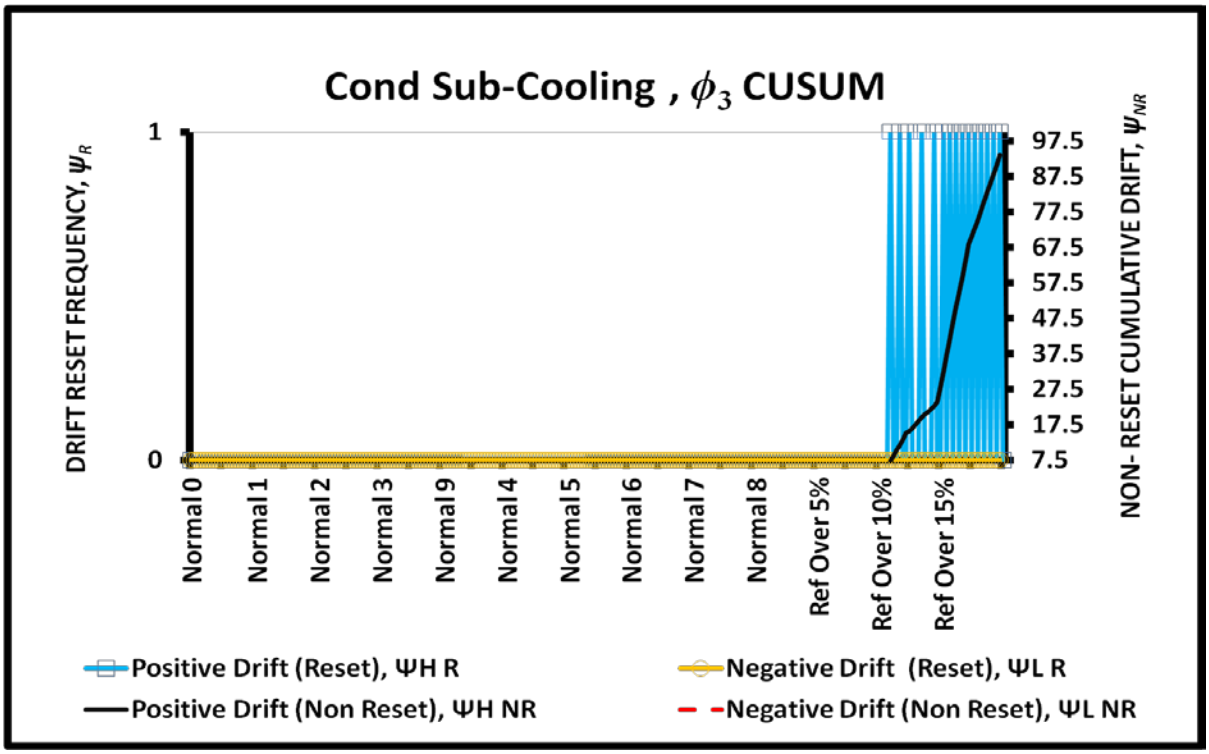

Figure 5.20: ϕ_3 CUSUM during refrigerant overcharge

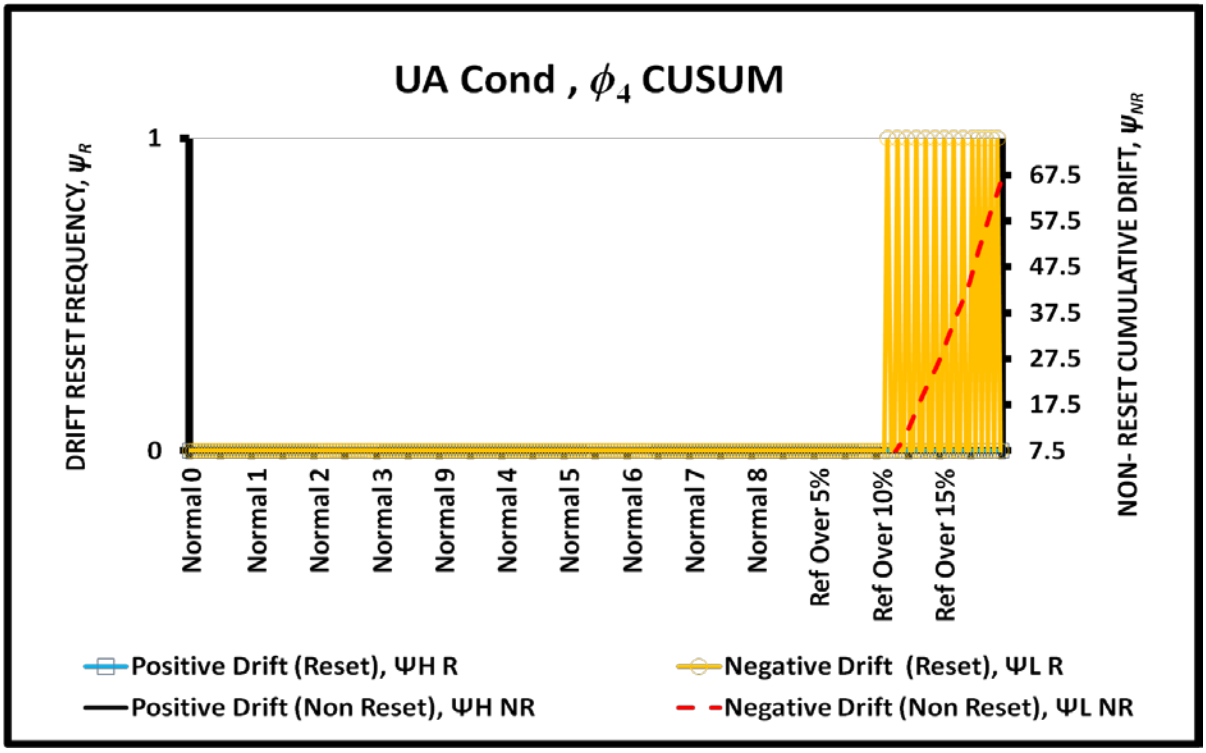

Figure 5.21: ϕ_4CUSUM during refrigerant overcharge

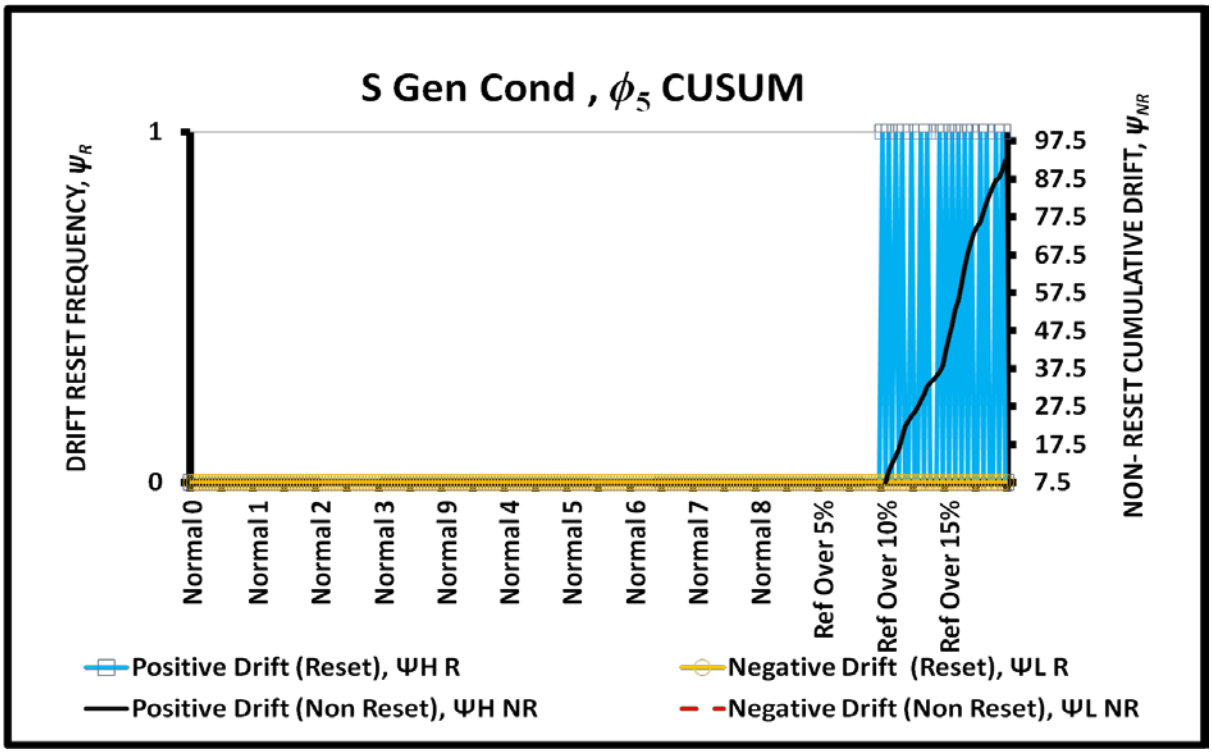

Figure 5.22: ϕ_5 CUSUM during refrigerant overcharge

5.4.4 After-service CUSUM Response

It is important for a fault detection technology to quickly recover from the influence of the previous faulty data once the system fault is identified and rectified. Figure 5.23 shows the quick recovery of the ϕ_4 CUSUM drift trend lines after the overcharge problem in the system was rectified. The after service condition was simulated by introducing the ϕ_4 CUSUM with the Normal 0 data at the end of 15% overcharge. From the figure, zero reset frequency can be observed after the set point of 15% overcharge. A sharp drop also can be observed that for the non-reset negative drift, $\psi_{L\,NR}$. The quick response of the CUSUM can be observed for all the other fault detection parameters and soft faults. Thus it suffices to demonstrate only one of the parameters.

A simple rule involving gradient of the non-reset trend line was incorporated in the CUSUM. From Equation 3.70 (or 3.69), it can be comprehended that drifts in the non-reset CUSUM is governed by the $\frac{(x_j-\mu)}{\sigma}$ term. This term is labelled as λ from hereinafter. Larger λ indicates larger deviations from the mean value. On the other hand, λ is much smaller during nominal test runs. Therefore a significant change in the λ can be observed before and after the service repairs. This sudden change in λ can be used to reinitialize the non-reset drifts. This explains the sudden drop of $\psi_{L\,NR}$ in Figure 5.23. The re-initialization for $\psi_{L\,NR}$ in this case is only performed when when the absolute value of λ is less than 1. It is very important to state that larger reset value can lead serious error due to rapid re-initializations.

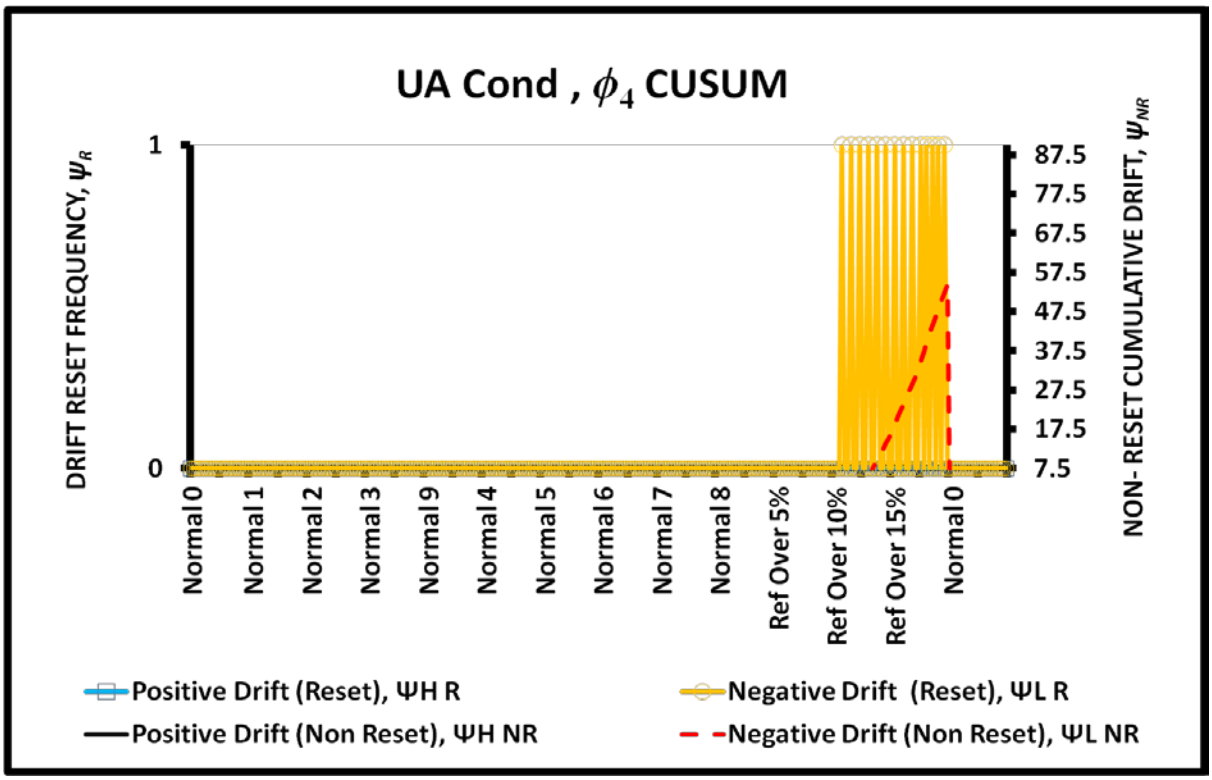

Figure 5.23: ϕ_5 CUSUM after the rectification of overcharge

5.5 Bayesian Diagnostics

As defined in the chapter three, the Bayes Rule is defined as following:

$$P(Fault_i|\boldsymbol{P}) = \frac{P(Fault_i)\ x\ P(\boldsymbol{P}|Fault_i)}{\sum_{j=1}^{3} P(Fault_j)P(\boldsymbol{P}|Fault_j)} \quad (3.92)$$

$P(Fault_i)$ is the prior probability of a fault

$P(Fault_i|\boldsymbol{P})$ is the posterior probability of a fault given CUSUM output vector, $\boldsymbol{P}$

$P(\boldsymbol{P}|Fault_i)$ is likelihood of fault for the observation of CUSUM vector, $\boldsymbol{P}$

The term on the left of the above equation is the probability that we are interested in. Known as posterior probability, it indicates the probability of a particular fault to occur with respect to the CUSUM vector. CUSUM vector, $\boldsymbol{P}$ represents the fault detection parameters and can be expressed as:-

$$\boldsymbol{P} = \begin{bmatrix} \phi_1 \\ \phi_2 \\ \phi_3 \\ \phi_4 \\ \phi_5 \end{bmatrix} = \begin{bmatrix} "1"\ or\ "-1"\ or\ "0" \\ "1"\ or\ "-1"\ or\ "0" \\ "1"\ or\ "-1"\ or\ "0" \\ "1"\ or\ "-1"\ or\ "0" \\ "1"\ or\ "-1"\ or\ "0" \end{bmatrix} \quad (3.78)$$

Each element of the vector, **P** is indicated in Boolean form:- (i) "1" for positive CUSUM drift, ψ_H (ii) "-1" for negative CUSUM drift, ψ_L and (iii) "0" for zero CUSUM drift. From the CUSUM fault detection results presented in the earlier section and Table 5.1, we can further reduce the diagnostic requirements for the soft faults studied in this thesis. The diagnostic trend of $T_{Cond,appr}, \phi_2$ is of opposite trend to the $(UA)_{Cond}$, ϕ_4 but similar to $S_{Gen,Cond}$, ϕ_5. Therefore, a surplus in the diagnostic is observed. Since $T_{Cond,appr}$ is easier to measure and has less measurement uncertainty, thus $(UA)_{Cond}$ and $S_{Gen,Cond}$ will be no

longer used in the Bayesian diagnostics. Superheat and sub-cooling temperatures also exhibit opposite trends during the occurrence of soft faults. Several researchers have pointed out that superheat drift is very much dependable on the type of the expansion valves used. For instance, refrigerant leakage can be easily detected using the superheat parameter if a system employs a capillary tube as expansion valves. However, a system operated using thermostatic or electronic expansion valve tend to compensate the leakage symptom by adjusting the refrigerant flow rate. Thus, superheat drift analysis is more system dependent. In the diagnostic study, the superheat analysis was excluded.

By ruling out the surplus fault detection parameters, the final CUSUM vector, $\boldsymbol{P}$ is redefined as:-

$$\boldsymbol{P} = [\phi_2, \phi_3]^T \tag{5.1}$$

In order to obtain the posterior probability, the prior probability and likelihoods need to be found. The prior probability is defined as the probability of a particular fault to occur. Since only three soft faults were considered in this thesis, the probabilities of leakage, fouling and overcharge need to be ascertained. Comstock and Braun (1999) conducted a survey and listed the frequency of common faults in centrifugal chillers. Approximately 15% of the total 170 service calls were due to leakage issue while about 8% of the calls attributed to condenser fouling. None was reported for refrigerant overcharge. Similar ranking was reported by Agami (2007) where a weighting factor of 1.5, 1.0 and 0.25 were assigned for leakage, fouling and overcharge respectively. In this study, we have adopted the similar ranking hierarchy. Prior probabilities for each fault were assigned after extensive discussion with several refrigerant experts and service personnel. The proposed prior probabilities are:-

$$P(Ref\ Leak) = 0.45 \qquad P(Cond\ Fouling) = 0.35 \qquad P(Ref\ Overcharge) = 0.20$$

Next, the likelihood probability $P(\boldsymbol{P}|Fault_i)$ needs to be computed to complete the Bayes diagnostic. As highlighted by Berry (1996), the likelihood can be calculated by multiplying the probabilities of each individual observation. This computation is best explained using the probability tree diagram, shown in the Figure 5.24. This figure consists of the two selected fault detection parameters namely (i) Condenser approach temperature (ϕ_2) and (ii) Condenser sub-cooling (ϕ_3). Each parameter is branched into 3 sub-diagrams to accommodate the results (e.g Positive (ψ_H), Negative (ψ_L) or Zero drift (ψ_Z) flagged by their respective CUSUM charts. A total of 9 different combinations can be flagged by the CUSUM vector, **P**. The probabilities of the vector element, P with respect to the three faults studied in this thesis is shown in Table 5.3.

Table 5.3: Probability of the vector element, ***P*** for each of the soft faults

FDD Vector, ***P***	Probability			
	Tag	Refrigerant Leakage	Condenser Fouling	Refrigerant Overcharge
ϕ_2, ψ_H	P(A)	0.10	0.80	0.80
ϕ_2, ψ_L	P(B)	0.80	0.10	0.10
ϕ_2, ψ_Z	P(C)	0.10	0.10	0.10
ϕ_3, ψ_H	P(D)	0.10	0.10	0.80
ϕ_3, ψ_L	P(E)	0.80	0.10	0.10
ϕ_3, ψ_Z	P(F)	0.10	0.80	0.10

For each fault detection parameter of a particular fault, the summation of the probabilities must be equal to “1”. For instance, the summation of P(A) +P(B) +P(C) that represent the positive (ϕ_2, ψ_H), negative (ϕ_2, ψ_L) and zero (ϕ_2, ψ_Z) drift of condenser approach temperature must be equivalent to 1. However, probability summation of a particular row shown in the Table 5.3 is not necessary “1” as the fault trees are built

independently for each soft fault. In order words, there will be 3 different probability tree diagrams that represent each fault.

The probability for each parameter of each fault was assigned based on diagnostic matrix formed in Table 5.1. During refrigerant leakage, condenser approach and sub-cooling temperatures experience negative drift. Thus, $\phi_2, \psi_L$and ϕ_3, ψ_L were assigned a higher probability of 0.8. On the other hand, the probabilities for ϕ_2, ψ_H and ϕ_2, ψ_Z that represent positive and zero drift in the approach temperature were assigned 0.1 respectively. Similar explanations can be provided for the rest of the faults based on Table 5.1.

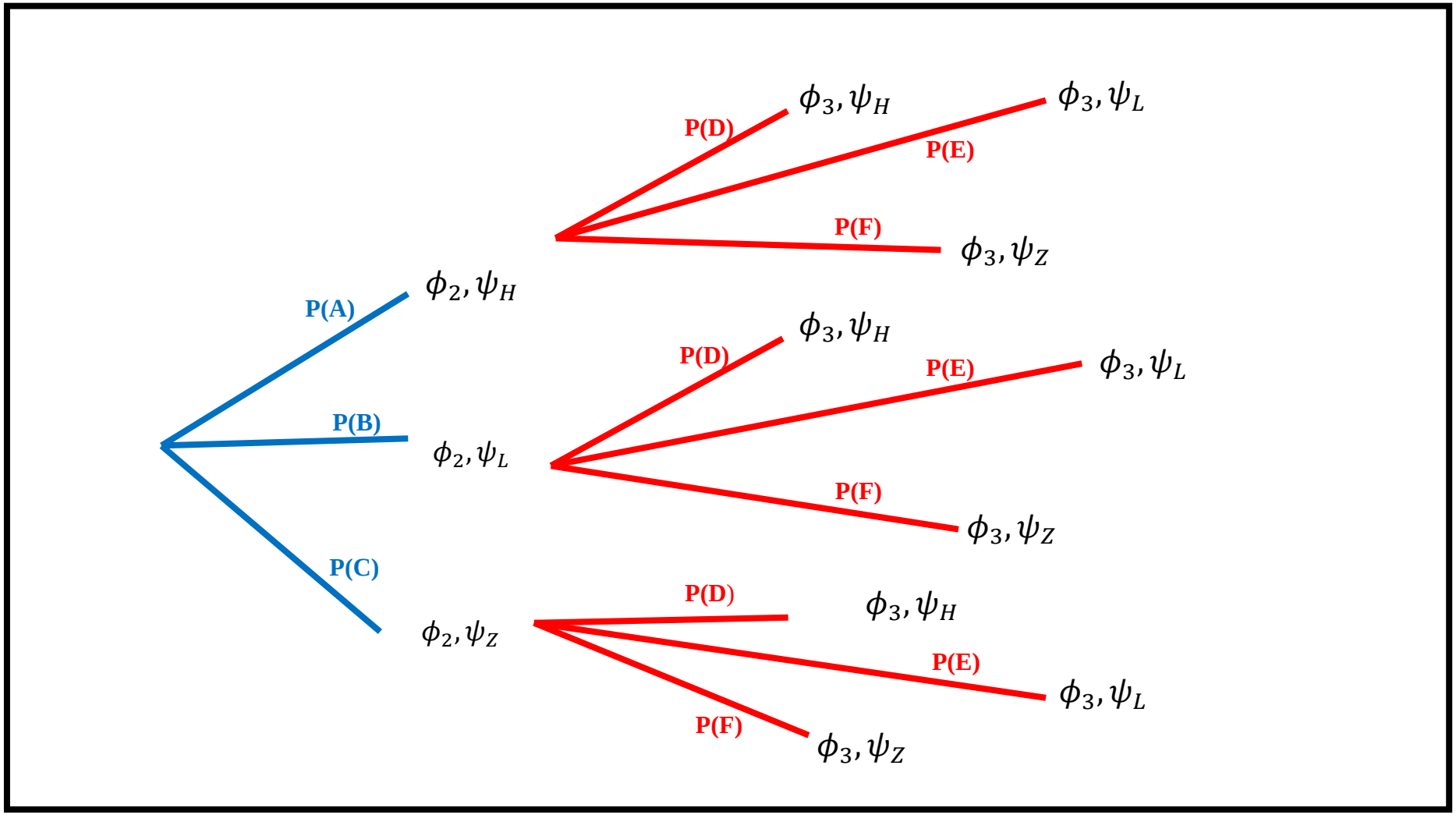

Figure 5.24: Probability tree diagram used to compute the likelihood

As mentioned earlier, the likelihood can be computed the multiplying the probabilities of each individual observation that lies in the path of the CUSUM vector, **P.** For instance, if a CUSUM vector indicates the following:- $\boldsymbol{P} = [\phi_2, \phi_3]^T = [1,1]^T$, then we can conclude that the positive drifts are detected in condenser approach and sub-cooling temperatures (note that "1"= positive drift; "-1" = negative drift and "0" =zero drift) by the respective CUSUM charts. Therefore likelihood path as shown in Figure 5.24 is traced as P(A) x P(D). On the other hand, if $\boldsymbol{P} = [0, -1]^T$, then the likelihood path is P(C) x P(E).

Finally, using the prior probability and likelihood, the posterior probability of each fault for a given vector, **P** can be computed. An example of fault diagnosis using the Bayes theorem is shown below.

Example 1: For a given $\boldsymbol{P} = [1,1]^T$, the likelihood is traced as P(A) x P(D). Using the prior probability and Equation 3.92, the posterior probabilities can be computed as shown in Table 5.4.

Table 5.4: Fault probability for a given CUSUM vector, $\boldsymbol{P} = [1,1]^T$

Fault	Prior	Likelihood	Prior x Likelihood	Posterior Fault Probability (%)
1. Ref leak	0.45	= 0.1 x 0.1 = 0.01	0.0045	=0.0045/0.1605*100 =2.8
2. Cond Foul	0.35	= 0.8 x 0.1 = 0.08	0.0280	=0.0280/0.1605*100 =17.2
3. Ref Over	0.20	= 0.8 x 0.8 = 0.64	0.1280	=0.1280/0.1605*100 =80.0
SUM	**1.00**		**0.1605**	**100.0**

The results shown in Table 5.4 clearly indicate that when positive drifts in condenser approach and sub-cooling temperatures are detected (e.g $\boldsymbol{P} = [1,1]^T$), there is a 80%

probability that the system is operating under overcharge condition. The possibility for fouling is 17.2% while almost zero probability for leakage.

Example 2: For a given $\boldsymbol{P} = [0, -1]^T$, the likelihood is traced as P(C) x P(E). Using the prior probability and Equation 3.92, the posterior probability can be computed as shown in Table 5.5.

Table 5.5: Fault probability for a given CUSUM vector, $\boldsymbol{P} = [0, -1]^T$

Fault	Prior	Likelihood	Prior x Likelihood	Posterior Fault Probability (%)
1. Ref leak	0.45	= 0.1 x 0.8 = 0.08	0.0360	=0.0360/0.0415*100 =86.8
2. Cond Foul	0.35	= 0.1 x 0.1 = 0.01	0.0035	=0.0035/0.0415*100 =8.4
3. Ref Over	0.20	= 0.1 x 0.1 = 0.01	0.0020	=0.0020/0.0415*100 =4.8
SUM	**1.00**		**0.0415**	**100.0**

The results shown in Table 5.5 clearly indicate that when a zero drift in condenser approach temperature and negative drift in the condenser sub-cooling temperatures are detected (e.g $\boldsymbol{P} = [0, -1]^T$), there is a 86.8% probability that the system is leaking. The possibility for fouling and overcharge is less than 10%.

Using all the nine possible combinations of CUSUM output $\boldsymbol{P}$, the computed probabilities of the three soft faults to occur with respect to each other are shown in Table 5.6. A unique diagnosis (labelled as "**Y**" in Table 5.6) can be assumed if the fault probability is more than 50%. In Table 5.6, seven unique diagnoses can be seen. Item No.9 of this table is misleading as the diagnosis routine is not activated when $\boldsymbol{P} = [0,0]^T$. Thus, this classification can be ignored. As for item No. 2, where $\boldsymbol{P} = [1, -1]^T$, there is no concrete

diagnosis can be made. In practice, it almost impossible for the condenser approach temperature to increase when sub-cooling temperature decreases.

Table 5.6: Fault probability for all the possible combination of CUSUM output, ***P***

No	ϕ_2	ϕ_3	**Ref leak (%)**	**Cond Foul (%)**	**Ref Over (%)**	**Unique Diagnosis**
1	1	1	2.8	17.4	**79.8**	**Y**
2	1	-1	45	35	20	
3	1	0	1.8	**91.6**	6.6	**Y**
4	-1	1	**64.9**	6.3	28.8	**Y**
5	-1	-1	**98.1**	1.2	0.7	**Y**
6	-1	0	**54.5**	42.4	3	**Y**
7	0	1	18.8	14.6	**66.7**	**Y**
8	0	-1	**86.7**	8.4	4.8	**Y**
9	0	0	13	81.2	5.8	

As of now, both the fault detection and diagnosis method have been adequately discussed. Before evaluating the diagnostics probabilities of the three soft faults evaluated in this study, it is important to study the lag between the two fault detection parameters (ϕ_2 and ϕ_3) used for diagnostic purposes. It has been outlined earlier that the diagnostic routine is activated when the one of the fault detection parameters exceeds the decision limit, Ω_2 . Thus, the other parameter will be definitely in the zero drift regions. The lag between these parameters could lead to serious error in diagnostic results as one of the parameters will be always flagged as non drift, ψ_Z. Nevertheless, this issue can be solved as we have adopted multiple thresholds (Ω_1 and Ω_2) in our proposed methodology. From the previous explanations presented in the Chapter 3, we knew that the reset drifts, ψ_R will be reinitialized to (Ω_1 /2) if the non-reset drift, ψ_{NR} exceeds the Ω_1 . As the fault severity increases, ψ_{NR} will increase over the time and eventually exceeds the second decision limit, Ω_2 and thus

triggering the diagnostic routine. To overcome the lag between the fault detection parameters (ϕ_2 and ϕ_3) when one of the ϕ reaches Ω_2, it is proposed that the diagnostic routine to judge the status of the lagged parameter using the first decision limit, Ω_1. For instance, if ϕ_2 reaches the Ω_2 and ϕ_3 is still below Ω_1 then it can be claimed that ϕ_2 is only the drifting parameter. However, if ϕ_2 reaches the Ω_2 and ϕ_3 is above Ω_1 then it can be concluded that both parameters have drifted from the nominal conditions. A better understanding of this concept can be obtained from Figure 5.25 that shows the lag between ϕ_2 and ϕ_3 during refrigerant overcharge.

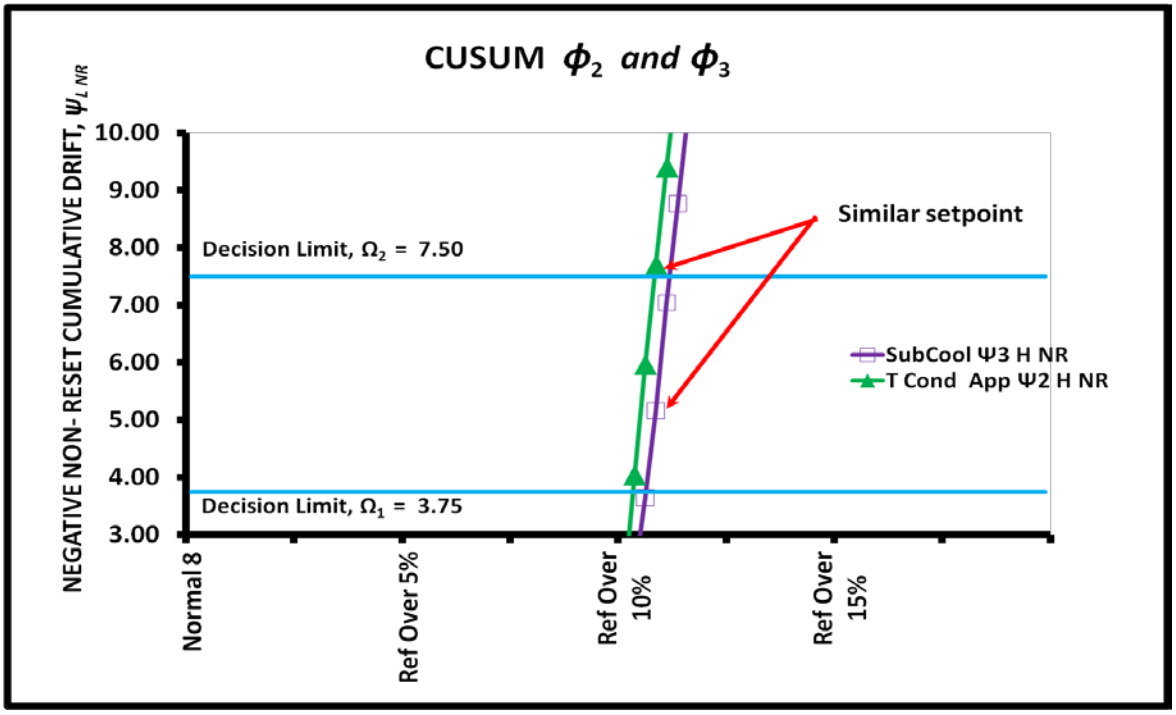

Figure 5.25: Lag between ϕ_2 and ϕ_3 during refrigerant overcharge

It can be from Figure 5.25 that $\phi_2\,\psi_H$ reached the second decision limit, $\Omega_2 = 7.5$ before $\phi_3\,\psi_H$. Thus, without considering the lag, the diagnostic routine will be computed using $\boldsymbol{P} = [1,0]^T$. Nevertheless, $\boldsymbol{P} = [1,1]^T$ will be used to in the diagnostic analysis if the lag in the $\phi_2\,\psi_H$ is considered. It can be seen from the figure that when $\phi_3\,\psi_H$ exceeded the Ω_2, $\phi_2\,\psi_H$ has already surpassed the first decision limit, $\Omega_1 = 3.75$. Thus, using the lagged

concept, both parameters were considered as positive drift and matched the diagnostic symptom for overcharge as indicated in Table 5.1.

Thus, using the proposed lagged concept and the CUSUM charts, the CUSUM output, ***P*** for the threes soft faults considered in this thesis is summarized in Table 5.7.

Table 5.7: Flagged CUSUM outputs for the simulated faults

FAULT DETECTION PARAMETER	RL 5%	RL 10%	RL 20%	CF 10%	CF 18%	CF 25%	RO 5%	RO 10%	RO 15%
Condenser Approach Temperature (ϕ_2)	ψ_Z	ψ_Z	ψ_L	ψ_H	ψ_H	ψ_H	ψ_Z	ψ_H	ψ_H
Condenser Sub-cooling Temperature (ϕ_3)	ψ_Z	ψ_L	ψ_L	ψ_Z	ψ_Z	ψ_Z	ψ_Z	ψ_H	ψ_H
CUSUM output, ***P***	$\begin{bmatrix}0\\0\end{bmatrix}$	$\begin{bmatrix}0\\-1\end{bmatrix}$	$\begin{bmatrix}-1\\-1\end{bmatrix}$	$\begin{bmatrix}1\\0\end{bmatrix}$	$\begin{bmatrix}1\\0\end{bmatrix}$	$\begin{bmatrix}1\\0\end{bmatrix}$	$\begin{bmatrix}0\\0\end{bmatrix}$	$\begin{bmatrix}1\\1\end{bmatrix}$	$\begin{bmatrix}1\\1\end{bmatrix}$

ψ_H = Positive drift, ψ_L = Negative drift, ψ_Z = Zero drift

Using the CUSUM outputs shown in Table 5.7, the Bayes diagnostic probabilities were then computed using the prior probabilities and likelihoods of each fault. The probability results are shown in Table 5.8.

Table 5.8: Computed fault probabilities

SOFT FAULT PROBABILITIES	RL 5%	RL 10%	RL 20%	CF 10%	CF 18%	CF 25%	RO 5%	RO 10%	RO 15%
REF LEAK (%)	ND	**86.8**	**98.1**	1.8	1.8	1.8	ND	2.8	2.8
COND FOUL (%)	ND	8.4	1.2	**91.6**	**91.6**	**91.6**	ND	17.4	17.4
REF OVER (%)	ND	4.8	0.7	6.6	6.6	6.6	ND	**79.8**	**79.8**
TOTAL (%)	-	100	100	100	100	100	-	100	100

From Table 5.8, it can be seen that refrigerant leakage has been successfully detected and diagnosed at the severity level of 10%. Although only one of the two parameters flagged by CUSUM (negative sub-cooling drift (ϕ_3, ψ_L), the proposed methodology was able to diagnose the leakage with a probability of 86.8%. The diagnostic capability progressively increased with additional parameter flagged by CUSUM as the fault severity increases. No detection (ND) was achieved at the severity level of 5%. As for the fouling, only an increase in the condenser approach temperature is detected for all the severity levels. The maximum diagnostic probability of 91.6% for condenser fouling is already achieved at the lowest severity level. Therefore, no further increase in the diagnostic probability can be seen for the other ascending severity levels. For refrigerant overcharge, there was no fault triggered by CUSUM at 5% overcharge. Thus, the diagnosis routine was not activated. Similar to the other faults, the probability of overcharge increases as the severity increases. At 10% overcharge, the maximum diagnostic probability for overcharge ($\boldsymbol{P}$= $[1,1]^T$) has been achieved as both parameters correctly flagged the symptoms.

.

5.6 Validation of the proposed FDD methodology

It has been clearly demonstrated that the proposed FDD scheme was able to detect and diagnose the occurrence of the soft fault at an acceptable probability. In this section, the proposed CUSUM-Bayes FDD methodology will be verified against an external laboratory chiller.

5.6.1 Overview of the External Laboratory Chiller Data

The 90 Rton McQuay centrifugal chiller used in this study was designed to meet the specification of ARI (Air-Conditioning and Refrigeration Institute) Standard 550 for Centrifugal and Rotary Screw Water-Chilling Packages. The chiller used R-134a as refrigerant and was operated from 25% to 100% cooling load in order to capture all the operating points of the chiller. The capacity control was achieved using inlet vanes. Three control variables were identified to form a 3x3x3 matrix for each data set where the variables ($T_{C,outlet}$, $T_{H,Inlet}$ and cooling load) were varied at three different ranges to obtain the 27 steady points. $T_{C,outlet}$ was varied from 277.59K (40^{o}F) to 283.15K (50^{o}F), $T_{H,Inlet}$was varied from 289.82K (62^{o}F) to 302.59.6K (85^{o}F) while cooling load was varied between 25% to 100%. The condenser and evaporator water flow rates were kept constant for all the faults studied (except for faults related to reduction in coolant flow rate). Table 5.9 summarizes the main components of the 90 Rton centrifugal chiller. Extended details on this FDD testing can be obtained from the extensive ASHRAE report by Comstock and Braun (1999).

Table 5.9: Specifications of the external laboratory chiller

Component	**Details**
Chiller	McQuay 90 Rton Centrifugal Chiller
Compressor	Centrifugal compressor with guide vane for capacity control
Expansion valve	Thermostatic expansion valve
Evaporator	Shell and Tube Type (Constant chilled water flow rate 216 gpm)
Condenser	Shell and Tube Type (Constant cooling water flow rate 270 gpm)
Refrigerant	R-134 a (in shell side for both evaporator and condenser)

5.6.2 Fault simulation of the External Chiller

In their study, Comstock and Braun (1999) investigated eight different types of fault that are possible to occur in large capacity chiller. The faults were (i) Reduction in condenser water (cooling water) flow rate (ii) Reduction in evaporator water (chilled water) flow rate (iii) Refrigerant leakage (iv) Refrigerant overcharge (v) Condenser fouling (vi) Presence of non-condensable (vii) Excessive oil and (viii) and Faulty expansion valve. In this section, we will only consider the leakage, overcharge and fouling analysis. The reduction of water flow rates can be easily detected by data logging the flow meters while the presence of non-condensable is virtually none for high pressure chiller. It is also difficult to simulate excess oil for our hermetic system.

5.6.3 Refrigerant Leakage simulation of the External Chiller

The leakage simulation was performed in the descending severity level. The system was initially evacuated to vacuum before being charged with 180lbs of R-134a to simulate the 40% leakage level 4, RL 40. Once the required data were collected, the system was then topped up with 30lbs to simulate, RL 30. Similar procedure was carried out until the system was nominally charged. Table 5.10 indicates the R-134a charge amount for each fault level.

Table 5.10: R-134a charge amount for each leakage level

Case	% Deviation	Absolute Charge
Nominal Operation	300 lbs refrigerant	300 lbs
Fault Level 1, RL 10	10% reduction in charge	270 lbs
Fault Level 2 , RL 20	20% reduction in charge	240 lbs
Fault Level 3 , RL 30	30% reduction in charge	210 lbs
Fault Level 4 , RL 40	40% reduction in charge	180 lbs

5.6.4 Condenser Fouling simulation of the External Chiller

Similar to our approach, fouling in the condenser was simulated by blocking the cooling water tubes. The effective heat transfer coefficient was lowered by reducing the surface area of the water tubes. Care was taken by the researchers to evenly distribute the plug in the 2 pass condenser. The condenser consists of 164 tubes and 4 different severity levels were simulated as shown in Table 5.11.

Table 5.11: Simulated condenser fouling levels

Case	% Deviation	Absolute Blockage
Normal Operation	164 unblocked tubes	No blocked tubes
Fault Level 1, CF 12	12% reduction in tubes	20 blocked tubes
Fault Level 2, CF 20	20% reduction in tubes	33 blocked tubes
Fault Level 3, CF 30	30% reduction in tubes	49 blocked tubes
Fault Level 4, CF 45	45% reduction in tubes	74 blocked tubes

5.6.5 Refrigerant Overcharge simulation of the External Chiller

The 90 Rton centrifugal chiller was overcharged at four different severity levels. For each fault level, an additional 30lbs of R 134-a were charged. The maximum overcharge level was capped at 40% of the nominal charge of 300lbs. Table 5.12 provides the details of the refrigerant overcharge simulation.

Table 5.12: Details of the refrigerant overcharge simulation

Case	% Deviation	Absolute Charge
Normal Operation	300 lbs refrigerant	300 lbs
Fault Level 1, RO 10	10% increase in charge	330 lbs
Fault Level 2, RO 20	20% increase in charge	360 lbs
Fault Level 3, RO 30	30% increase in charge	390 lbs
Fault Level 4, RO 40	40% increase in charge	420 lbs

5.6.6 CUSUM Fault- Free Model for External Chiller

This section describes on the CUSUM fault detection methodology for the three soft faults simulated on the external chiller. Similar to the previous analysis of the scroll chiller, the slack values, ζ_1 1 and ζ_1 were kept at 0.75 while the decision limits, Ω_1 and $\Omega_2$was fixed at 3.75 and 7.5 respectively. The sigma value can be obtained from the maximum MAD as outlined in Equation 4.10. The fault-free models for condenser approach and sub-cooling temperatures were developed using simple regression techniques. A total of eight nominal data sets were used as the nominal fault-free data sets. Of the eight, three data sets (where each data set comprised of 27 different operating points) were used to regress the required coefficients. The obtained regressed values were then used to predict the other five nominal data sets. The accuracies of the predictions were verified using the MAD technique described in Chapter 4. Tables 5.13 and 5.14 describe the fault-free models of the external 90Rton chiller for condenser approach and sub-cooling temperatures.

Table 5.13: Regressed coefficients of ϕ_2 and prediction accuracy of the model for all the normal data sets (90 Rton Chiller)

Fault Free Condenser Approach Temperature Prediction		
Data Sets	MAD (K)	
Normal	0.33	$T_{Cond,appr} = 5.16 - 0.09\,T_{H,Inlet} + 0.09P_{in}$
Normal 2	0.29	
Normal CF	0.30	
Normal 1	0.38	
Normal CF6	0.38	
Normal EO	0.32	
Normal NC	0.36	
Normal CF4	0.39	
Maximum MAD	0.39	

Table 5.14: Regressed coefficients of ϕ_3 and prediction accuracy of the model for all the normal data sets (90 Rton Chiller)

Fault Free Condenser Sub-cooling Prediction		
Data Sets	MAD (K)	$T_{subcool} = 4.15 - 0.07\,T_{H,Inlet} + 0.14\,P_{in}$
Normal	0.44	
Normal 2	0.42	
Normal CF	0.52	
Normal 1	0.60	
Normal CF6	0.52	
Normal EO	0.42	
Normal NC	0.49	
Normal CF4	0.52	
Maximum MAD	0.60	

5.6.7 CUSUM-Bayes Refrigerant Leakage Diagnosis for External Chiller

Figures 5.26 and 5.27 show the CUSUM charts of condenser approach and sub-cooling temperatures with respect to refrigerant leakage of the 90 Rton chiller. It can be seen that both condenser approach and sub-cooling temperatures exhibited negative drift as the leakage severity increased. However, the earliest detection was only observable at the end of 20% leakage for the approach temperature. A false spike was also noticeable in the condenser approach temperature, ϕ_2 CUSUM chart at a nominal data set labelled, Normal R. However, the diagnosis routine is not activated as the non-reset drift, ψ_{NR} was less than the decision limit, $\Omega_2 = 7.5$. The occurrence of false spike can be minimized by imposing stricter steady state filters and better fault-free models. As for sub-cooling, the non-reset negative drift, $\psi_{L\,NR}$ crossed the decision limit at the end of 30% leakage. A single reset can be observed at the 20% leakage level, thus indicating a possibility of lag between ϕ_2 and ϕ_3. The lag between ϕ_2 and ϕ_3 is shown in Figure 5.28. It can be seen that at 20% leakage level, ϕ_2 surpassed the decision limit, $\Omega_2 = 7.5$, thus triggering the diagnostic routine. However at

this point of time, ϕ_3 has exceed the first decision limit, $\Omega_1 = 3.75$. Therefore, the CUSUM output at this point was considered as $\boldsymbol{P} = [-1, -1]^T$.

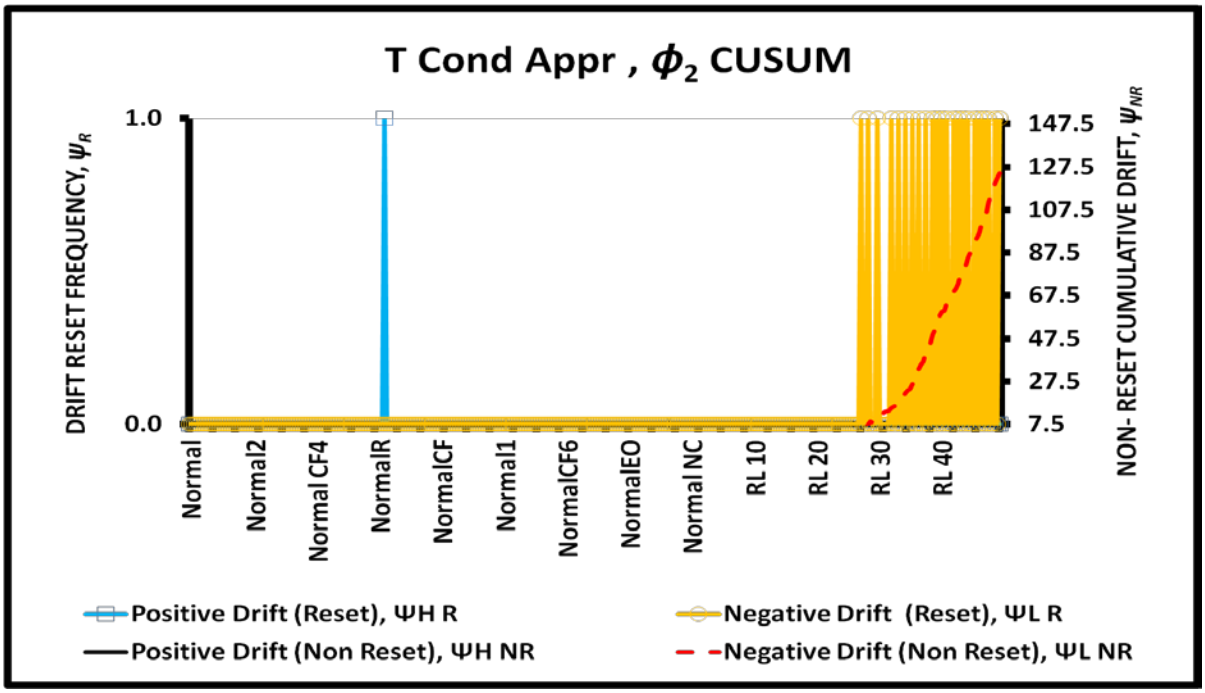

Figure 5.26: ϕ_2 during refrigerant leakage (90 Rton Chiller)

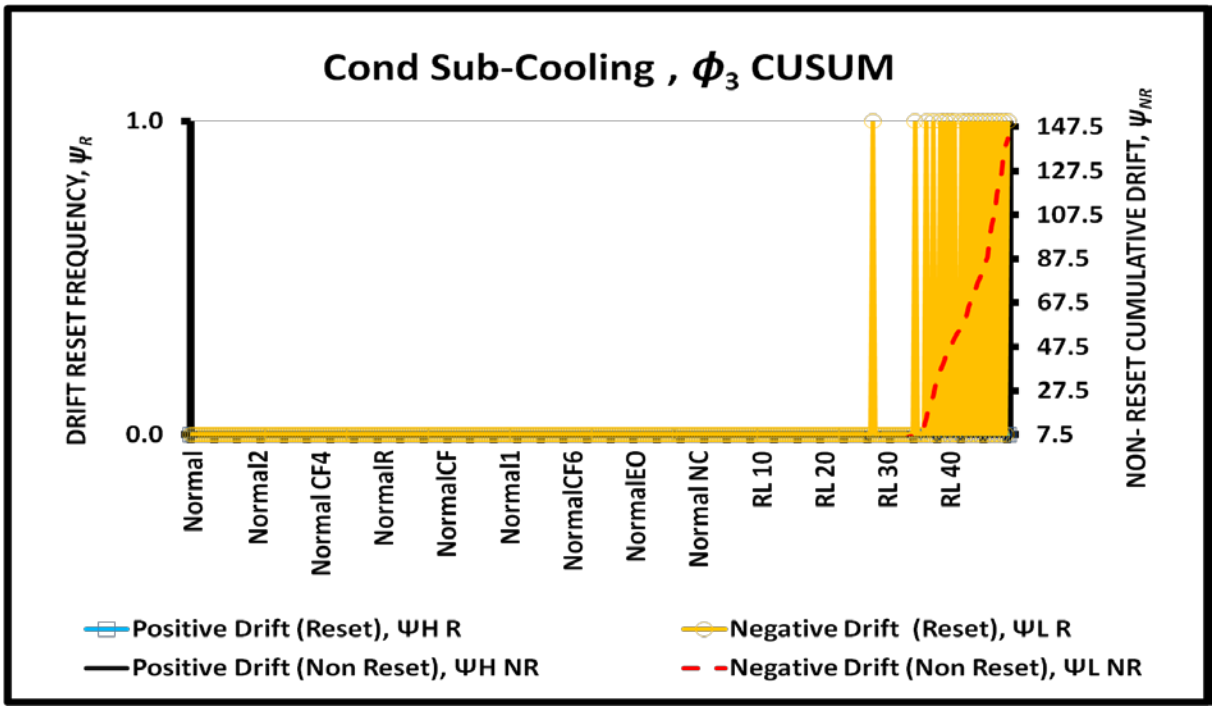

Figure 5.27: ϕ_3 during refrigerant leakage (90 Rton Chiller)

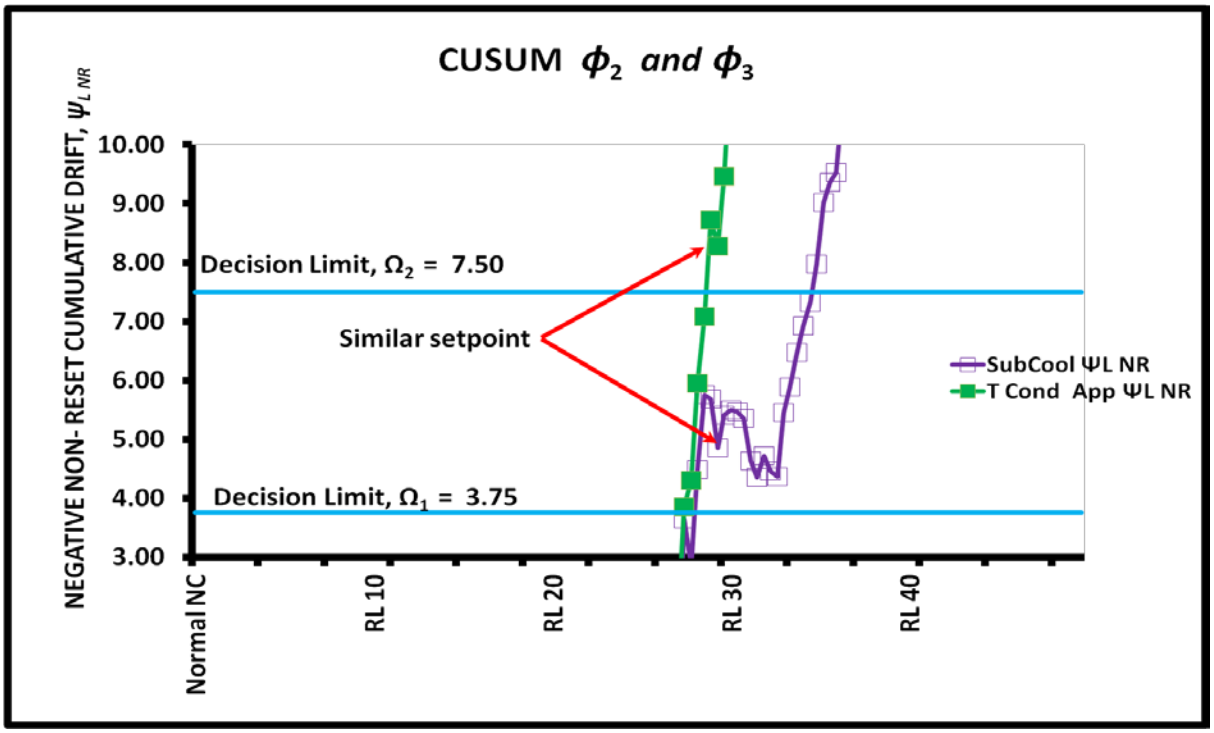

Figure 5.28: Lag between ϕ_2 and ϕ_3 during leakage (90 Rton Chiller)

Based on the CUSUM outputs, the computed Bayes probabilities during refrigerant leakage are shown in Table 5.15. The same prior probabilities and likelihoods used for the previous scroll chiller analyses were applied here.

Table 5.15: Diagnostic outputs for the leakage simulation (90 Rton Chiller)

FAULT DETECTION PARAMETER	**RL 10%**	**RL 20%**	**RL 30%**	**RL 40%**	
Condenser Approach Temperature (ϕ_2)	ψ_Z	ψ_L	ψ_L	ψ_L	**CUSUM**
Condenser Sub-cooling Temperature (ϕ_3)	ψ_Z	ψ_L	ψ_L	ψ_L	
CUSUM output, ***P***	$\begin{bmatrix}0\\0\end{bmatrix}$	$\begin{bmatrix}-1\\-1\end{bmatrix}$	$\begin{bmatrix}-1\\-1\end{bmatrix}$	$\begin{bmatrix}-1\\-1\end{bmatrix}$	
REF LEAK (%)	ND	**98.1**	**98.1**	**98.1**	**BAYES**
COND FOUL (%)	ND	1.2	1.2	1.2	
REF OVER (%)	ND	0.7	0.7	0.7	

Table 5.15 shows the diagnostic result obtained during refrigerant leakage simulation of the 90 Rton chiller. A very high probability (98.1%) of leakage can be confirmed from leakage severity of 20% and above.

5.6.8 CUSUM-Bayes Condenser Fouling Diagnosis for External Chiller

Figures 5.29 and 5.30 shows the CUSUM charts of condenser approach and sub-cooling temperatures with respect to the fouling increment in the condenser of the 90 Rton chiller.

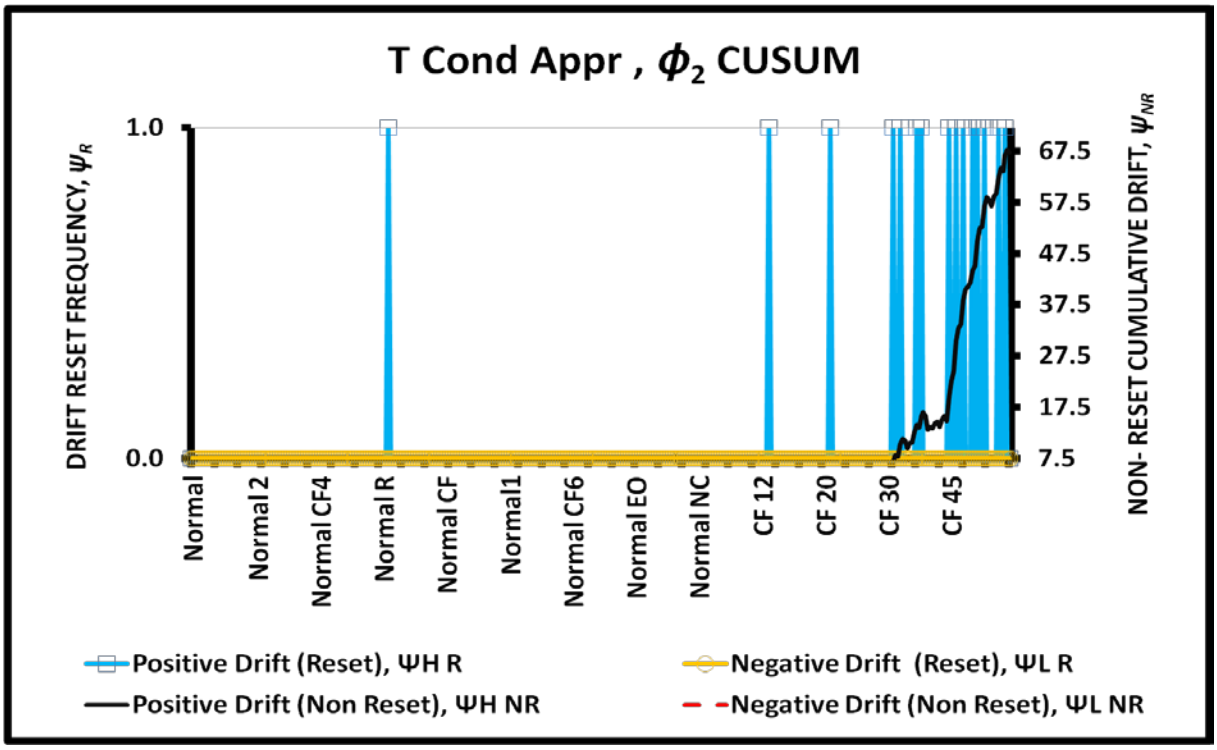

Figure 5.29: ϕ_2 during condenser fouling (90 Rton Chiller)

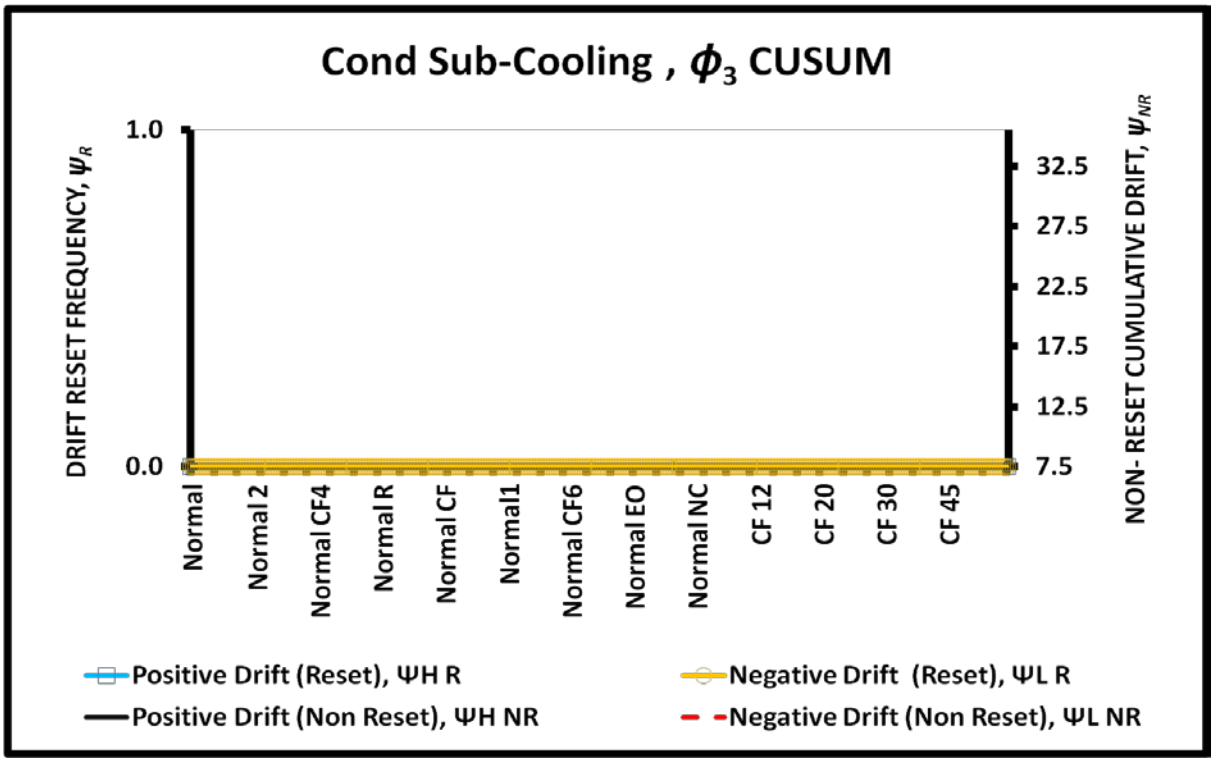

Figure 5.30: ϕ_3 during condenser fouling (90 Rton Chiller)

As for the ϕ_2 CUSUM, single resets can be observed from Figure 5.29 at CF 12 and CF 20. However these evidence is too weak and vague for the diagnosis routine to be activated as they were below Ω_2 . The first multiple reset was recorded at fouling severity of 30%. The steady climb of the non-reset positive drift substantiates the detection of the increment in the approach temperature thus triggering the diagnosis routine. Higher reset frequencies can be observed at 45% fouling level. On the other hand, ϕ_3 CUSUM as shown in Figure 5.30 indicates zero drift for all the fault levels. The lag analysis is not needed as there was no reset observed in the sub-cooling throughout the data sets. Finally, the diagnosis probability for the fouling simulation was computed using the Bayes Theorem. The diagnosis routine was not activated for the initial two fault levels. For fouling level of 30% and above, the Bayes theorem indicated that there was a probability of 91.6% for fouling to occur.

Table 5.16: Diagnostic outputs for the fouling simulation (90 Rton Chiller)

FAULT DETECTION PARAMETER	CF12%	CF 20%	CF 30%	CF 45%	
Condenser Approach Temperature (ϕ_2)	ψ_Z	ψ_Z	ψ_H	ψ_H	**CUSUM**
Condenser Sub-cooling Temperature (ϕ_3)	ψ_Z	ψ_Z	ψ_z	ψ_Z	
CUSUM output, ***P***	$\begin{bmatrix}0\\0\end{bmatrix}$	$\begin{bmatrix}0\\0\end{bmatrix}$	$\begin{bmatrix}1\\0\end{bmatrix}$	$\begin{bmatrix}1\\0\end{bmatrix}$	
REF LEAK (%)	ND	ND	1.8	1.8	**BAYES**
COND FOUL (%)	ND	ND	**91.6**	**91.6**	
REF OVER (%)	ND	ND	6.6	6.6	

5.6.9 CUSUM-Bayes Refrigerant Overcharge Diagnosis for External Chiller

Figures 5.31 and 5.32 show the trends of ϕ_2 and ϕ_3 during overcharge of the 90 Rton chiller. Both were detected at 10% overcharge level. The lag between ϕ_2 and ϕ_3 is shown in Figure 5.33. Both exhibited positive drifts as they satisfy the proposed lag criterion where the lagged parameter, ϕ_3 is above the Ω_1 when ϕ_2 exceeds, Ω_2. The diagnostic results shown in Table 5.17 revealed that there was 79.8% possibility for overcharge to occur.

Table 5.17: Diagnostic outputs for the overcharge simulation (90 Rton Chiller)

FAULT DETECTION PARAMETER	RO 10%	RO 20%	RO 30%	RO 40%	
Condenser Approach Temperature (ϕ_2)	ψ_Z	ψ_H	ψ_H	ψ_H	**CUSUM**
Condenser Sub-cooling Temperature (ϕ_3)	ψ_Z	ψ_H	ψ_H	ψ_H	
CUSUM output, ***P***	$\begin{bmatrix}0\\0\end{bmatrix}$	$\begin{bmatrix}1\\1\end{bmatrix}$	$\begin{bmatrix}1\\1\end{bmatrix}$	$\begin{bmatrix}1\\1\end{bmatrix}$	
REF LEAK (%)	ND	2.8	2.8	2.8	**BAYES**
COND FOUL (%)	ND	17.4	17.4	17.4	
REF OVER (%)	ND	**79.8**	**79.8**	**79.8**	

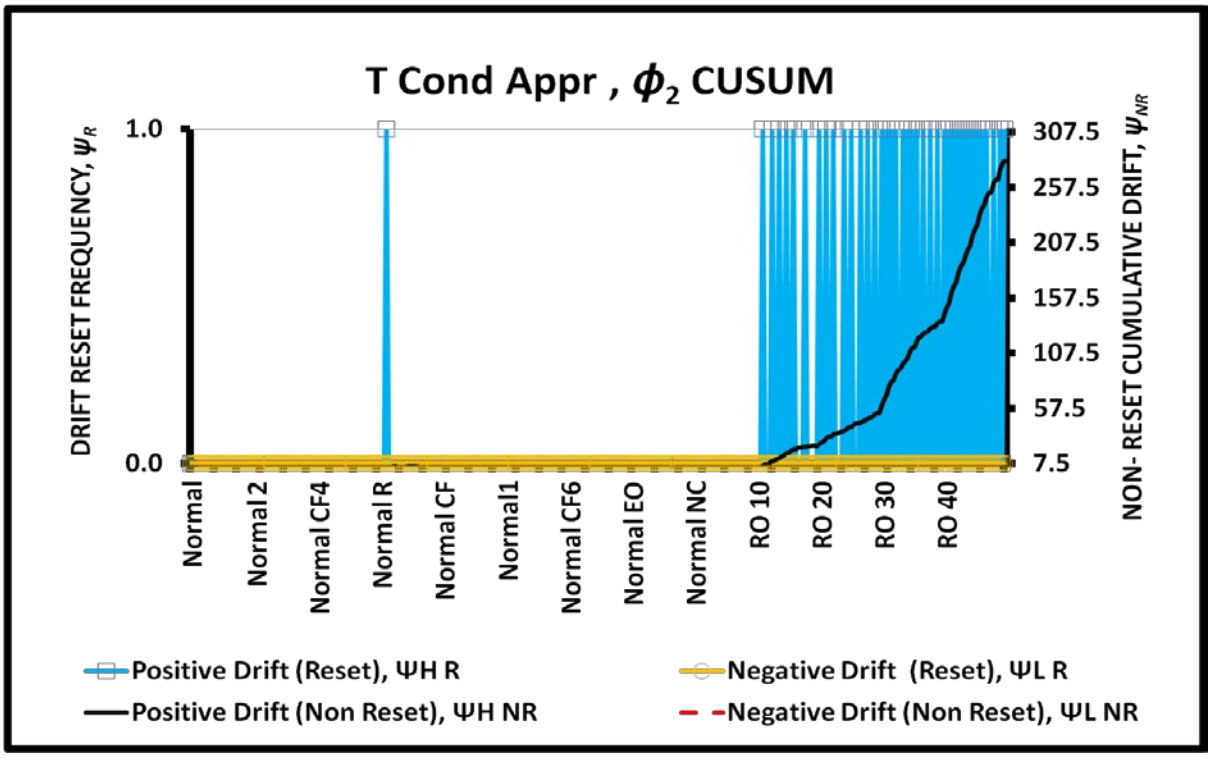

Figure 5.31: ϕ_2 during refrigerant overcharge (90 Rton Chiller)

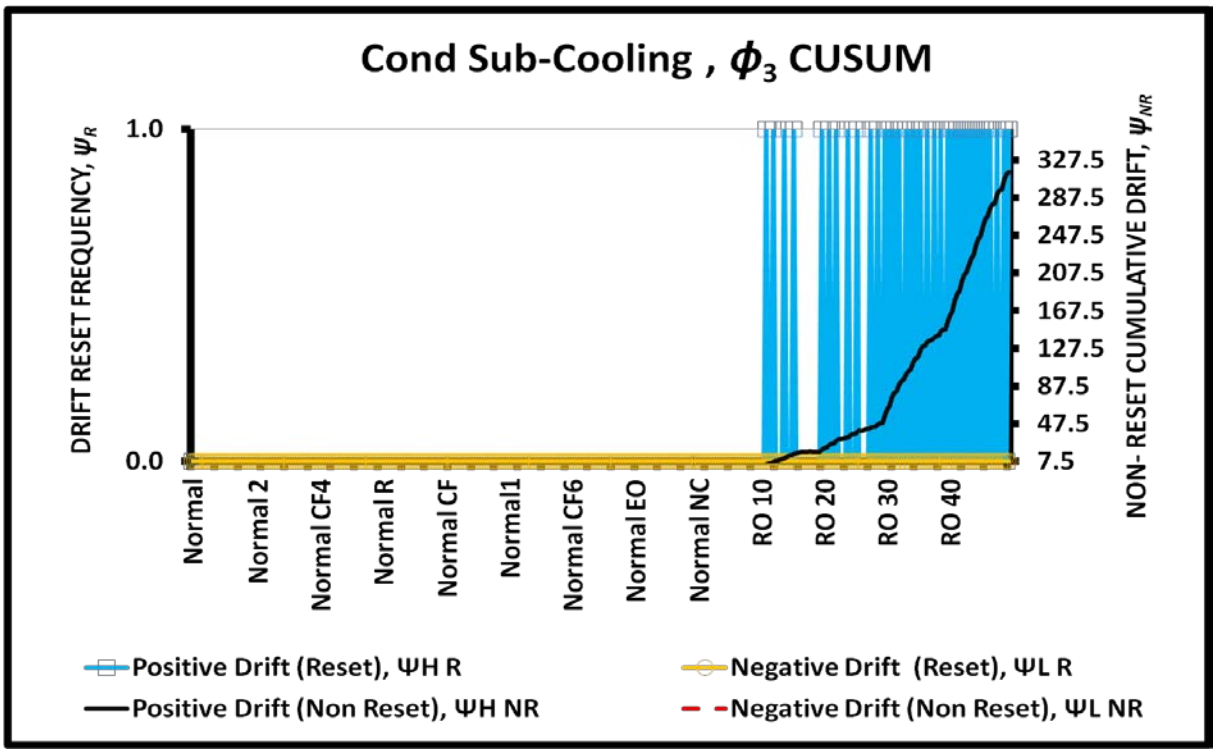

Figure 5.32: ϕ_3 during refrigerant overcharge (90 Rton Chiller)

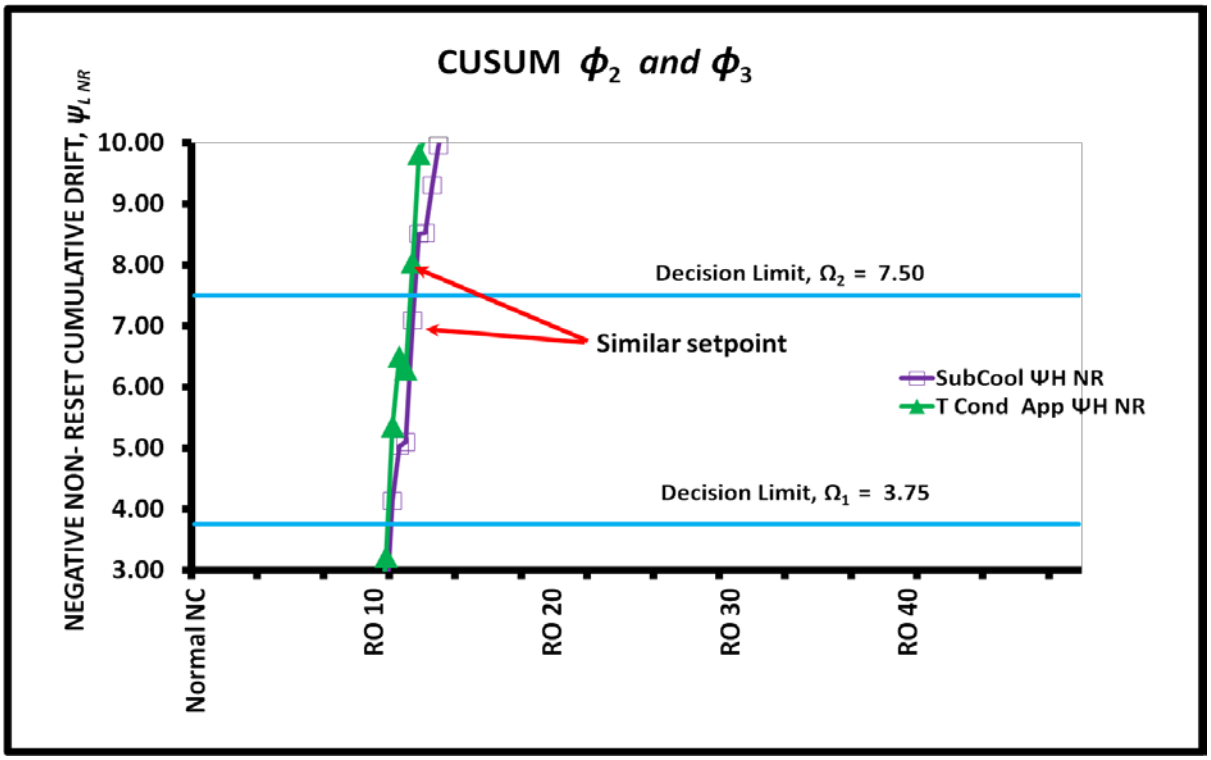

Figure 5.33: Lag between ϕ_2 and ϕ_3 during overcharge (90 Rton Chiller)

5.7 Proposed CUSUM-BAYES Fault Detection and Diagnosis Scheme

It has been demonstrated earlier that the proposed CUSUM-Bayes technology is capable of diagnosing the three soft faults considered in this study. The following flow chart as shown in Figure 5.34 summarizes the proposed FDD scheme. The extended details of the scheme are described in the following steps:-

1. Start

The start command activates the data acquisition system.

2. Data Input

The desired temperature, pressure, power and flow rate measurements are data logged and stored in the database.

3. Steady State (SS) Computation

The scroll chiller is assumed to be in a steady state if deviations in the steady indicators were below the allowable tolerances for a minimum period of 15 minutes. The maximum allowable deviation for each steady indicator is as follows:-

i. 0.15 K tolerance for the leaving chilled water temperature
ii. 0.15 K tolerance for the entering cooling water temperature
   a. Hz tolerance for the compressor frequency
iii. 5% tolerance in the cooling load for full load data and 7.7% tolerance at a part load of 70%
iv. 5% tolerance in the overall system energy balance for full load data and 7.7% tolerance at a part load of 70%

Apart from the above criteria, the cooling and chilled water flow rates are to be maintained at 48.6 Lpm and 38.7 Lpm (for this particular Scroll Chiller testing), respectively. Maximum deviation of 5% is allowed for both measurements.

4. Steady State criterion

A decision block is required to confirm the steady state operation. If any of the criterions mentioned in step 3 is not met, then the system is categorized as unsteady and the data acquisition process repeats. If the criterions are met, the next step is triggered.

5. Steady State Data Points

This step is required so that different steady state points can be used to trigger the CUSUM analysis. This step is important to prevent a single steady state point from dominating the drift accumulation in the CUSUM charts. If a different steady state point is detected then CUSUM analysis is executed.

6. CUSUM Analysis

The CUSUM analysis as described earlier is carried out at this step. The positive and negative drifts are kept accumulated from the previous steady state data points. The fault free model is used to compute the deviations.

7. Bayes Diagnostic

Once one of the fault detection parameters exceeds the second decision limit Ω_2, the diagnostic routine is activated. The lag between parameters need to be considered before the executing the probability computation. The data acquisition resumes after the diagnostic computation is completed.

5.8 Summary

The proposed CUSUM-Bayes diagnostics methodology was tested on two different vapor compression systems:- (i) a 15 kW water cooled scroll chiller (the test rig developed specifically for this study and (ii) a 90 R-ton centrifugal chiller (external chiller data obtained from ASHRAE RP). Both systems were simulated for leakage, overcharge and condenser fouling fault. For the leakage simulation on the scroll chiller, the proposed FDD scheme was able to detect the fault at lowest severity level of 10% with an acceptable probability of

86.8%. The occurrence of 10% fouling was also successfully diagnosed with a probability of 91.6%. Finally, for overcharge simulation on the similar chiller, the fault was not detected (missed detection) at the lowest severity level of 5%. However, an overcharge of 10% and above was correctly diagnosed with a probability of 79.8%. For the 90 Rton centrifugal chiller, the leakage was diagnosed with a high probability (98.1%) from the severity of 20% and above. As for the fouling, the diagnostic was only possible from 30% severity level and above with a probability of 91.6%. On the other hand, overcharge was successfully diagnosed at the lowest severity level of 10% with a probability of 79.8%. It can be concluded that the proposed CUSUM-Bayes technique can be successfully applied in detecting the soft faults simulated in this study.

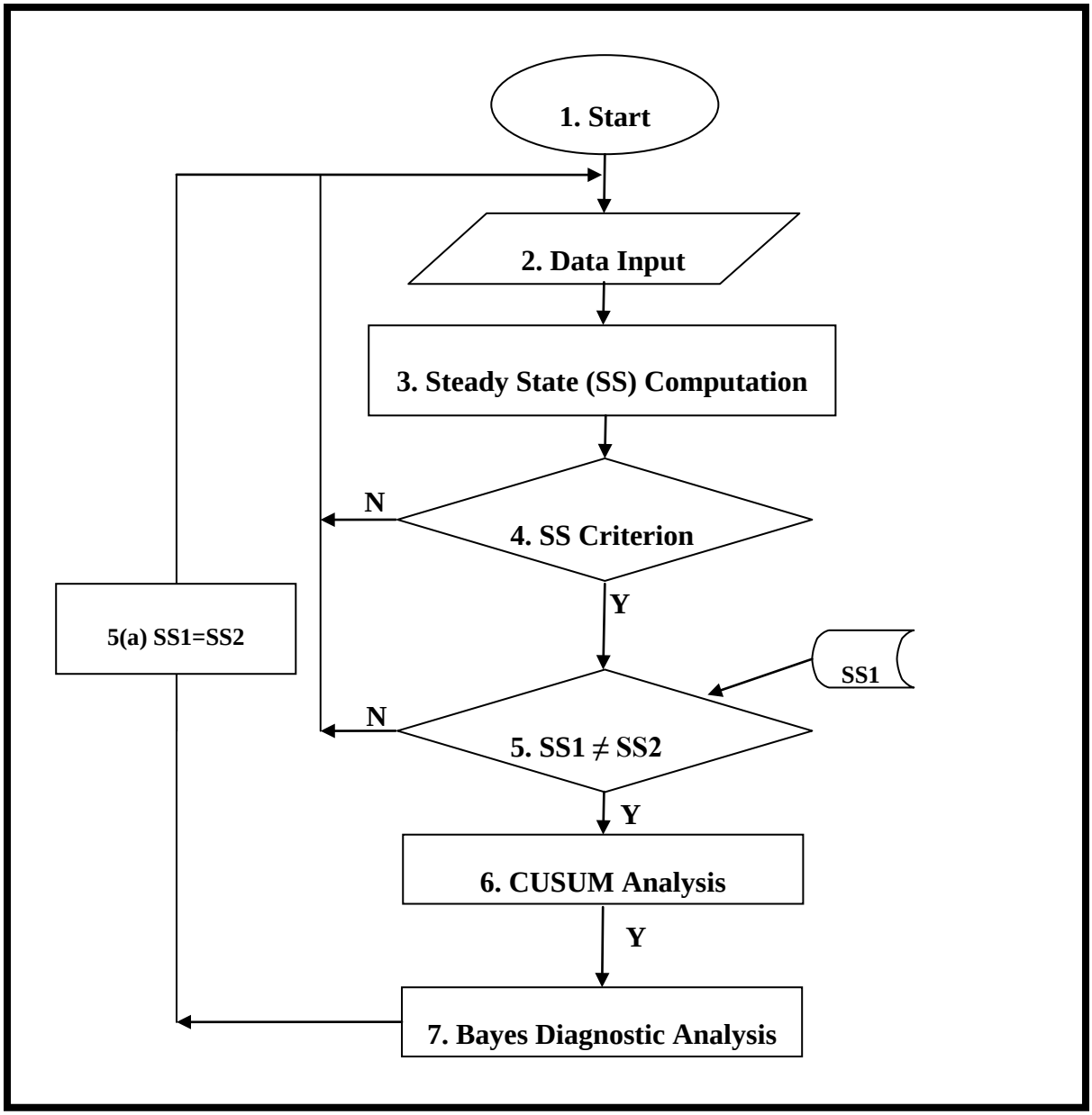

Figure 5.34: Proposed FDD scheme

Chapter 6: Conclusion and Future Work

6.1 Conclusion and Summary of the Thesis

The current study demonstrates the significance of developing a reliable and accurate fault detection and diagnosis (FDD) analysis for vapor compression chillers. As chillers consume approximately 50% of the total electricity of a commercial building, dedicated FDD software can play a pivotal role in detecting and diagnosing faults at preliminary stages. Earlier fault detections will result in significant savings in terms of breakdowns and maintenance costs. In this regard, we have developed simple yet reliable FDD scheme that is capable of capturing *soft* faults at initial stages.

In this study, an inverter driven scroll chiller test facility was designed in accordance to the industrial standards complete with high accuracy instruments. The test facility consisted of two primary systems, namely the coolant and the refrigerant system. The coolant system was developed to simulate artificial building loads by mixing the evaporator and condenser leaving water. A mixing chamber with staggered internal baffles was designed to achieve this purpose. The temperature control mechanism to obtain the desired temperature set points was accomplished using four units of electric linear modulating valves. The valves were modulated by PID controllers that were developed using LabView 8.6. The inputs for the controllers were: (i) evaporator leaving water temperature (ii) condenser return water temperature and (iii) cooling tower return water temperature. Based on experimental test data it was obvious that the designed mixing chamber aided with the modulating valves effortlessly achieved the desired set points. The temperature variations of the desired set points were less than 0.15 K for both the condenser return water and evaporator leaving water

respectively. Precisely controlled set points were important in this study. The set points act as fixed inputs for all the test runs, thus allowing direct comparison between the faulty and fault-free data. Large variations in the temperature set points lead to erroneous comparison and raise ambiguity on the quality of the test data and the fault analysis. In short, the entire analysis of this study is neither possible nor accurate without precisely controlled set points. The temperature set points of this study were achieved using PID controllers that transmitted DC analog inputs to the electrical actuators that opened or closed the two-way globes. It was noticed that the valves responded at a relatively slower rate compared to incoming DC Volt inputs. The slow dynamic responses of the valves resulted in a mismatch between the controllers and valves, thus resulting in longer time to achieve the set points. Although timing in achieving the set points is not critical for this study (which is only focusing on steady state analysis), future analysis will be mainly revolving around the transient responses of refrigerant system. The slower valve dynamics will have undesired effects on the transient analysis. It is recommended that the valves and actuators to be replaced with swift response valves to obtain a good quality transient data.

A significant portion of this thesis focused on the performance and thermodynamics characteristics of a 15 kW R22 scroll chillers due to the presence of *soft* faults (also commonly referred as degrading faults). It was widely reported in the literature that heat exchanger fouling (particularly condenser) and refrigerant leakage were the two foremost common *soft* faults in vapor compression chillers. These two faults along with refrigerant overcharge were extensively studied and analyzed based on collected data which comprised of: - (i) seven temperature and pressure readings of the refrigerant system (ii) 5 temperature readings of the coolant system (iii) three volumetric flow rates readings (condenser water, evaporator water and refrigerant R22) and (iv) compressor power reading. The test runs were firstly conducted at fault-free conditions. They were then followed by another series of faulty

test runs with an increasing step of 10% in the severity level of a particular fault. Fouling phenomenon was artificially introduced to the system by blocking the condenser water tubes accordingly to the fault severity level. On the other hand, refrigerant leakage was simulated by undercharging the system. Conversely, overcharge was performed by topping up the system with additional refrigerant. To safeguard the compressor from the liquid flood back effect, the maximum overcharge was limited to 15%. Both the nominal and faulty data were collected at twenty different steady state set points. The primary and secondary criterions for the steady state analysis were clearly described in the chapter 4.

Once the steady state filtration was accomplished, fault-free models were developed for the selected fault detection parameters namely, (i) suction superheat temperature (ii) condenser approach temperature (iii) condenser sub-cooling (iv) overall condenser heat transfer coefficient and (v) condenser entropy generation. Simple regression technique was adopted to generate the fault free model for each of the parameters mentioned above using leaving chilled water temperature, $T_{C,outlet}$, entering cooling water temperature, $T_{H,Inlet}$ and compressor power, P_{in} as independent variables. Details of regression technique were elaborated in the chapter 4. The prediction accuracies of the regressed models were judged using Mean Average Deviation (MAD). The smaller the MAD, the better the predictions are. The MAD values are important for the fault detection analysis. In this study, the faults were detected using the CUSUM technique. CUSUM is a very useful statistical technique that is capable of detecting minute shifts or drifts. As soft faults developed gradually in chillers, the need for a detection technique that captures “slow” faults at the earliest possible time frame is crucial. In this regard, CUSUM is one of the best yet simple available techniques. In order to develop a CUSUM framework, the following parameters: - (i) slack parameter (ζ), (ii) sigma (σ), and (iii) decision limits $\Omega_1$and Ω_2 need to be established. These details were also sufficiently covered in the Chapter 3. A fault is considered detected if the non-reset drift

(negative or positive) of any of the CUSUM parameters surpasses the decision limit, $\Omega_2 = 7.5$. A simple lag analysis was also proposed in order to enhance the diagnostic results. Once a fault is detected, the diagnosis routine is then activated. The diagnostic routine worked using the principle of Bayes probability which was already extensively covered in the chapter 3 and 5. Although five fault detection parameters were investigated, it was found out that condenser approach and condenser sub-cooling temperatures were more than sufficient to evaluate the three soft faults investigated in this study. These parameters are readily available in industrial chillers and have less measurement uncertainties.

The proposed CUSUM-Bayes diagnostics methodology was tested on two different vapor compression systems:- (i) a 15 kW water cooled scroll chiller (the test rig developed specifically for this thesis and (ii) a 90 R-ton centrifugal chiller (external chiller data obtained from ASHRAE RP). Both systems were simulated for leakage, overcharge and condenser fouling fault. For the leakage simulation on the scroll chiller, the proposed FDD scheme was able to detect the fault at lowest severity level of 10% with an acceptable probability of 86.8%. The occurrence of 10% fouling was also successfully diagnosed with a probability of 91.6%. Finally, for overcharge simulation on the similar chiller, the fault was not detected (missed detection) at the lowest severity level of 5%. However, an overcharge of 10% and above was correctly diagnosed with a probability of 79.8%. For the 90 Rton centrifugal chiller, the leakage was diagnosed with a high probability (98.1%) from the severity of 20% and above. As for the fouling, the diagnostic was only possible from 30% severity level and above with a probability of 91.6%. On the other hand, overcharge was successfully diagnosed at the lowest severity level of 10% with a probability of 79.8%. Finally, a flow diagram that outlined the FDD scheme was presented. This flow diagram is vital for software development purposes. The scheme was developed using only a handful number of measurements that is usually available in commercial and industrial chillers. Apart from that, the proposed scheme

can be easily programmed as commercial software due to its simple and straight forward equations.

It has to be pointed out that refrigerant leakage diagnosis for both chillers was only possible from minimum 10% severity level and above. As 10% leakage level is considered as a serious issue, it is believed that inability of the proposed model to detect this fault at much earlier level could be due to the design (oversize) of chiller itself and the type of expansion valve. It is believed that if a chiller is designed as a critically charge system, then leakage fault can be detected at a much earlier rate. Apart from that, over-sizing of expansion valves also could be a factor as valves tend to compensate the leakage effect by regulating refrigerant flow rate.

6.2 Future Work

Two primary areas for future work are identified in this study. They are (i) transient fault detection and diagnostics analysis and (ii) the development of computer software using the proposed analysis.

As the current work has only considered the occurrence of soft faults over a period of time, steady analysis is sufficient to detect and diagnose the faults. However, there is a high possibility for the chillers to operate in highly transient loadings such as in supermarket and office buildings. This emphasizes the need for a FDD scheme that is able to capture the soft faults at transient conditions.

The other task is primarily focused in packaging the FDD scheme into commercial software. As the current data acquisition is accomplished using the LabView environment, the proposed scheme can be easily developed using the similar environment. Another

advantage of choosing LabView as the development platform is due to the ability of the platform to be converted into executable standalone files. This exe file can be easily installed on the client workstation that operates on WINDOWS, MAC of LINUX platforms. The final software will also be packaged with the p-H diagram and other standard GUIs related to chiller operations.

References

Anderson, D., L. Graves, W. Reinert, J.F. Kreider,, J. Dow and H. Wubbena, 1989. A quasi-real-time expert system for commercial building HVAC diagnostics, ASHRAE Tran.95(2)2.

ASHRAE, 1996. Fault Detection and Diagnosis for HVAC Systems, ASHRAE Technical Data Bulletin Vol. 12, no.2.

Babnik,T., and Gubina, F., 2001. Two approaches to power transformer fault classification based on protection signals, Electrical Power and Energy Systems 24 (2002) 459-468.

Badavas, P.C., 1993. Real-Time Statistical Process Control, Prentice-Hall.

Berry, D.A., 1996, Statistics A Bayesian Perspective, Wadsworth Publishing Company

Bourdouxhe, J.P., M. Grodent, and J.LeBrun, 1999. HVAC1 Toolkit- A Toolkit for Primary HVAC System Energy Calculations, American Society of Heating, Refrigerating and Air-conditioning Engineers, Atlanta, GA.

Browne, M.W. and P.K. Bansal, 1998. Steady-state model of centrifugal liquid chillers, International Journal of Refrigeration, Volume 21, Issue 5, Pages 343-358

Browne, M.W., and P.K. Bansal, 1998. Challenges in modeling vapor compression liquid chillers, ASHRAE Tran. 104(1):474-486.

Browne, M.W., and P.K. Bansal, 2001. Different modelling strategies for in situ liquid chillers Proceedings of the Institution of Mechanical Engineers, Part A: Journal of Power and Energy , Volume 215, Issue 3, Pages 357-374

References

Braun, J.E. 1999. Automated fault detection and diagnostics for the HVAC&R industry, IJHVAC&R Research, 5(2):85-86.

Breuker, M.S. and J.E. Braun. 1998a. Common faults and their impacts for rooftop air conditioners, IJHVAC&R Research 4(3).

Breuker, M.S. and J.E. Braun. 1998b. Evaluating the performance of a fault detection and diagnostic system for vapor compression equipment, IJHVAC&R Research 4 (4).

Bolstad, W.M., 2004. Introduction to Bayesian Statistics, Wiley-Interscience.

Castro, N.S.,2002. Performance evaluation of a reciprocating chiller using experimental data and model predictions for fault detection and diagnosis, ASHRAE Trans, 108(1).

Cengel, Y.A., and Boles, M.A., 2002. Thermodynamics An Engineering Approach 4th Edition, McGraw-Hill Higher Education

Chen, B. and J.E. Braun, 2001. Simple rule-based methods for fault detection and diagnostics applied to packaged air conditioners, ASHRAE Trans., 107(1).

Comstock, M. C., B. Chen, and J.E. Braun. 1999. Literature Review for Applications of Fault Detection and Diagnostic Methods to Vapor Compression Cooling Equipment. Ray W. Herrick Laboratories. Purdue University. HL 99-19: Report #4036-2, December.

Comstock, M.C. and J.E. Braun, 1999. Development of Analysis Tools for the Evaluation of Fault Detection and Diagnostics in Chillers, ASHRAE Research Project 1043-RP; also, Ray W. Herrick Laboratories. Purdue University. HL 99-20: Report #4036-3, December.

Corcoran, J.P. and Reddy, T.A., 2003. Improving the process of certified and witnessed factory testing for chiller procurement, ASHRAE Tran.109(1), January.

References

Cui J., and Wang S., 2005. A model-based online fault detection and diagnosis strategy for centrifugal chiller systems. International Journal of Thermal Sciences, 44 (10), pp. 986-999.

Demirel, Y. , 2007. Nonequilibrium Thermodynamics: Transport and Rate Processes in Physical and Biological Systems 2nd Edition, Elsevier

Dexter, A.L. and M. Benouarets, 1997. Generic approach to identifying faults in HVAC plants, ASHRAE Trans., 102(1): 550-556.

Dexter, A.L. and D.Ngo, 2001. Fault diagnosis in air-conditioning systems: A multi-step fuzzy model-based approach, ASHRAE Trans., 107(1), AT-01-14-3.

Gordon, J.M. and K.C. Ng., 1995. Predictive and diagnostic aspects of a universal thermodynamic model for chillers, International Journal of Heat and Mass Transfer Volume 38, Issue 5, Pages 807-818

Gordon, J.M. and K.C. Ng, 2000. Cool Thermodynamics, Cambridge International Scientific Publishers, Cambridge, UK.

Gordon, J.M., Ng, K.C., Chua, H.T , 2000. How varying condenser coolant flow rate affects chiller performance: thermodynamic modeling and experimental confirmation, Applied Thermal Engineering 20, 1149 1159

Grimmelius, H.T., J.K.. Woud, and G. Been. 1995. On-line Failure Diagnosis for Compression Refrigeration Plants, International Journal of Refrigeration, 18(1): pp. 31-41.

Grimmelius, H.T., Meiler, P.P., Maas, H.L.M.M., Bonnier., Grenvik, J.S., and Robert, F.V.K, 1999. Thress State-of-the-Art Methods for Condition Monitoring, IEEE Trans on Industrial Electronics, Vol. 46. No.2

References

Hawkins, D.M., and Olwell, D.H., 1997.Cumulative Sum Charts and Charting for Quality Improvement, Springer-Verlag

Haves, P., T.I. Salsbury and J.A. Wright, 1996. Condition monitoring in HVAC subsystems using first principles models, ASHRAE Tran., 102(1), AT-96-3-1.

Henke, J.E., and Wichern, D.W., 2005. Business Forecasting 8th Edition, Prentice Hall

Holman, J.P., 1989. Experimental Methods for Engineers 5th Edition, McGraw-Hill Book Company

Hydeman, M. et al. 2002. Development and testing of a reformulated regression based electric chiller model, ASHRAE Transactions 108(2) 1118-27.

Isserman, R. and P. Balle, 1997. Trends in the application of model-based fault detection and diagnosis of technical processes, Control. Eng. Practice, 5(5): 709-719.

Jia, Y., and T.A. Reddy,, 2003. Characteristic physical parameter approach to modeling chillers suitable for fault detection, diagnosis and evaluation, ASME Journal of Solar Energy Eng., 125: 258-265, August.

Jensen, F.V., and Nielsen, T.D., 2007. Bayesian Networks and Decision Graphs 2nd Edition, Springer

Jiang, W. and T.A. Reddy, 2003. Reevaluation of the Gordon-Ng performance models for water-cooled chillers, ASHRAE Trans., 109(2), June.

J.M. Gordon, K.C. Ng and H.T. Chua, 1997. Optimizing chiller operation based on finite-time thermodynamics: universal modeling and experiment confirmation, Int J. Refrig, Vol 20, No.3, pp. 191 – 200.

References

J.M. Gordon, K.C. Ng and H.T. Chua., 1995. Centrifugal chillers: thermodynamic modelling and a diagnostic case study, Int. J. Refrig, 18(4):253-257

Katipamula, S. and M.R. Brambley, 2005a. Methods for fault detection, diagnostics and prognostics for building systems- A review, Part I, IJHVAC&R Research, vol.11 (1):3-25, January.

Katipamula, S. and M.R. Brambley, 2005b. Methods for fault detection, diagnostics and prognostics for building systems- A review, Part II, IJHVAC&R Research, vol.12 (2):169-187.

Kim, M., Kim, M.S., 2005. Performance investigation of a variable speed vapor compression system for fault detection and diagnosis, International Journal of Refrigeration Volume 28, Issue 4, Pages 481-488.

Navarro-Esbrí, J., Torrella, E.b, Cabello, R.,2006. A vapour compression chiller fault detection technique based on adaptative algorithms. Application to on-line refrigerant leakage detection, International Journal of Refrigeration, Volume 29, Issue 5,Pages 716-723.

Ng, K. C., Chua, H.T., Ong, W., Lee, S. S., and Gordon, J.M., 1997. Diagnostics and optimization of reciprocating chillers: theory and experiment, Applied Thermal Engineering, 17(3):263-276

Li, H. and J.E. Braun, 2003. An improved method for fault detection and diagnosis applied to packaged air conditioners, ASHRAE Trans., 109(2).

McIntosh, I.B.D., J.W. Mitchell and W.A. Beckman, 2000. Fault detection and diagnosis in chillers- Part 1: Model development and application, ASHRAE Trans., 106(2).

References

Peitsman, H.C. and V. Bakker, 1996. Application of black-box models to HVAC systems for fault detection, ASHRAE Trans., 102(1): 628-640.

Reddy, T.A. and Andersen, K.K., 2002. An evaluation of classical steady-state off-line linear parameter estimation methods applied to chiller performance data, IJHVAC&R Research, 8(1):101-124.

Reddy, T.A., Niebur, D., Gordon, J., Seem, J., Cabrera, G., Jia, Y., Andersen, K., and Pericolo P., 2001. Development and Comparison of On-line Model Training Techniques for Model-Based FDD Methods Applied to Vapor Compression Chillers- Evaluation of Mathematical Models and Training Techniques, Final Project Report of the ASHRAE Research Project 1139, September.

Reddy, T.A., 2006. Evaluation and assessment of fault detection and diagnostic methods for centrifugal chillers- phase II, ASHRAE Research Project RP-127

Reddy, T.A., 2007. Formulation of a generic methodology for assessing FDD methods and its specific adoption to large chillers. ASHRAE Transactions 113(1). 281–95.

Reddy, T.A., 2007. Application of a generic methodology to assess four different chiller FDD methods (RP-1275). HVAC&R Research (13).

Reddy, T.A., 2007. Development and Evaluation of a Simple Model-Based Automated Fault Detection and Diagnosis (FDD) Method Suitable for Process Faults of Large Chillers, ASHRAE Transactions 113.

Rueda, E.Show., Tassou, S.A.,Grace, I.N.S., 2005. Proceedings of the Institution of Mechanical Engineers, Part E: Journal of Process Mechanical Engineering Volume 219, Issue 2, Pages 117-125

References

Riemer, P.L., J.W. Mitchell and W.A. Beckman, 2002. The use of time series analysis in fault detection and diagnosis methodologies", ASHRAE Tran.108 (2).

Rossi, T.M. & J.E. Braun. 1997. A Statistical, rule-based fault detection and diagnostic method for vapor compression air conditioners, IJHVAC&R Research 3(1): 19-37.

Saad, M.A., 1993. Compressible Fluid Flow, Prentice-Hall

Saththasivam, J. and Ng, K.C., 2008. Predictive and Diagnostic Methods for Centrifugal Chillers, ASHRAE Transactions 114, Part 1, pp. 282-287.

Saththasivam, J., Tang, G., Ng. K.C., 2010. Evaluation of the Simple Thermodynamic Model (Gordon and Ng Universal Chiller Model) as a Fault Detection and Diagnosis Tool for On-Site Centrifugal Chillers. International Journal of Air Conditioning and Refrigeration, Volume No.18, Issue No. 1

Saththasivam, J., Ng. K.C. 2010, Automated Performance Monitoring of a Standard Inverter Split Unit R-410A, Automated Test Summit 2010

Saththasivam, J., Ng. K.C. 2010. Performance Study of Thermostatic and Electronic Expansion Valve of Water Cooled Scroll Chiller. Fifth Asian Conference on Refrigeration and Air Conditioning.

Schein, J. and J.M. House, 2003. Application of control charts for detecting faults in variable-air-volume boxes, ASHRAE Tran.109(2), July.

Sreedharan, P., and Haves.,P, 2001. Comparison of Chiller Models for Use in Model-Based Fault Detection, International Conference for Enhanced Building Operations

References

Stylianou, M. and D. Nikanpour, 1996. Performance monitoring, fault detection, and diagnosis of reciprocating chillers, ASHRAE Tran, 102(1):615-627.

Stylianou, M.P.1997. Application of classification functions to chiller fault detection and diagnosis, ASHRAE Tran., 103(1):641-648.

Swider, D.J., 2002. A comparison of empirically based steady-state models for vapor compression liquid chillers, Applied Thermal Engineering Volume 23, Issue 5, Pages 539-556

Tsuitsui, H. and K. Kimmura, 1996. Chiller condition monitoring using topological case-based modeling, ASHRAE Trans., 102(1): 641-648.

Venkatasubramanian, V., R. Rengaswamy, K. Yin and S.N. Kavuri, 2003a. A review of process fault detection and diagnosis, Part I: Quantitative model-based methods, Computers in Chemical Engineering, 27:293-311.

Venkatasubramanian, V., R. Rengaswamy, K. Yin and S.N. Kavuri, 2003b. A review of process fault detection and diagnosis, Part II: Quantitative models and search strategies, Computers in Chemical Engineering, 27:313-326.

Venkatasubramanian, V., R. Rengaswamy, K. Yin and S.N. Kavuri, 2003c. A review of process fault detection and diagnosis, Part III: Process history based methods, Computers in Chemical Engineering, 27:327-346.

Appendix

MQSO

PACKAGED WATER - COOLED CHILLER
(68 - 394 MBH)

fujiair
AIR-CONDITIONERS

PHYSICAL & ELECTRICAL DATA

MODEL "MQSO"		007 H	009 H	010 H	012 H	013 H	015 S	020 S	025 S	030 S	040 S
NOMINAL CAPACITY	MBH	68.0	80.5	104.7	118.7	131.4	157.0	203.0	274.0	303.0	394.0
	kW	20.5	23.6	30.7	34.8	38.5	46.0	59.5	80.3	88.8	115.5
COMPRESSOR	TYPE	← HERMETIC →					← SEMI-HERMETIC →				
	POWER SUPPLY	← 380-415 V / 3 ϕ / 50 Hz. →									
	HP.	6.8	8.5	10.0	12.0	13.0	15.0	20.0	25.0	30.0	40.0
	RATED LOAD AMP. (each)	10.6	12.5	16.50	18.6	18.6	20.5	26.5	36.2	40.6	57.8
	FULL LOAD AMP. (each)	12.5	14.7	19.4	21.8	21.8	28.6	42.0	55.0	62.0	92.0
	LOCKED ROTOR AMP. (each)	72	77	80	126	126	115	146	200	214	292
CONDENSER	TYPE	← SHELL AND TUBE →									
	FLOW RATE GPM	18	21	28	31	35	41	53	72	79	103
	PRESSURE DROP PSI.	1.6	3.3	1.2	1.2	1.2	3.5	5.2	5.1	6.1	8.6
	CONNECTIONS IN / OUT MPT.	1 1/4	1 1/4	1 1/4	1 1/4	1 1/4	2	2	2	2 1/2	2 1/2
	Q' TY	1	1	1	1	1	1	1	1	1	1
CHILLER	TYPE	← SHELL AND TUBE →									
	FLOW RATE GPM	13.6	16.1	21.0	23.7	26.3	31.4	40.6	54.8	60.6	78.8
	PRESSURE DROP PSI.	0.60	0.76	1.00	1.04	1.04	1.30	1.65	2.10	2.30	2.40
	CONNECTIONS IN / OUT MPT.	1 1/2	1 1/2	1 1/2	1 1/2	1 1/2	2	2	2	2 1/2	2 1/2
	Q' TY	1	1	1	1	1	1	1	1	1	1
REFRIGERANT	TYPE	← R - 22 →									
	CHARGED	← HOLDING →									
DIMENSION	WIDTH (mm.) , A	1,470	1,470	1,770	2,020	2,020	1,370	1,480	1,780	2,270	1,820
	DEPTH (mm.) ,B	400	400	400	400	400	550	550	550	550	700
	HEIGHT (mm.) , C	1,200	1,219	1,219	1,219	1,219	1,400	1,400	1,400	1,400	1,500
NET WEIGHT	kg.	250	250	275	320	320	440	530	715	780	920

Remarks: - Nominal capacity based onchilled water temperatre 12°C / 7°C (55°F / 45°F)and condenser 32°C /37°C (90°C /100°C)
- Nominal capacity : MBH = 1,000 BTUH , kW = 1,000 W
- Specifications subject to change without notice

STANDARD ACCESSARIES :

Refrigeration parts
- Thermostatic expansion valves
- Suction and liquid lines shut off & service valves
- Hot gas muffler
- Liquid line solinoid valves
- Sight glass and moisture indicator
- Liquid line filter drier

Electrical parts
- Compressor starter and overload relay
- Time delay relay
- High-low pressure switch
- Oil pressure switch (semi-hermetic only)
- Crankcase heater
- Electronic temperature control
- Electronic freezestat

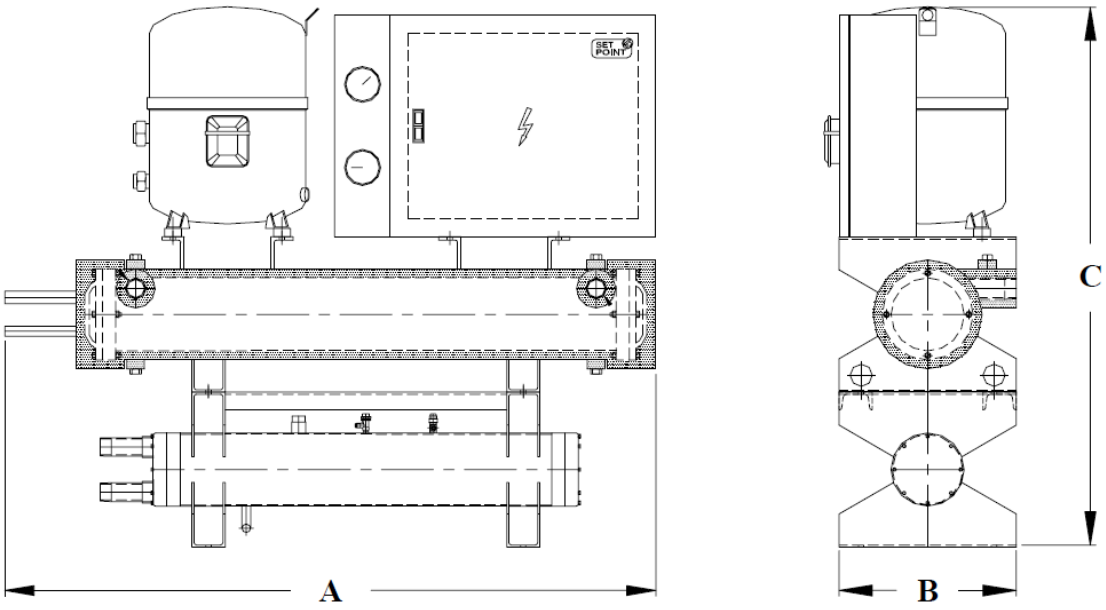

MQSO 007H - 013H

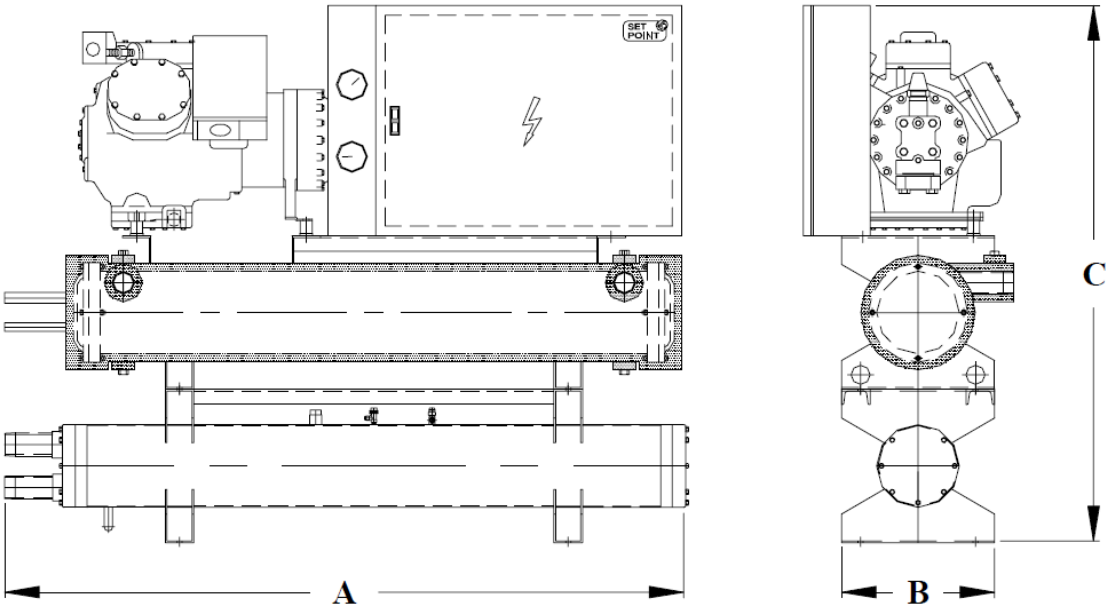

ZR81KC-TFD

HCFC, R-22, Mid Point, 50 Hz, 3 - Phase, 380/420 V
Air Conditioning
Production Status: Available for sale to all U.S. customers. Please check with your local Emerson Climate Technologies Representative for international availability.

Performance

Evap(°F)/Cond(°F)	45/130	45/100
RG(°F)/Liq(°F)	65/115	65/85
Capacity (Btu/hr):	68000	79500
Power(Watts):	5800	4140
Current (Amps):	10.5	8.8
EER (Btu/Wh):	11.7	19.2
Mass Flow (lbs/hr):	995.0	1020.0

Sound Power (dBA):	72 Ave 77 Max
Vibration (mils(peak-peak)):	2.0 Ave 3.0 Max

Mechanical

Number of Cylinders:	0	CIR (in^3/Rev):	6.577
Bore Size (in):	0.0	CFH (ft^3/hr):	662.2644
Stroke(in):	0.0		
Overall Length (in):	9.48	Mounting Length (in):	7.5
Overall Width (in):	9.71	Mounting Width(in):	7.5
Overall Height(in):	17.955	Mounting Height(in):	18.205*

Suction Size (in):	7/8 Stub
Discharge Size(in):	3/4 Stub
Initial Oil Charge (oz):	60
Oil Recharge (oz):	56
Net Weight(lbs):	86.0
HorsePower	

*Overall compressor height on Copeland Brand Product's specified mounting grommets.

Electrical

LRA-High*:	101.0	MCC(Amps):	17.0	UL File No.:	SA-2337
LRA-Half Winding:		RPM:	2900	UL File Date:	26-Jul-1993
LRA-Low*:	90.5	Max Operating Current:	15.0	CSA File No.:	LR3104C

RLA(=MCC/1.4; use for contactor selection): 12.1
RLA (=MCC/1.56; use for breaker & wire size selection): 10.9

Alternate Applications

Refrigerant	Frequency(Hz)	Phase	Voltage	Application
R-22 HCFC	60	3	460	Air Conditioning

Appendix

08-MAR-2009 10:41 2PT.CO.,LTD. 027262674 P.03

2 PT.CO.,LTD.
26/3 M.12 SUKHUMVIT 103 RD. DOKMAI
PRAWET BANGKOK 10250
TEL.0-2726-2675-7 FAX.0-2726-2674

CUSTOMER :

DATE : 26/09/2008
REFERENCE : S/ 2007/ -

PROJECT :

30 CONDENSER SPECIFICATION (SHELL AND TUBE)

DUTY REQUIREMENT

		R22			WATER	
FLUID						
FLOW RATE	FLOWRATE LIQUID	297.9	liter/hr	FLOW RATE	21.0	GPM
	FLOWRATE VAPOR	4800	liter/hr			
CONDENSATION TEMP (DEW)		42.0	^{0}C	TEMPERATURE-OUT	35.0	^{0}C
CONDENSER INLET TEMP		90.0	^{0}C	TEMPERATURE -IN	30.0	^{0}C
DENSITY	LIQUID	1.12	kg/liter	SPECIFIC HEAT	0.998	kcal / kg ^{0}C
	VAPOR	0.069	kg/liter	DENSITY	994	kg / m^3
EVAPORATION TEMP (DEW)		2	^{0}C			
SUBCOOL		1	^{0}C			

HEAT EXCHANGER (STAINLESS TUBE)

COOLING LOAD CAPACITY	(EXCLUDE HEAT REJECT 1.25 %)	92816	BTU/hr	27.2	Kw/hr	23391	Kcal/hr
COOLING LOAD CALCULATION	(EXCLUDE HEAT REJECT 1.25 %)	75000	BTU/hr	22.0	Kw/hr	18901	Kcal/hr
SAFETY FACTOR		23.8		%			
K-VALUE		1416		BTU/ft^2-hr-^{0}C			
LOG-MEAN-TEMP.-DIFF		9.5		^{0}C			
VELOCITY LIQUID(<6 ft/sec)	1.24 ft/sec	VELOCITY(4-10 ft/sec)		3.36 ft/sec			
VELOCITY HOT GLASS	14 ft/sec						
WATER PRESSURE DROP				1.40		mH_2O	
FOULING FACTOR				0.00025	ft^2 hr.^{0}F / BTU		
PASS OF WATER	4 pass						
MAX PRESSURE	400 lb/in^2			10		kg / cm^2	
PRESSURE TEST	450 lb/in^2			15		kg / cm^2	

CONSTRUCTION DATA

CONDENSER MODEL		VCC 7.5-1-06 S	
SURFACE		84.5	ft^2
WATER VOLUME		4	liter
WEIGHT -DRY		50.5	kg
SIDE OF TUBE		5/8	inch
NUMBER OF TUBE / CIRCUIT		28 / 1	pcs/circuit
SHELL OUT DIAMETER		6 1/2"	inch
REFRIGERANT PUMPDOWN CAPACITY		12	liter
REFRIGERANT OPERATION CHARGE(APPROXIMANT)		2	liter
CONNECTION	WATER CONNECTION IN & OUT	1 1/2	inch
	HOT GAS CONNECTION	7/8	inch
	LIQUID CONNECTION	3/4	inch
MATERIAL	SHELL	CARBON STEEL	
	TUBE	STAINLESS 304	
	FINED	ALUMINIUM HIARED FINED TUBE	
	TUBE SHEET	CARBON STEEL	
	HOT GAS CONNECTION (OD)	NYLON	
	LIQUID CONNECTION (OD)	NATIONAL RUBBER	
CAPACITY OF FOULING FACTOR	0.00025 ft^2.hr.^{0}F/BTU	100%	
	0.0005 ft^2.hr.^{0}F/BTU	98%	
	0.00075 ft^2.hr.^{0}F/BTU	95%	

2 PT.CO..LTD.
26/3 M.12 SUKHUMVIT 103 RD. DOKMAI
PRAWET BANGKOK 10250
TEL.0-2726-2675-7 FAX.0-2726-2674

CUSTOMER : -

DATE : 12/06/2007
REFERENCE : 2007/S- 00003

PROJECT : -

30 COOLER SPECIFICATION (SHELL AND TUBE)

DUTY REQUIREMENT

		R22			WATER	
FLUID						
FLOW RATE	FLOWRATE LIQUID	440.6	liter/hr	FLOW RATE	16.5	GPM
	FLOWRATE VAPOR	26663	liter/hr			
EVAPORATION TEMP		0.0	°C	TEMPERATURE-IN	12.0	°C
SUPER HEAT		7.0	°C			
EVAPORATOR (SUCTION TEMP)		7.0	°C	TEMPERATURE -OUT	7.0	°C
DENSITY	LIQUID	1.28	kg/liter	SPECIFIC HEAT	1.0	kcal / kg °C
	VAPOR	0.021	kg/liter	DENSITY	999	kg / m³

HEAT EXCHANGER (STAINLESS TUBE)

COOLER CAPACITY			100743	BTU/hr		
COOLER CALCULATION			80000	BTU/hr		
SAFETY FACTOR(<10%)			25.9	%		
K-VALUE			3965	BTU/ft²-hr-°C		
LOG-MEAN-TEMP.-DIFF			8.3	°C		
PASS OF REFRIGERENT			4.0	pass/pcs		
VELOCITY LIQUID(<6 ft/sec)	1.30	ft/sec	VELOCITY(4-10 ft/sec)		2.58	ft/sec
VELOCITY SUCTION(7-60 ft/sec)	45	ft/sec				
PRESSURE DROP	5.4	lb/in²			0.80	mH_2O
FOULING FACTOR					0.00025	ft² hr. °F / BTU
REFRIGERENT PASS	4	pass				
MAX PRESSURE	200	lb/in²			10	kg / cm²
PRESSURE TEST	250	lb/in²			15	kg / cm²

CONSTRUCTION DATA

COOLER MODEL		CST 008-1-06 S		
SURFACE		26		ft²
WATER VOLUME		16		liter
WEIGHT -DRY(TUBE SHEET CIRCLE/REGULAR)		74.4	/ ###	kg
SIDE OF TUBE		1/2		inch
NUMBER OF TUBE		54		pcs
NOMBER OF CIRCUIT		100%	/	circuit
SHELL OUT DIAMETER		6 1/2"		inch
CONNECTION	WATER CONNECTION	1 1/2		inch
	SUCTION CONNECTION	1 1/8		inch
	LIQUID CONNECTION	7/8		inch
MATERIAL	SHELL	CARBON STEEL		
	TUBE	STAINLESS 304		
	TUBE SHEET	CARBON STEEL		
	COVER	CARBON STEEL		
	GASKET	ASBESTOS"TESIT SOLVENIT"0.9mm.THICK		
	BUFFER	STAINLESS 304 &MILA		
CAPACITY OF FOULING FACTOR	0.00025 ft².hr.°F/BTU	100%		
	0.0005 ft².hr.°F/BTU	98%		

EMERSON Climate Technologies

EX2

Pulse Modulated Electronic Expansion Valve

Technical Data

ALCO CONTROLS

ALCO Controls EX2 Series is an electronically controlled expansion device. The capacity is defined through pulse width modulation. The EX2 can be driven by any electronic system providing the necessary electric power. However we recommend to use the ALCO EC2 Series.

Features

- Shut off function eliminates the necessity of a separate solenoid valve
- Dampened plunger reduces noise an effects of water hammer
- Wide regulation range 10% ... 100%
- One valve body can be combined with 6 orifices to make 7 capacity ranges, up to 17,2 kW, R22
- Applicable to all common refrigerants (CFC, HCFC, HFC).
- Available with ODF connections
- Utilising standard ASC coils (to be ordered separately)
- Long lifetime, high reliability

EX2-000

Pulse Modulated Electronic Expansion Valve

Introduction

Since the introduction of microprocessor systems more than 20 years ago it has been proven in millions of different applications that electronic control systems are very reliable and can do a much better job than mechanical solutions. The key point in most applications is the interface between the electronics and the media to be controlled.

The EX2 is the key to electronic control of refrigerant flow for refrigeration and air conditioning systems up to 17,2 kW (R22). The EX2 is designed for pulse width modulation and therefore able to provide a very precise temperature control. It is applicable to all common CFC, HCFC, HFC refrigerants and may be used on conventional, multiple evaporator or compressor systems.

The EX2 valve is a slide type solenoid valve with an orifice for expansion. This construction ensures noise free operation and avoids the „water hammer" due to soft closing. It is either completely open or completely closed. One common valve body can be combined with 6 interchangeable orifices to cover 7 capacity ranges (see selection chart). The table quotes capacities at 100% duty cycle. i.e. valve open continuously. However, it is recommended to operate the valve at partial load (50-80%) to allow for system load fluctuations. When used with an EC2 case controller, the valve operates with a 6 second pulse width cycle. Partial capacity can be calculated by proportioning the actual pulse time relative to 6 sec. i.e. 3 sec. pulse width cycle time = 50% valve capacity.

The standard ASC coil which operates the EX2 valve is available in a wide range of AC or DC voltages.

We recommend to use the EC2 Electronic display case controller from ALCO together with the EX2 valve which operates on a 24V AC supply.

Selection Chart

Function	Type	Order Nr.	Capacity Q_n at 100% Open Valve (kW)				
Electronic Expansion Valve			R 134a	R 22	R 404A	R 507	R 407C
10 mm inlet / 12 mm outlet	EX2-M00	801 091	13.3	17.2	12.1	12.1	18.7
3/8" inlet / 1/2" outlet	EX2-I00	801 090					
Orifice 4	EXO-004	801 089	8.5	10.9	7.7	7.7	11.8
Orifice 3	EXO-003	801 088	5.6	7.2	5.1	5.1	7.8
Orifice 2	EXO-002	801 087	3.3	4.3	3.0	3.0	4.7
Orifice 1	EXO-001	801 086	2.5	3.2	2.3	2.3	3.5
Orifice 0	EXO-000	801 085	1.2	1.6	1.1	1.1	1.7
Orifice X	EXO-00X	801084	0.7	0.9	0.6	0.6	1.0

Nominal capacities at 38°C condensing temperature, +4°C evaporating temperature and 1 K liquid sub-cooling at the inlet of the exp. valve.

Coil 24 VAC / 50 - 60 Hz (10 W)	ASC	801 062	for use with the ALCO EC2-controller (other coils voltages upon request)